AD_____

Award Number: W81XWH-13-1-0130

TITLE: Understanding Selective Downregulation of c-Myc Expression through Inhibition of General Transcription Regulators in Multiple Myeloma

PRINCIPAL INVESTIGATOR: Dr. Charles Lin

CONTRACTING ORGANIZATION:

Dana-Farber Cancer Institute, Inc.
Boston, MA 02115-6013

REPORT DATE: June 2014

TYPE OF REPORT: Annual Report

PREPARED FOR: U.S. Army Medical Research and Materiel Command
Fort Detrick, Maryland 21702-5012

REPORT DOCUMENTATION PAGE

Form Approved
OMB No. 0704-0188

1. REPORT DATE	2. REPORT TYPE	3. DATES COVERED
June 2014	Annual	15 June 2013 - 14 June 2014

4. TITLE AND SUBTITLE

Understanding Selective Downregulation of c-Myc Expression through Inhibition of General Transcription Regulators in Multiple Myeloma

5a. CONTRACT NUMBER

5b. GRANT NUMBER
W81XWH-13-1-0130

5c. PROGRAM ELEMENT NUMBER

6. AUTHOR(S)

Dr. Charles Lin

E-Mail: Charles_lin@dfci.harvard.edu

5d. PROJECT NUMBER

5e. TASK NUMBER

5f. WORK UNIT NUMBER

7. PERFORMING ORGANIZATION NAME(S) AND ADDRESS(ES)
Dana-Farber Cancer Institute
Boston, MA 02115-5450

8. PERFORMING ORGANIZATION REPORT NUMBER

9. SPONSORING / MONITORING AGENCY NAME(S) AND ADDRESS(ES)
U.S. Army Medical Research and Materiel Command
Fort Detrick, Maryland 21702-5012

10. SPONSOR/MONITOR'S ACRONYM(S)

11. SPONSOR/MONITOR'S REPORT NUMBER(S)

12. DISTRIBUTION / AVAILABILITY STATEMENT
Approved for Public Release; Distribution Unlimited

13. SUPPLEMENTARY NOTES

14. ABSTRACT

Chemical inhibitors that affect regulators of chromatin and transcription have emerged as powerful candidates for targeted cancer therapy. Through analysis of the chromatin and transcriptional landscape of Multiple Myeloma (MM), this project has endeavored to provide an explanatory mechanism for how treatment with inhibitors of chromatin regulators can selectively target oncogene transcription, and to understand how chromatin and transcription are altered in MM to promote tumorigenesis. Here we report the first comprehensive map of the chromatin and transcriptional landscape of MM in both cell lines and primary patient MM. Analysis of these maps revealed a striking asymmetry in the distribution of chromatin co-activators, most notably at a set of clustered enhancer regions we have termed "super-enhancers" which contain disproportionate levels of chromatin co-activators and are found near key oncogenes in MM. Due to their extreme occupancy by chromatin co-activators, target genes of super-enhancers are exquisitely sensitive to perturbations in chromatin co-activator binding, suggesting a mechanism underlying the observed selective downregulation of oncogene transcription by BET-bromodomain inhibitors, a class of inhibitors currently in clinical trials. In other tumor systems, super-enhancers associate with tumor specific oncogenes and dependencies and provide a rationale for super-enhancer mapping to characterize tumor oncogees and dependencies.

15. SUBJECT TERMS
Multiple myeloma, chromatin, computational biology

16. SECURITY CLASSIFICATION OF:			17. LIMITATION OF ABSTRACT	18. NUMBER OF PAGES	19a. NAME OF RESPONSIBLE PERSON
a. REPORT	b. ABSTRACT	c. THIS PAGE			USAMRMC
U	U	U	UU	62	19b. TELEPHONE NUMBER *(include area code)*

Table of Contents

Introduction: Multiple Myeloma (MM) is an aggressive and incurable plasma cell malignancy often characterized by IgH Enhancer/*MYC* (IgH/*MYC*) translocations that drive excess levels of the c-Myc oncoprotein. Recently, the Bradner laboratory has shown that inhibition of the general transcriptional co-activator BRD4 with a selective chemical probe (JQ1) leads to dramatic down regulation of c-Myc expression and cell death in MM cell lines (Delmore et al., 2011). In other tumors, BRD4 inhibition does not lead to down regulation of the IgH/*MYC* translocation gene, but rather causes the selective down regulation of other key cancer genes (Dawson et al., 2011; Ott et al., 2012; Zuber et al., 2011). BRD4 is a BET (bromodomain and extra-terminal) family protein (Filippakopoulos et al., 2010) that binds to acetyl-lysine residues on histones and other chromatin associated factors. BRD4 is a key co-activator of the elongation factor P-TEFb and has been shown to co-activate transcription through co-operative interactions with master regulator transcription factors (Huang et al., 2009). P-TEFb is required for the transcription elongation of essentially all active genes (Rahl et al., 2010) suggesting a general role for BRD4 in broadly co-activating transcription. Thus, it is unexpected based on current paradigms of mammalian transcriptional regulation and chromatin structure, how inhibition of BRD4 can selectively inhibit the transcriptional activity of oncogenes in tumors.

Body: *To explore the mechanisms by which inhibition of BRD4 leads to selective effects on oncogene transcription, we have undertaken the following aims:*

To map Brd4 onto the transcriptional and epigenomic landscape of MM. Reported in Loven et al., Cell 2013: Using genome wide ChIP-Seq (chromatin immunoprecipitation coupled to high throughput sequencing) approaches, we have mapped the comprehensive transcriptional and epigenomic landscape of MM in steady state and in response to treatment with increasing doses of JQ1 (Loven et al., Cell 2013 and attached). These data have been curated and made publically available on the Epigenome gateway browser in the "Multiple Myeloma Epigenome Portal" (http://epigenomegateway.wustl.edu/browser/). To map the activity of chromatin regulator bound cis-regulatory elements, we have developed and made openly available analysis software that can quantify normalized factor occupancy genome wide to identify and rank super-enhancers, genomic regions of asymmetric chromatin co-activator loading (http://younglab.wi.mit.edu/super_enhancer_code.html). We have employed this framework in patient MM samples to investigate changes to the enhancer landscape of MM induced by the primary tumor microenvironment (Figure 1) and have identified candidate primary tumor specific super-enhancers. We have also used this framework to explore epigenetic changes in B-cell acute lymphoblastic leukemia (Lane et al., 2014), and additional studies have employed our computational methods to characterize the epigenomes of healthy and disease cells (Shi et al., 2013; Wang et al., 2014; Whyte et al., 2013).

To examine the kinetic, transcriptional response to BET bromodomain inhibition Reported in Loven et al., Cell 2013; Chapuy et al., Cancer Cell 2013; Anand et al., Cell 2013: We have mapped JQ1 induced changes in gene expression and RNA Pol II genomic occupancy in both a time and concentration dependent manner in MM and other disease model systems (Anand et al., 2013; Chapuy et al., 2013; Loven et al., 2013). These data consistently show that BET bromodomain inhibition by JQ1 treatment leads to a global decrease in transcriptional activity, specifically a decrease in elongating RNA Pol II. This inhibition of transcription is most pronounced at super-enhancer proximal target genes and is supported at the chromatin level by evidence that both BRD4 and the active kinase subunit of the elongation P-TEFb are preferentially lost at super-enhancer loci upon JQ1 treatment. In MM, JQ1 treatment leads to rapid downregulation of *MYC* and other super-enhancer associated oncogenes. Interestingly in diffuse large B-cell lymphoma (DLBC), super-enhancers associate with different oncogenes and thus JQ1 treatment does not preferentially downregulate *MYC* transcription. Instead, in DLBCL, super-enhancers associate with other prominent B-cell factors including *BCL6* and *PAX5* that are strongly downreguated upon JQ1 treatment (Chapuy et al., 2013).

Thus we have shown that BET bromodomains act predominantly as transcription elongation co-activators and that their inhibition causes transcriptional effects commensurate with their local genomic density, in particular at super-enhancers which are disproportionately loaded by the factor.

To explore the contribution of cooperative binding and disproportionate load by Brd4 to transcriptional response: The initial description of super-enhancers in MM revealed additional features of super-enhancers with potential utility in characterizing tumor epigenomes. First, super-enhancers differ from typical enhancers in their underlying sequence composition, their response to perturbation, and their ability to drive extremely high levels of transcription at target genes. Towards a mechanistic understanding of these features, we are in the process of developing computational approaches to map transcription factor binding sites within super-enhancer loci (Figure 2). We have also established enhancer reporter constructs to test the activity of individual enhancer constituents. Finally, we are developing CRISPR based genetic editing systems to endogenously alter underlying sequences of super-enhancer regions (Cong et al., 2013). Second, in MM, the association of super-enhancers with key genes in MM biology suggest that super-enhancer mapping can be used as a tool to characterize unknown tumors and discover novel tumor dependencies. As a proof of concept, we have used maps of super-enhancers to successfully characterize primary DLBCL samples into their relevant clinical classifications (Chapuy et al., 2013). We have also targeted super-enhancer associated genes as candidate tumor dependencies — work that has lead to the characterization of the transcriptional co-activator *OCA-B* as a novel tumor dependency in DLBCL (Chapuy et al., 2013). Finally, to interrogate the dynamic epigenome in response to therapy, we are establishing novel methods to profile epigenomes from primary patient samples such as the newly developed assay for transposase accessible chromatin (ATAC-Seq) (Buenrostro et al., 2013) protocol which identifies DNAse hypersensitive cis-regulatory elements from small biological samples (Figure 3). Combined these efforts will allow further elucidation of the mechanisms by which super-enhancers regulate the tumor epigenome.

Key research accomplishments:

- Characterized super-enhancers in the epigenome of MM and other tumors
- Established super-enhancers as an explanatory mechanism to explain selective inhibition of tumor oncogenes in multiple contexts
- Utilized super-enhancers to discover novel tumor dependencies in DLBCL
- Established experimental protocols to profile epigenomes of primary patient tumors
- Established and distributed computational tools for quantifying enhancer landscapes

Reportable outcomes:

- *Publications:* Loven et al., Cell 2013; Anand et al., Cell 2013; Chapuy et al., Cancer Cell 2013; Lane et al., Nature Genetics 2014. (See Appendix and References)
- *Presentations:* Cell Symposia Cancer Epigenomics, Sitges Spain, October 2013
- *Databases:* Multiple Myeloma Epigenome Portal (http://epigenomegateway.wustl.edu/)
- *Informatics:* ROSE Rank Order of Super-Enhancers software (http://younglab.wi.mit.edu/super_enhancer_code.html)

Conclusion: The work described herein establishes super-enhancers as a conceptually novel feature of the epigenomic regulatory landscape in tumor cells. Super-enhancers are large genomic domains that are asymmetrically bound by chromatin co-activators. In different tumor cells, they associate with and drive the expression of tumor specific oncogenes and dependencies. Due to their disproportionate binding by chromatin co-activators, small molecule inhibitors of those co-activators, including BET bromodomain inhibitors, preferentially downregulate genes driven by super-enhancers. BET bromodomain inhibitors are currently in clinical trials and the use of these compounds in different tumor systems as well as measurements of their efficacy are currently being guided in large part by the conceptual framework of super-enhancers. More broadly, super-enhancers provide an explanatory mechanism for how inhibition of general chromatin co-activators can have gene selective effects and provide a rationale for targeting other chromatin co-activator proteins. Finally the unique features of super-enhancers suggest that their identification in poorly characterized tumors may allow better classification of patient tumor samples, identification of druggable targets, and discovery of novel tumor dependencies. These findings illustrate the importance of super-enhancers as a conceptual framework for understanding how tumor cells regulate their epigenomes.

References:

Anand, P., Brown, J.D., Lin, C.Y., Qi, J., Zhang, R., Artero, P.C., Alaiti, M.A., Bullard, J., Alazem, K., Margulies, K.B.*, et al.* (2013). BET bromodomains mediate transcriptional pause release in heart failure. Cell *154*, 569-582.
Buenrostro, J.D., Giresi, P.G., Zaba, L.C., Chang, H.Y., and Greenleaf, W.J. (2013). Transposition of native chromatin for fast and sensitive epigenomic profiling of open chromatin, DNA-binding proteins and nucleosome position. Nature methods *10*, 1213-1218.
Chapuy, B., McKeown, M.R., Lin, C.Y., Monti, S., Roemer, M.G., Qi, J., Rahl, P.B., Sun, H.H., Yeda, K.T., Doench, J.G.*, et al.* (2013). Discovery and characterization of super-enhancer-associated dependencies in diffuse large B cell lymphoma. Cancer cell *24*, 777-790.
Cong, L., Ran, F.A., Cox, D., Lin, S., Barretto, R., Habib, N., Hsu, P.D., Wu, X., Jiang, W., Marraffini, L.A.*, et al.* (2013). Multiplex genome engineering using CRISPR/Cas systems. Science *339*, 819-823.
Dawson, M.A., Prinjha, R.K., Dittmann, A., Giotopoulos, G., Bantscheff, M., Chan, W.I., Robson, S.C., Chung, C.W., Hopf, C., Savitski, M.M.*, et al.* (2011). Inhibition of BET recruitment to chromatin as an effective treatment for MLL-fusion leukaemia. Nature *478*, 529-533.
Delmore, J.E., Issa, G.C., Lemieux, M.E., Rahl, P.B., Shi, J., Jacobs, H.M., Kastritis, E., Gilpatrick, T., Paranal, R.M., Qi, J.*, et al.* (2011). BET bromodomain inhibition as a therapeutic strategy to target c-Myc. Cell *146*, 904-917.
Filippakopoulos, P., Qi, J., Picaud, S., Shen, Y., Smith, W.B., Fedorov, O., Morse, E.M., Keates, T., Hickman, T.T., Felletar, I.*, et al.* (2010). Selective inhibition of BET bromodomains. Nature *468*, 1067-1073.
Huang, B., Yang, X.D., Zhou, M.M., Ozato, K., and Chen, L.F. (2009). Brd4 coactivates transcriptional activation of NF-kappaB via specific binding to acetylated RelA. Mol Cell Biol *29*, 1375-1387.
Lane, A.A., Chapuy, B., Lin, C.Y., Tivey, T., Li, H., Townsend, E.C., van Bodegom, D., Day, T.A., Wu, S.C., Liu, H.*, et al.* (2014). Triplication of a 21q22 region contributes to B cell transformation through HMGN1 overexpression and loss of histone H3 Lys27 trimethylation. Nature genetics.
Loven, J., Hoke, H.A., Lin, C.Y., Lau, A., Orlando, D.A., Vakoc, C.R., Bradner, J.E., Lee, T.I., and Young, R.A. (2013). Selective inhibition of tumor oncogenes by disruption of super-enhancers. Cell *153*, 320-334.
Ott, C.J., Kopp, N., Bird, L., Paranal, R.M., Qi, J., Bowman, T., Rodig, S.J., Kung, A.L., Bradner, J.E., and Weinstock, D.M. (2012). BET bromodomain inhibition targets both c-MYC and IL7R in high-risk acute lymphoblastic leukemia. Blood.
Rahl, P.B., Lin, C.Y., Seila, A.C., Flynn, R.A., McCuine, S., Burge, C.B., Sharp, P.A., and Young, R.A. (2010). c-Myc regulates transcriptional pause release. Cell *141*, 432-445.
Shi, J., Whyte, W.A., Zepeda-Mendoza, C.J., Milazzo, J.P., Shen, C., Roe, J.S., Minder, J.L., Mercan, F., Wang, E., Eckersley-Maslin, M.A.*, et al.* (2013). Role of SWI/SNF in acute leukemia maintenance and enhancer-mediated Myc regulation. Genes & development *27*, 2648-2662.
Wang, H., Zang, C., Taing, L., Arnett, K.L., Wong, Y.J., Pear, W.S., Blacklow, S.C., Liu, X.S., and Aster, J.C. (2014). NOTCH1-RBPJ complexes drive target gene expression through dynamic interactions with superenhancers. Proc Natl Acad Sci U S A *111*, 705-710.
Whyte, W.A., Orlando, D.A., Hnisz, D., Abraham, B.J., Lin, C.Y., Kagey, M.H., Rahl, P.B., Lee, T.I., and Young, R.A. (2013). Master transcription factors and mediator establish super-enhancers at key cell identity genes. Cell *153*, 307-319.
Zuber, J., Shi, J., Wang, E., Rappaport, A.R., Herrmann, H., Sison, E.A., Magoon, D., Qi, J., Blatt, K., Wunderlich, M.*, et al.* (2011). RNAi screen identifies Brd4 as a therapeutic target in acute myeloid leukaemia. Nature *478*, 524-528.

Supporting Data:

Figure 1:

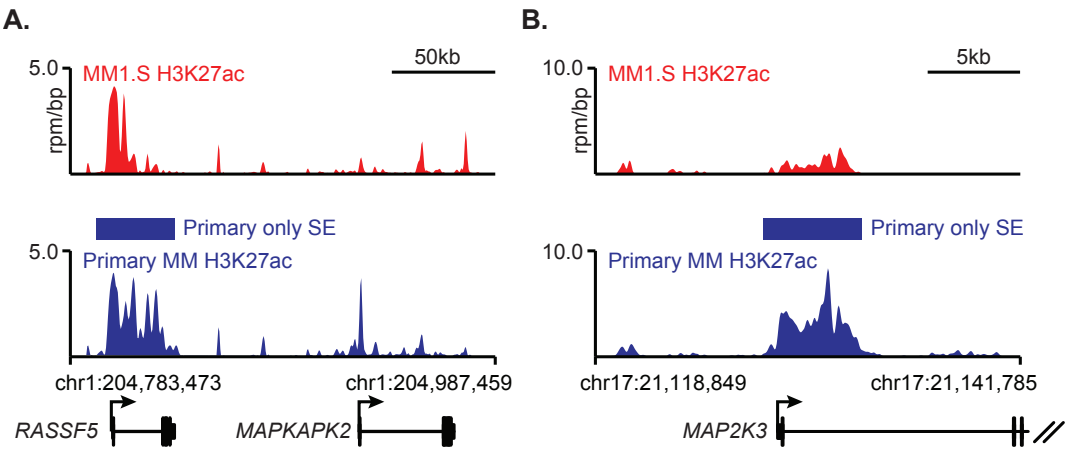

Gene tracks showing H3K27ac ChIP-Seq density in the MM1.S cell line (red) and in primary pleural effusion MM (blue) at MAPK pathway genes **A)** *MAPKAPK2* and **B)** *MAP2K3*. The x-axis shows linear genomic coordinates with genes containing regions displayed as boxes (exons) and lines (introns). Transcription start sites and gene orientation are shown with an arrow. The y-axis shows normalized ChIP-Seq density in units of reads per million per basepair (rpm/bp). Scale bars are provided in the top right. Super-enhancers found only in primary MM are shown as blue bars.

Figure 2:

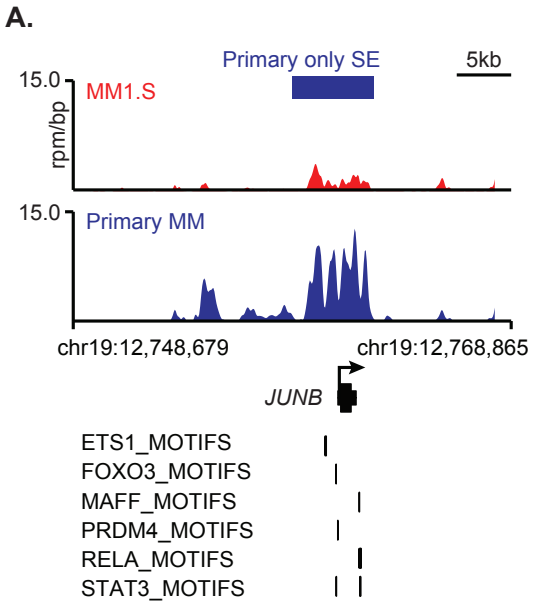

Gene tracks showing H3K27ac ChIP-Seq density in the MM1.S cell line (red) and in primary pleural effusion MM (blue) at the A) *JUN* locus. Super-enhancers found only in primary MM are shown as blue bars. Black bars underneath gene tracks illustrate computationally predicted transcription factor binding sites for transcription factors active in primary MM.

Figure 3:

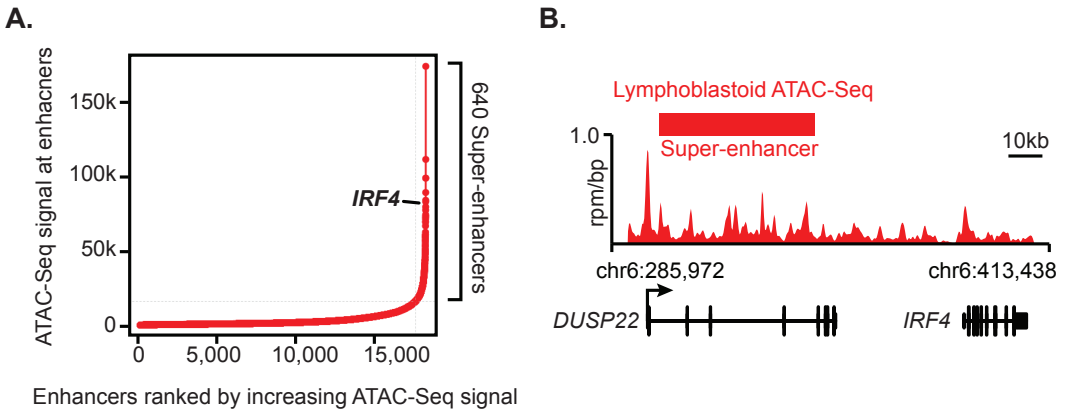

A) Enhancers in MM1.S cells ranked in increasing order by ATAC-Seq signal in units of total reads per million per enhancer (total rpm). 640 super-enhancers with asymmetric ATAC-Seq signal are identified along with the enhancer upstream of the *IRF4* gene. **B)** Gene track showing ATAC-Seq density in the MM1.S cell line (red) at the plasma cell lineage defining transcription factor *IRF4* locus. The x-axis shows linear genomic coordinates with genes containing regions displayed as boxes (exons) and lines (introns). Transcription start sites and gene orientation are shown with an arrow. The y-axis shows normalized ATAC-Seq density in units of reads per million per basepair (rpm/bp). Scale bars are provided in the top right. Super-enhancers found only in ATAC-Seq data are shown as a red bar.

Appendices:

I. Loven et al., Cell 2013

II. Anand et al., Cell 2013

III. Chapuy et al., Cancer Cell 2013

IV. Lane et al., Nature Genetics 2014

Cell

Selective Inhibition of Tumor Oncogenes by Disruption of Super-Enhancers

Jakob Lovén,[1,7] Heather A. Hoke,[1,2,7] Charles Y. Lin,[1,3,5,7] Ashley Lau,[1,2] David A. Orlando,[1] Christopher R. Vakoc,[4] James E. Bradner,[5,6] Tong Ihn Lee,[1] and Richard A. Young[1,2,*]
[1]Whitehead Institute for Biomedical Research, 9 Cambridge Center, Cambridge, MA 02142, USA
[2]Department of Biology
[3]Computational and Systems Biology Program
Massachusetts Institute of Technology, Cambridge, MA 02139, USA
[4]Cold Spring Harbor Laboratory, 1 Bungtown Road, Cold Spring Harbor, NY 11724, USA
[5]Department of Medical Oncology, Dana-Farber Cancer Institute, 44 Binney Street, Boston, MA 02115, USA
[6]Department of Medicine, Harvard Medical School, 25 Shattuck Street, Boston, MA 02115, USA
[7]These authors contributed equally to this work
*Correspondence: young@wi.mit.edu
http://dx.doi.org/10.1016/j.cell.2013.03.036

SUMMARY

Chromatin regulators have become attractive targets for cancer therapy, but it is unclear why inhibition of these ubiquitous regulators should have gene-specific effects in tumor cells. Here, we investigate how inhibition of the widely expressed transcriptional coactivator BRD4 leads to selective inhibition of the *MYC* oncogene in multiple myeloma (MM). BRD4 and Mediator were found to co-occupy thousands of enhancers associated with active genes. They also co-occupied a small set of exceptionally large super-enhancers associated with genes that feature prominently in MM biology, including the *MYC* oncogene. Treatment of MM tumor cells with the BET-bromodomain inhibitor JQ1 led to preferential loss of BRD4 at super-enhancers and consequent transcription elongation defects that preferentially impacted genes with super-enhancers, including *MYC*. Super-enhancers were found at key oncogenic drivers in many other tumor cells. These observations have implications for the discovery of cancer therapeutics directed at components of super-enhancers in diverse tumor types.

INTRODUCTION

Chromatin regulators are attractive as therapeutic targets for cancer because they are deregulated in numerous cancers (Baylin and Jones, 2011; Elsässer et al., 2011; Esteller, 2008; Feinberg and Tycko, 2004; You and Jones, 2012) and are amenable to small-molecule inhibition (Cole, 2008; Dawson and Kouzarides, 2012; Geutjes et al., 2012). Inhibition of some chromatin regulators has already proven to be efficacious for treatment of certain cancers (Issa and Kantarjian, 2009; Marks and Xu, 2009). Most chromatin regulators, however, are expressed in a broad range of healthy cells and contribute generally to gene expression, so inhibition of these important genome-associated proteins might be expected to adversely affect global gene expression in healthy cells and thus produce highly toxic effects. Nonetheless, inhibitors of some chromatin regulators, such as BRD4, have been shown to selectively inhibit transcription of key oncogenic drivers such as *c-MYC* (hereafter referred to as *MYC*) in multiple tumor types (Dawson et al., 2011; Delmore et al., 2011; Mertz et al., 2011; Zuber et al., 2011). It is important to understand how inhibition of a widely expressed, general regulator such as BRD4 can exert a selective effect on the expression of a small number of genes in specific cells.

BRD4 is a member of the bromodomain and extraterminal (BET) subfamily of human bromodomain proteins, which includes BRDT, BRD2, BRD3, and BRD4. These proteins associate with acetylated chromatin and facilitate transcriptional activation (LeRoy et al., 2008; Rahman et al., 2011). BRD4 was first identified as an interaction partner of the murine Mediator coactivator complex (Jiang et al., 1998) and was subsequently shown to associate with Mediator in a variety of human cells (Dawson et al., 2011; Wu and Chiang, 2007). BRD4 is involved in the control of transcriptional elongation by RNA polymerase II (RNA Pol II) through its recruitment of the positive transcription elongation factor P-TEFb (Jang et al., 2005; Yang et al., 2005). Almost all human cells express the *BRD4* gene, based on analysis of human tissue expression data across 90 distinct tissue types (human body index - transcriptional profiling, see Extended Experimental Procedures), and BRD4 is found to be associated with a large population of active genes in $CD4^+$ T cells (Zhang et al., 2012). It is not yet clear whether the BRD4 protein is generally involved in the transcription of active genes in tumor cells or if it is selectively associated with a subset of these genes.

Two recently developed bromodomain inhibitors, JQ1 and iBET, selectively bind to the amino-terminal twin bromodomains of BRD4 (Filippakopoulos et al., 2010; Nicodeme et al., 2010). These BET inhibitors cause selective repression of the potent *MYC* oncogene in a range of tumors, including multiple myeloma (MM), Burkitt's lymphoma (BL), acute myeloid leukemia (AML), and acute lymphoblastic leukemia (ALL) (Dawson et al., 2011; Delmore et al., 2011; Mertz et al., 2011; Ott et al., 2012; Zuber et al., 2011). The inhibition of *MYC* apparently occurs as a consequence of BRD4 depletion at the enhancers that drive *MYC* expression (Delmore et al., 2011). Although BRD4 is widely expressed in mouse tissues, mice are reasonably tolerant of the levels of BET bromodomain inhibition that inhibit certain tumors in mouse models (Dawson et al., 2011; Delmore et al., 2011; Filippakopoulos et al., 2010; Mertz et al., 2011; Zuber et al., 2011).

The MM cell line (MM1.S) used to study the effects of JQ1 has an *IgH-MYC* rearrangement, and *MYC* gene expression is driven by factors associated with the *IgH* enhancer (Dib et al., 2008; Shou et al., 2000). Enhancers function through cooperative and synergistic interactions between multiple transcription factors and coactivators (Carey et al., 1990; Giese et al., 1995; Kim and Maniatis, 1997; Thanos and Maniatis, 1995). Cooperative binding and synergistic activation confer increased sensitivity so that small changes in activator concentration can lead to dramatic changes in activator binding and transcription of associated genes (Carey, 1998). Furthermore, enhancers with large numbers of transcription factor binding sites can be more sensitive to small changes in factor concentration than those with smaller numbers of binding sites (Giniger and Ptashne, 1988; Griggs and Johnston, 1991). This concept led us to postulate that some features of the *IgH* enhancer might account for the selective effect of BRD4 inhibition.

We show here that BRD4 and Mediator are associated with most active enhancers and promoters in MM1.S tumor cells, but exceptionally high levels of these cofactors occur at a small set of large enhancer regions, which we call super-enhancers. Super-enhancers are associated with *MYC* and other key genes that feature prominently in the biology of MM, including many lineage-specific survival genes. Treatment of MM tumor cells with the BRD4 inhibitor JQ1 caused a preferential loss of BRD4, Mediator, and P-TEFb at super-enhancers and caused preferential loss of transcription at super-enhancer-associated genes, including the *MYC* oncogene. Tumor cell addiction to high-level expression of these oncogenes may then contribute to their vulnerability to super-enhancer disruption (Chin et al., 1999; Felsher and Bishop, 1999; Jain et al., 2002; Weinstein, 2002). We find super-enhancers in additional tumor types, where they are similarly associated with key oncogenes. Thus, key oncogene drivers of tumor cells are regulated by super-enhancers, which can confer disproportionate sensitivity to loss of the BRD4 coactivator and thus cause selective inhibition of transcription.

RESULTS

BRD4 and Mediator Co-occupy Promoters of Active Genes in Multiple Myeloma

Transcription factors bind to enhancers and recruit the Mediator coactivator, which in turn becomes associated with RNA Pol II at the transcription start site (TSS), thus forming DNA loops between enhancers and core promoters (Kagey et al., 2010). BRD4 is known to associate with Mediator in some mammalian cells (Dawson et al., 2011; Jiang et al., 1998; Wu et al., 2003). To identify active promoter and enhancer elements and to determine how BRD4 and Mediator occupy the genome in MM1.S MM cells, we used chromatin immunoprecipitation coupled to high-throughput sequencing (chromatin immunoprecipitation [ChIP]-seq) with antibodies against the Mediator subunit MED1, BRD4, the enhancer-associated histone modification H3K27Ac, and the TSS-associated histone modification H3K4Me3 (Figure 1). ChIP-seq signals for both Mediator and the histone modification H3K27Ac have previously been shown to occur at both enhancers and TSSs (Creyghton et al., 2010; Heintzman et al., 2009; Rada-Iglesias et al., 2011), and enhancers can be distinguished from TSSs by the absence of TSS annotation and relatively low levels of H3K4Me3. We found that BRD4 co-occupied enhancers and TSSs with MED1 throughout the genome (Figures 1A and 1B) and that the levels of BRD4 and MED1 were strongly correlated (Figure S1 available online).

To confirm that BRD4 and Mediator are generally associated with active genes in MM1.S cells, we compared the ChIP-seq data for these regulators with that for RNA Pol II and the histone modification H3K4Me3. The levels of BRD4 and Mediator correlated with the levels of RNA Pol II genome wide (Figure 1C). Signals for BRD4 and Mediator were found together with those for the histone modification H3K4Me3 and RNA Pol II at ~10,000 annotated TSSs, and these were considered active TSSs (Table S1). Signals for BRD4 and the enhancer-associated histone modification H3K27Ac were found in ~8,000 Mediator-occupied regions either lacking TSSs or extending beyond the immediate vicinity of the TSS, and these were considered enhancer regions (Table S2, Data S1, and Extended Experimental Procedures).

Super-Enhancers Are Associated with Key Multiple Myeloma Genes

Further analysis of the ~8,000 enhancer regions revealed that the MED1 signal at 308 enhancers was significantly greater than at all other enhancers and promoters (Figures 2A and S2A and Table S2). These 308 super-enhancers differed from typical enhancers in both size and Mediator levels (Figure 2B). Remarkably, ~40% of all enhancer-bound Mediator and BRD4 occupied these 308 super-enhancers. Whereas the typical enhancer had a median size of 1.3 kb, the super-enhancers had a median size of 19.4 kb. These super-enhancers were thus 15-fold larger than typical enhancers and were occupied, based on ChIP-seq signal, by 18-fold more Mediator and 16-fold more BRD4. Similarly high levels of H3K27Ac were observed in these large regions (Figure 2B). Examples of gene tracks showing super-enhancers at either end of the spectrum of Mediator occupancy (Figure 2A) are shown in Figure 2C. The largest super-enhancer was found associated with the *IGLL5* gene, which encodes an immunoglobulin lambda peptide expressed at high levels in these cells.

We next sought to identify the complete set of MM1.S genes that are most likely associated with super-enhancers. Enhancers tend to loop to and associate with adjacent genes in order to activate their transcription (Göndör and Ohlsson, 2009; Lelli

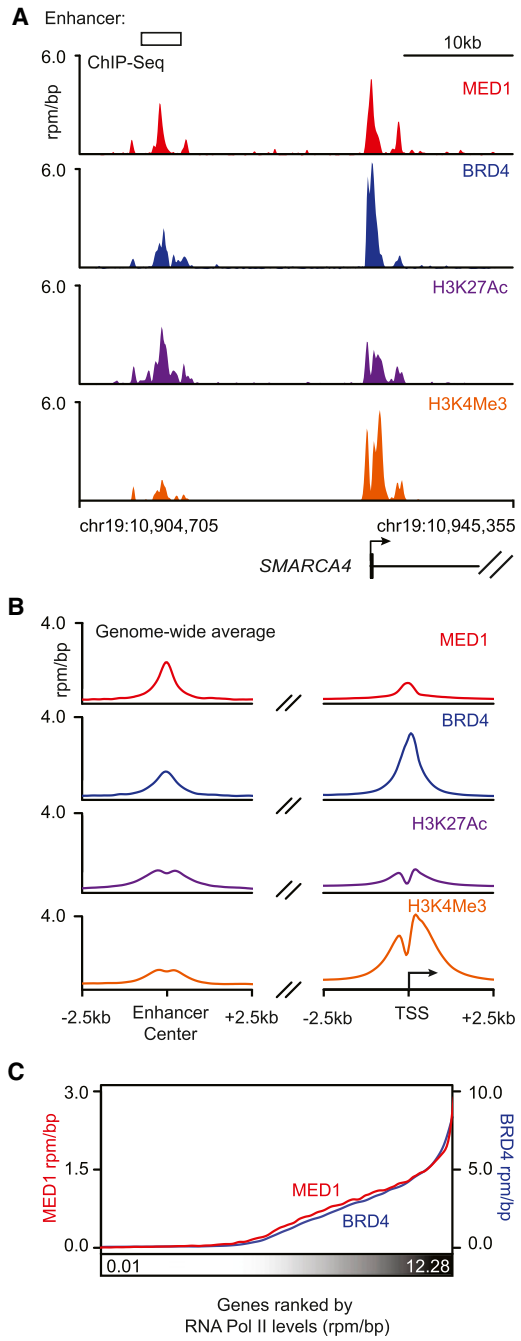

Figure 1. Mediator and BRD4 Co-occupy Promoters of Active Genes in Multiple Myeloma

(A) Gene tracks of MED1, BRD4, H3K27Ac, and H3K4Me3 ChIP-seq occupancy at the enhancer (left) and promoter (right) of *SMARCA4* in MM1.S MM cells. The x axis shows genomic position, and enhancer-containing regions are depicted with a white box. The y axis shows signal of ChIP-seq occupancy in units of reads per million mapped reads per base pair (rpm/bp).

(B) Metagene representation of global MED1, BRD4, H3K27Ac, and H3K4Me3 occupancy at enhancers and promoters. The x axis shows the ±2.5 kb region flanking either the center of enhancer regions (left) or the TSS of active genes (right). The y axis shows the average background subtracted ChIP-seq signal in units of rpm/bp.

(C) Median MED1 and BRD4 levels in the ±1 kb region around the TSSs of actively transcribed genes ranked by increasing RNA Pol II occupancy in MM1.S cells. Levels are in units of rpm/bp, with the left y axis showing levels of MED1 and the right y axis showing levels of BRD4. Promoters were binned (50/bin), and a smoothing function was applied to median levels.

See also Figure S1.

et al., 2012; Ong and Corces, 2011; Spitz and Furlong, 2012). Most of these interactions occur within a distance of ~50 kb of the enhancer (Chepelev et al., 2012). Using a simple proximity rule, we assigned all transcriptionally active genes (TSSs) to super-enhancers within a 50 kb window, a method shown to identify a large proportion of true enhancer/promoter interactions in embryonic stem cells (Dixon et al., 2012). This identified 681 genes associated with super-enhancers (Table S3), and 307 of these had a super-enhancer overlapping a portion of the gene, as shown for *CCND2* in Figure 2C.

Super-enhancer-associated genes were generally expressed at higher levels than genes with typical enhancers and tended to be specifically expressed in MM1.S cells (Figure 2D). To test whether components of super-enhancers confer stronger activity compared to typical enhancers, we cloned representative super-enhancer or typical enhancer fragments of similar size into luciferase reporter constructs and transfected these into MM1.S cells. Cloned sequence fragments from super-enhancers generated 2- to 3-fold higher luciferase activity compared to typical enhancers of similar size (Figure 2E and Extended Experimental Procedures). These results are consistent with the notion that super-enhancers help to activate high levels of transcription of key genes that regulate and enforce the MM1.S cancer cell state.

The super-enhancer-associated genes included most genes that have previously been shown to have important roles in MM biology, including *MYC*, *IRF4*, *PRDM1/BLIMP-1*, and *XBP1* (Figure 3A). *MYC* is a key oncogenic driver in MM (Chng et al., 2011; Dib et al., 2008; Holien et al., 2012; Shou et al., 2000), and the MM1.S *MYC* locus contains a chromosomal rearrangement that places *MYC* under the control of the *IgH* enhancer, which qualifies as a super-enhancer in MM1.S cells. The *IRF4* gene encodes a key plasma cell transcription factor that is frequently deregulated in MM (Shaffer et al., 2008). *PRDM1/BLIMP-1* encodes a transcription factor that is considered a master regulator of plasma cell development and is required for the formation of plasma cell tumors in a mouse model (Shapiro-Shelef et al., 2003; Turner et al., 1994). *XBP1* encodes a basic-region leucine zipper (bZIP) transcription factor of the CREB-ATF family that governs plasma cell differentiation (Reimold et al., 2001). *XBP1* is frequently overexpressed in human MM and can drive the development of MM in a mouse model (Carrasco et al., 2007; Claudio et al., 2002).

Super-enhancers were associated with many additional genes that have important roles in cancer pathogenesis more generally (Figure 3B). Cyclin D2 (*CCND2*) is deregulated in many human cancers, including MM (Bergsagel et al., 2005; Musgrove et al., 2011). The PIM1 kinase has been implicated in the biology of many different cancers (Shah et al., 2008). *MCL1* and *BCL-xL*, members of the BCL-2 family of apoptosis regulators, are frequently deregulated in cancer, promoting cell survival and

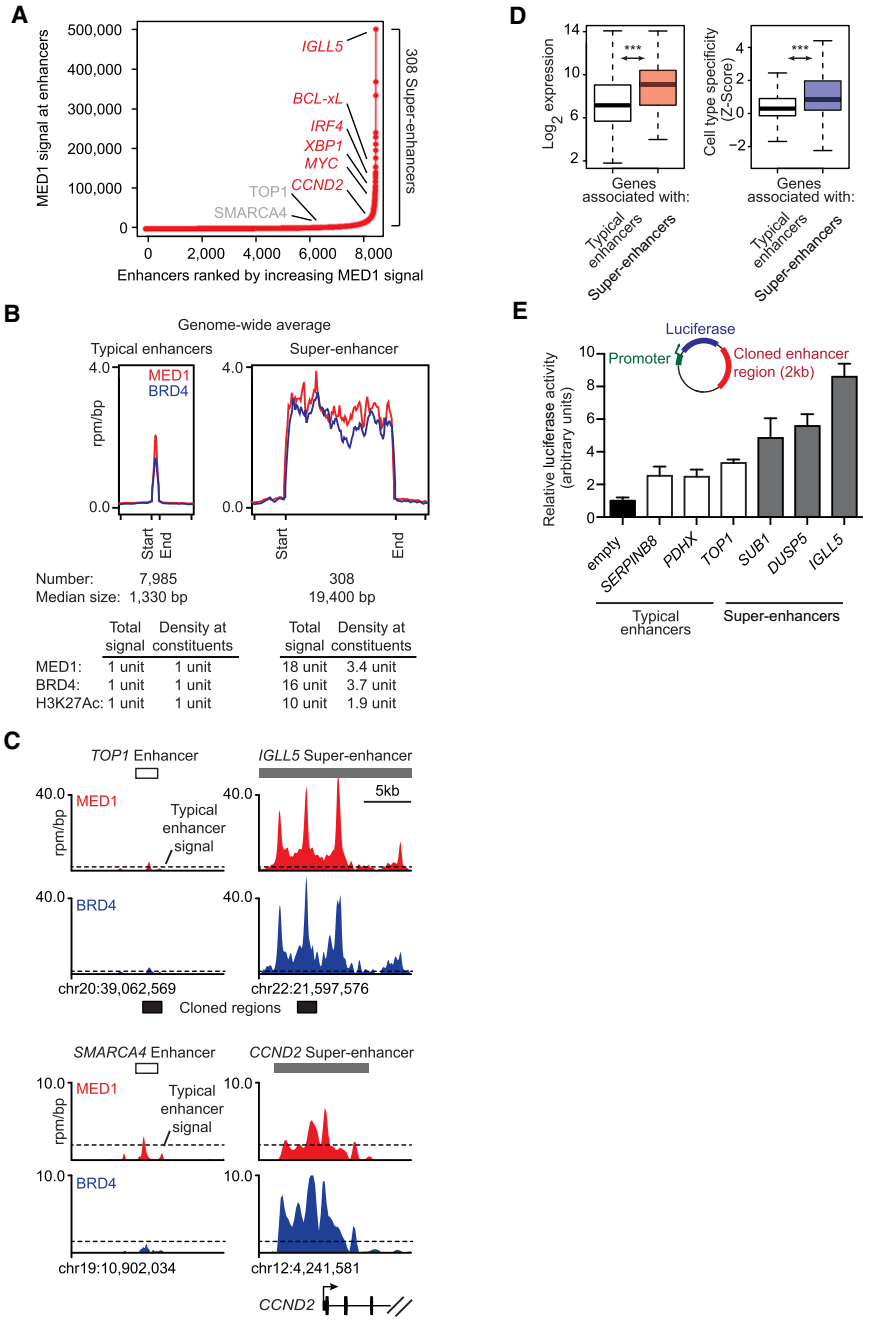

Figure 2. Super-Enhancers Identified in Multiple Myeloma

(A) Total MED1 ChIP-seq signal in units of reads per million in enhancer regions for all enhancers in MM1.S. Enhancers are ranked by increasing MED1 ChIP-seq signal.

(B) Metagene representation of global MED1 (red line) and BRD4 (blue line) occupancy at typical enhancers and super-enhancers. The x axis shows the start and end of the enhancer (left) or super-enhancer (right) regions flanked by ±5 kb of adjacent sequence. Enhancer and super-enhancer regions on the x axis are relatively scaled. The y axis shows the average signal in units of rpm/bp.

(C) Gene tracks of MED1 (top) and BRD4 (bottom) ChIP-seq occupancy at the typical enhancer upstream of *TOP1*, the super-enhancer downstream of *IGLL5*, the typical enhancer upstream of *SMARCA4*, and the super-enhancer overlapping the *CCND2* gene TSS. The x axis shows genomic position, and super-enhancer-containing regions are depicted with a gray box. The y axis shows signal of ChIP-seq occupancy in units of rpm/bp.

(D) Left: box plots of expression values for genes with proximal typical enhancers (white) or with proximal super-enhancers (pink). The y axis shows expression value in Log2 arbitrary units. Right: box plots of cell-type specificity values for genes with proximal typical enhancers (white) or with proximal super-enhancers (purple). The y axis shows the *Z* score of the Jensen-Shannon (JS) divergence statistic for genes, with higher values corresponding to a more cell-type-specific pattern of expression. Changes between expression levels are significant (two-tailed Welch's t test, $p < 2 \times 10^{-16}$), as are changes between cell-type-specificity levels (two-tailed Welch's t test, $p = 1 \times 10-14$).

(E) Bar graph depicting luciferase activity of reporter constructs containing cloned fragments of typical enhancers and super-enhancers in MM1.S cells. 2 kb fragments of three super-enhancers, IGLL5, DUSP5, and SUB1, and three typical enhancers, PDHX, SERPINB8, and TOP1, ranked 1, 129, 227, 2352, 4203, and 4794, respectively, in terms of MED1 occupancy, were cloned into reporter plasmids downstream of the luciferase gene, driven by a minimal *MYC* promoter. Luciferase activity is represented as fold over empty vector. Error bars represent SD of triplicate experiments.

See also Figure S2 and Data S1.

chemoresistance (Beroukhim et al., 2010). We conclude that super-enhancers are frequently associated with genes that feature prominently in the biology of MM and other human cancers.

Inhibition of BRD4 Leads to Displacement of BRD4 Genome Wide

BRD4 interacts with chromatin-associated proteins such as transcription factors, the Mediator complex, and acetylated histones (Dawson et al., 2011; Dey et al., 2003; Jang et al., 2005; Jiang et al., 1998; Wu and Chiang, 2007; Wu et al., 2013). Previous studies have shown that treatment of MM1.S cells with JQ1 leads to reduced levels of BRD4 at the *IgH* enhancer that drives *MYC* expression (Delmore et al., 2011), but it is not clear whether such treatment causes a general reduction in the levels of BRD4 associated with the genome. We found that treatment of MM1.S cells with 500 nM JQ1 for 6 hr reduced the levels of BRD4 genome wide by ~70% (Figures 4A and 4B). This reduction in BRD4 occupancy was evident both by inspection of individual gene tracks (Figure 4C) and through global analysis of the average effects at enhancers and TSSs

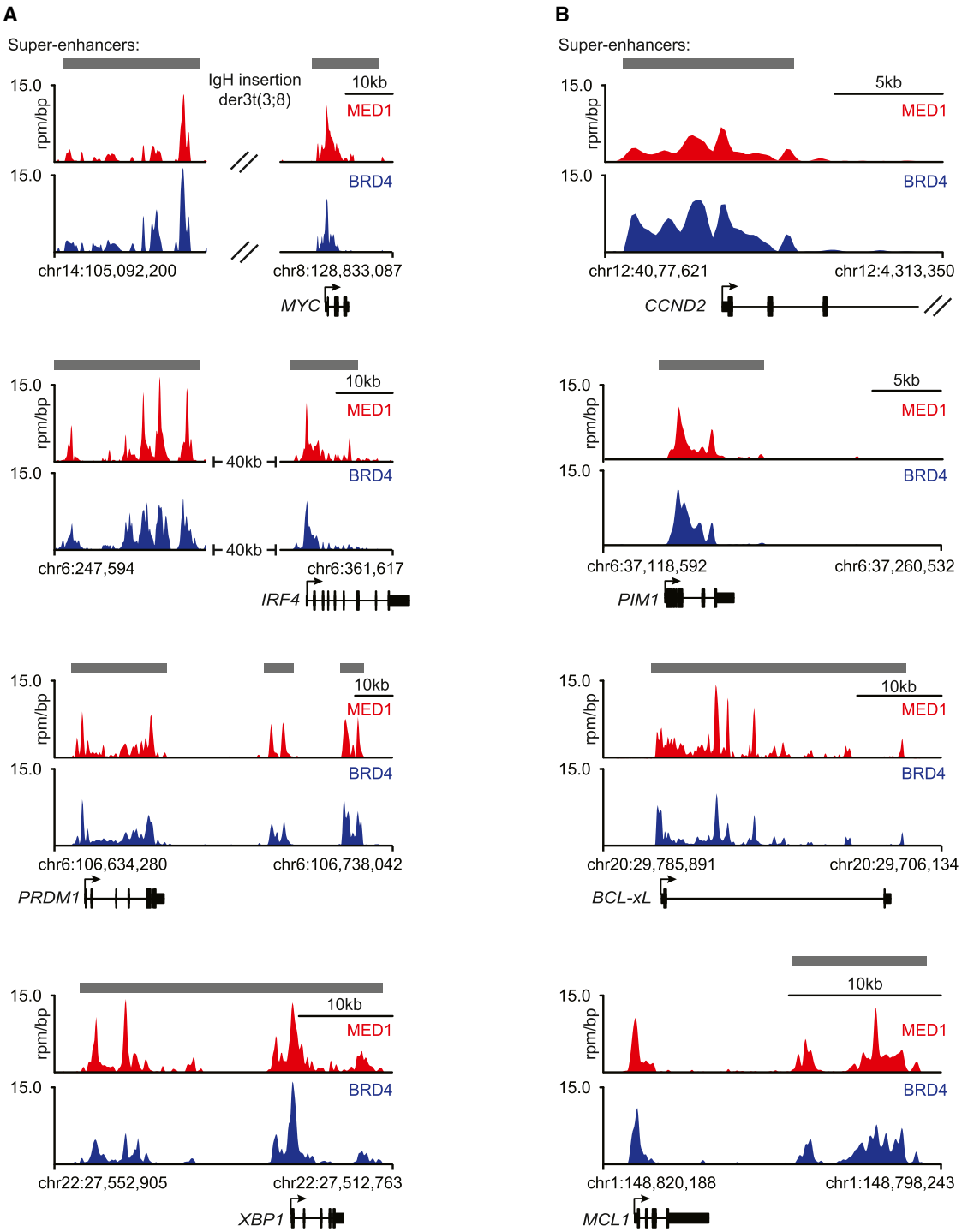

Figure 3. Super-Enhancers Are Associated with Key Multiple Myeloma Genes

(A and B) Gene tracks of MED1 and BRD4 ChIP-seq occupancy at super-enhancers near genes with important roles in MM biology (A) or genes with important roles in cancer (B). Super-enhancers are depicted in gray boxes over the gene tracks. The x axis shows genomic position, and super-enhancer-containing regions are depicted with a gray box. The y axis shows signal of ChIP-seq occupancy in units of rpm/bp.

(Figure 4D). JQ1 treatment led to ~60% reduction in BRD4 signal at enhancers and ~90% reduction at promoters (Figure 4D). The reduction in BRD4 was more profound at super-enhancers such as those associated with *IgH-MYC* and *CCND2* (Figure 4E), where the loss of BRD4 was nearly complete. We conclude that BET bromodomain inhibition of BRD4

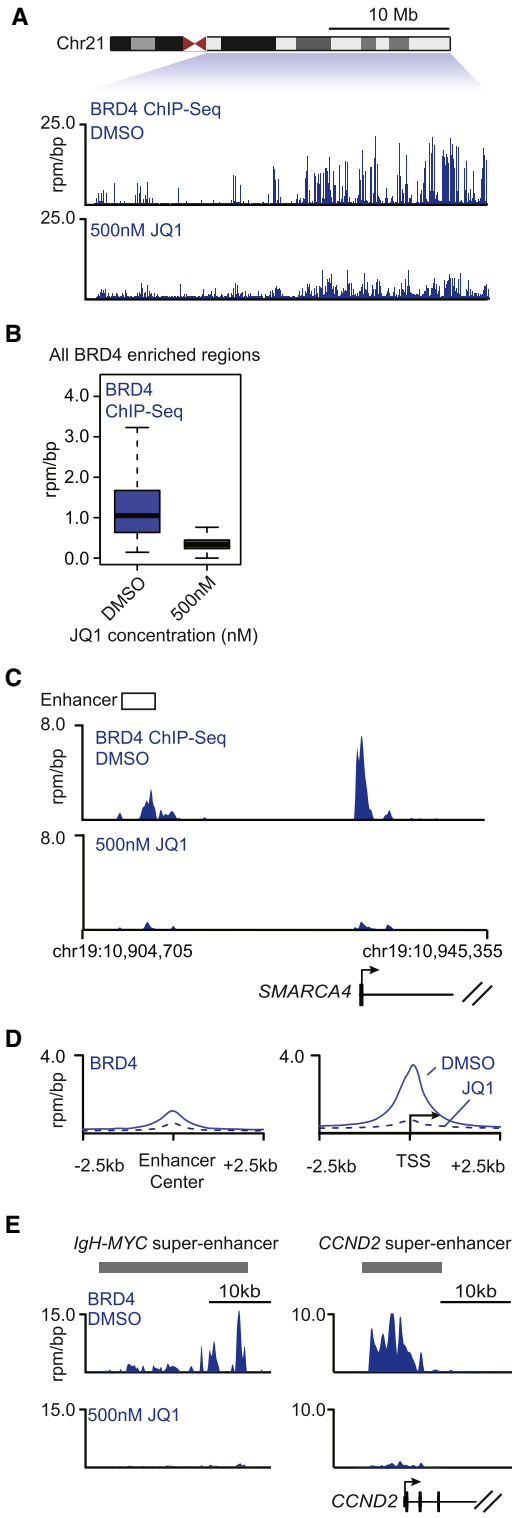

Figure 4. Inhibition of BRD4 Leads to Loss of BRD4 Genome Wide

(A) Tracks showing BRD4 ChIP-seq occupancy on the 35 Mb right arm of chromosome 21 after DMSO (top) or 500 nM JQ1 (bottom) treatment. The chromosome 21 ideogram is displayed above the gene tracks with the relevant region highlighted in blue. The x axis of the gene tracks shows genomic position, and the y axis shows BRD4 ChIP-seq signal in units of rpm/bp.

(B) Box plot showing the distributions of BRD4 ChIP-seq signal at BRD4-enriched regions after DMSO (left) or 500 nM JQ1 (right) treatment. BRD4-enriched regions were defined in MM1.S cells treated with DMSO. The y axis shows BRD4 ChIP-seq signal in units of rpm/bp. The loss of BRD4 occupancy at BRD4-enriched regions after JQ1 is highly significant (p value $< 1 \times 10^{-16}$, Welch's t test).

(C) Gene tracks of BRD4 ChIP-seq occupancy at the enhancer (left) and promoter (right) of *SMARCA4* in MM1.S cells after DMSO (top) or 500 nM JQ1 (bottom) treatment for 6 hr. The x axis shows genomic position, and enhancer-containing regions are depicted with a white box. The y axis shows signal of ChIP-seq occupancy in units of rpm/bp.

(D) Metagene representation of global BRD4 occupancy at enhancers and promoters after DMSO (solid line) or 500 nM JQ1 (dotted line) treatment. The x axis shows the ±2.5 kb region flanking either the center of enhancer regions (left) or the TSS of active genes. The y axis shows the average background subtracted ChIP-seq signal in units of rpm/bp.

(E) Gene tracks of BRD4 binding at super-enhancers after DMSO (top) or 500 nM JQ1 (bottom) treatment. The x axis shows genomic position, and super-enhancer-containing regions are depicted with a gray box. The y axis shows signal of ChIP-seq occupancy in units of rpm/bp.

leads to reduced levels of BRD4 at enhancers and promoters throughout the genome in MM1.S cells.

Transcription of Super-Enhancer-Associated Genes Is Highly Sensitive to BRD4 Inhibition

Enhancers are formed through cooperative and synergistic binding of multiple transcription factors and coactivators (Carey, 1998; Carey et al., 1990; Giese et al., 1995; Kim and Maniatis, 1997; Thanos and Maniatis, 1995). As a consequence of this binding behavior, enhancers bound by many cooperatively interacting factors lose activity more rapidly than enhancers bound by fewer factors when the levels of enhancer-bound factors are reduced (Giniger and Ptashne, 1988; Griggs and Johnston, 1991). The presence of super-enhancers at *MYC* and other key genes associated with MM led us to consider the hypothesis that super-enhancers are more sensitive to reduced levels of BRD4 than typical enhancers and that genes associated with super-enhancers might then experience a greater reduction of transcription than genes with average enhancers when BRD4 is inhibited (Figure 5A).

To test this hypothesis, we first examined the effects of various concentrations of JQ1 on BRD4 occupancy genome wide (Figure 5B). JQ1 had little effect on MM1.S cell viability when treated for 6 hr at these various concentrations, whereas at later time points, JQ1 had a significant antiproliferative effect (Figure 5C). As expected, MYC protein levels were significantly depleted by exposure of MM1.S cells to 50 nM or greater doses of JQ1 for 6 hr (Figure 6D) (Delmore et al., 2011). In contrast, JQ1 did not affect total BRD4 protein levels within the cells and did not significantly reduce ChIP efficiency (Figure 5E). When BRD4 occupancy was examined genome wide in cells exposed to increasing concentrations of JQ1, it was evident that super-enhancers showed a greater loss of BRD4 occupancy than typical enhancer regions (Figure 5F). For example, the *IgH* super-enhancer showed significantly greater reduction in BRD4 occupancy in cells treated with 5 nM or 50 nM JQ1 than typical enhancer regions such as that upstream of *SMARCA4* (Figure 5G). Ultimately, virtually all BRD4 occupancy was lost at the *IgH* super-enhancer (97% reduction versus DMSO control)

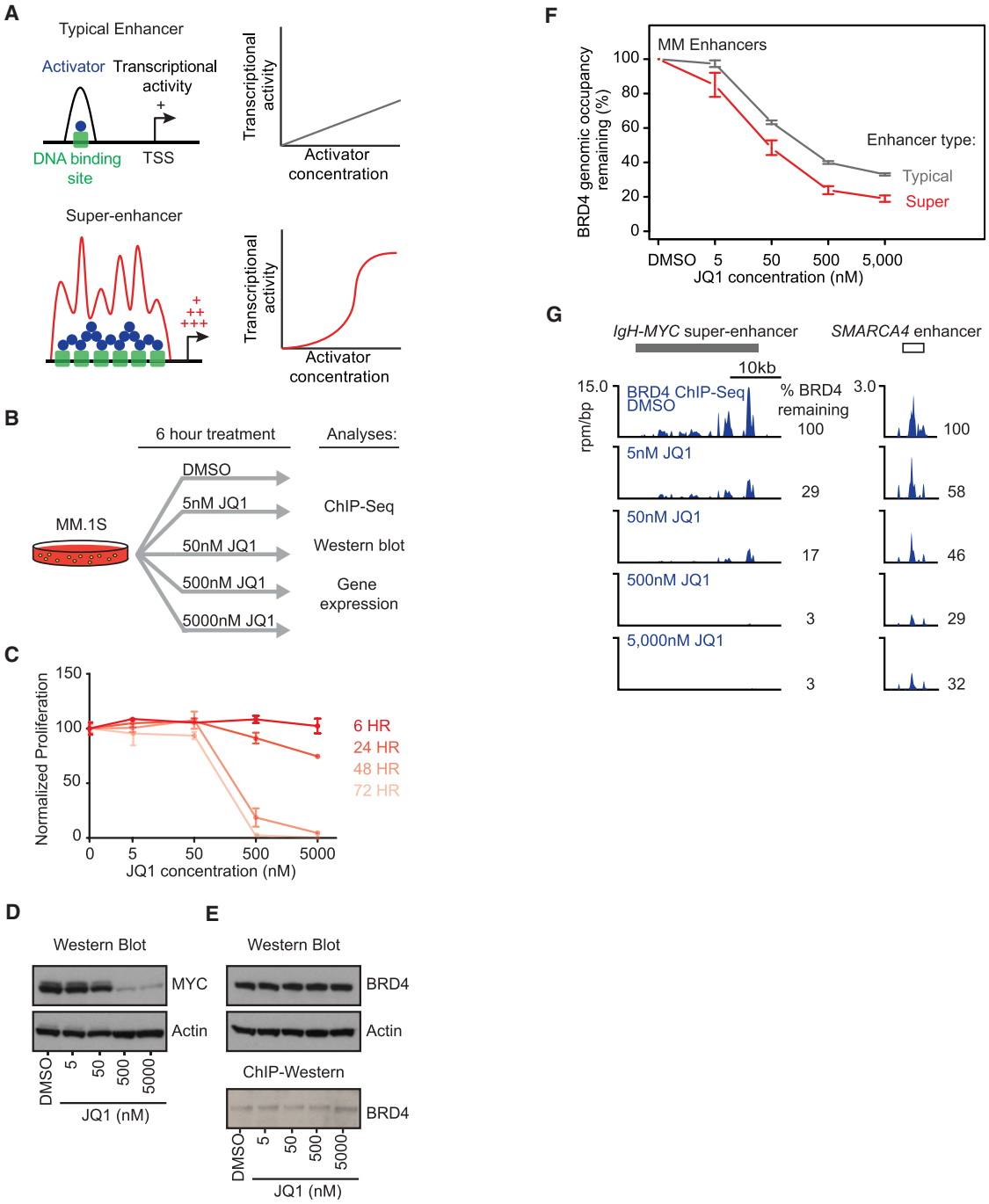

Figure 5. BRD4 Occupancy at Super-Enhancers Is Highly Sensitive to Bromodomain Inhibition

(A) Schematic example of how cooperative interactions of enhancer-associated factors at super-enhancers lead to both higher transcriptional output and increased sensitivity to factor concentration.

(B) Measuring the effects of various concentrations of JQ1 genome wide on BRD4 occupancy. Schematic depicting the experimental procedure.

(C) Short-term JQ1 treatment (6 hr) has little effect on MM1.S cell viability. JQ1 sensitivity of MM1.S cells by measurement of ATP levels (CellTiterGlo) after 6, 24, 48, and 72 hr of treatment with JQ1 (5, 50, 500, or 5,000 nM) or vehicle (DMSO, 0.05%). Error bars represent the SD of triplicate experiments.

(D) Western blot of relative MYC levels after 6 hr of JQ1 or DMSO treatment.

(E) Western blot of relative BRD4 levels after 6 hr of JQ1 or DMSO treatment. ChIP-western blot of the relative levels of immunoprecipitated BRD4 after 6 hr of JQ1 or DMSO treatment.

(F) Line graph showing the percentage of BRD4 occupancy remaining after 6 hr treatment at various JQ1 concentrations for typical enhancers (gray line) or super-enhancers (red line). The y axis shows the fraction of BRD4 occupancy remaining versus DMSO. The x axis shows different JQ1 concentrations (DMSO [none], 5 nM, 50 nM, and 500 nM). Error bars represent 95% confidence intervals of the mean (95% CI).

(legend continued on next page)

after treatment with 500 nM JQ1, whereas loss of BRD4 occupancy at the typical enhancer for *SMARCA4* was less pronounced (71% reduction versus DMSO control) (Figure 5G).

We next investigated whether genes associated with super-enhancers might experience a greater reduction of transcription than genes with average enhancers when BRD4 is inhibited. As expected, treatment of MM1.S cells with 500 nM JQ1 led to progressive reduction in global messenger RNA (mRNA) levels over time (Figures 6A and S3A). Similarly, treatment with increasing concentrations of JQ1 caused progressive reductions in global mRNA levels (Figures 6A and S3B). There was a selective depletion of mRNAs from super-enhancer-associated genes that occurred in both temporal (Figure 6B) and concentration-dependent manners (Figure 6C). Notably, *MYC* and *IRF4* mRNA levels were more rapidly depleted than other mRNAs that are expressed at similar levels (Figure 6D). The levels of transcripts from super-enhancer-associated genes were somewhat more affected than those from genes that have multiple typical enhancers bound by BRD4 (Figures S3C and S3D). Thus, BET bromodomain inhibition preferentially impacts transcription of super-enhancer-driven genes.

To further test the model that super-enhancers are responsible for the special sensitivity to BRD4 inhibition, we transfected MM1.S cells with luciferase reporter constructs containing super-enhancer and typical enhancer fragments and examined the effects of various JQ1 concentrations on luciferase activity. Upon treatment with JQ1, MM1.S cells transfected with a super-enhancer reporter experienced a greater reduction in luciferase activity than those transfected with a typical enhancer reporter (Figure 6E). Interestingly, the dose-response curve observed for luciferase activity of the super-enhancer construct is consistent with that expected for enhancers that are bound cooperatively by multiple factors (Figure 5A) (Giniger and Ptashne, 1988; Griggs and Johnston, 1991). These results are also consistent with the model that super-enhancers are responsible for the special sensitivity of gene transcription to BRD4 inhibition.

BRD4 Inhibition and Transcription Elongation

At active genes, enhancers and core promoters are brought into close proximity, so factors associated with enhancers can act on the transcription apparatus in the vicinity of TSSs and thereby influence initiation or elongation. BRD4 is known to interact with Mediator and P-TEFb and to be involved in the control of transcriptional elongation by RNA Pol II (Conaway and Conaway, 2011; Dawson et al., 2011; Jang et al., 2005; Krueger et al., 2010; Rahman et al., 2011; Yang et al., 2005). This suggests that the preferential loss of BRD4 from super-enhancers might affect the levels of Mediator and P-TEFb at these sites and, furthermore, that the reduced levels of mRNAs from super-enhancer-associated genes might be due to an effect on transcription elongation.

To test these predictions, we carried out ChIP-seq for the Mediator component MED1 and the catalytic subunit of the P-TEFb complex CDK9 in MM1.S cells treated with DMSO or 500 nM JQ1 for 6 hr. In control cells, MED1 and CDK9 were found at enhancers and promoters of active genes throughout the MM genome, as expected (Figures 1A, 1B, and S3E). In cells treated with JQ1, reduced levels of MED1 and CDK9 were observed primarily at enhancers, with the greatest loss at super-enhancers (Figure 6F). As many super-enhancers span contiguous regions that encompass or overlap the TSS, we analyzed MED1 and CDK9 loss in either TSS proximal or TSS distal regions of super-enhancers and again observed loss of MED1 and CDK9 predominantly at TSS distal regions (Figure S3F). We conclude that inhibition of BRD4 genomic binding leads to a marked reduction in the levels of Mediator and P-TEFb at genomic regions distal to TSSs, with the greatest reduction occurring at super-enhancers.

To determine whether reduced levels of BRD4 lead to changes in transcription elongation, we quantified changes in transcription elongation by performing ChIP-seq of RNA Pol II before and after treatment of MM1.S cells with 500 nM JQ1. We then calculated the fold loss of RNA Pol II occupancy in the gene body regions for all transcriptionally active genes and found that more than half of these genes show a decrease in elongating RNA Pol II density after JQ1 treatment (Figure 6G). Importantly, genes associated with super-enhancers showed a greater decrease of RNA Pol II in their elongating gene body regions compared to genes associated with typical enhancers (Figures 6H and S3G). Inspection of individual gene tracks revealed pronounced elongation defects at super-enhancer-associated genes such as *MYC* and *IRF4*, with the greatest effects observed with *MYC* (Figures 6I and 6J). Thus, the selective effects of JQ1 on the transcription of *MYC* and other super-enhancer-associated genes can be explained, at least in part, by the sensitivity of super-enhancers to reduced levels of BRD4, which leads to a pronounced effect on pause release and transcription elongation.

Super-Enhancers Are Associated with Disease-Critical Genes in Other Cancers

To map enhancers and to determine whether super-enhancers occur in additional tumor types, we investigated the genome-wide occupancy of Mediator (MED1), BRD4, and the enhancer-associated histone modification H3K27Ac using ChIP-seq in glioblastoma multiforme (GBM) and small-cell lung cancer (SCLC) (Figure 7). Mediator (MED1) occupancy was used to identify enhancer elements because enhancer-bound transcription factors bind directly to Mediator (Borggrefe and Yue, 2011; Conaway and Conaway, 2011; Kornberg, 2005; Malik and Roeder, 2010; Taatjes, 2010) and because it has proven to produce high-quality evidence for enhancers in mammalian cells (Kagey et al., 2010). Global occupancy of BRD4 and H3K27Ac was used as corroborative evidence to identify enhancer elements (Figure S4 and Table S4). Analysis of the regions occupied by Mediator revealed that, as in

(G) Gene tracks of BRD4 ChIP-seq occupancy after various concentrations of JQ1 treatment at the *IgH-MYC*-associated super-enhancer (left) and the *SMARCA4*-associated typical enhancer (right). The x axis shows genomic position, and gray boxes depict super-enhancer regions. The y axis shows signal of ChIP-seq occupancy in units of rpm/bp. The percent of BRD4 remaining after each concentration of JQ1 treatment is annotated to the right of the gene tracks.

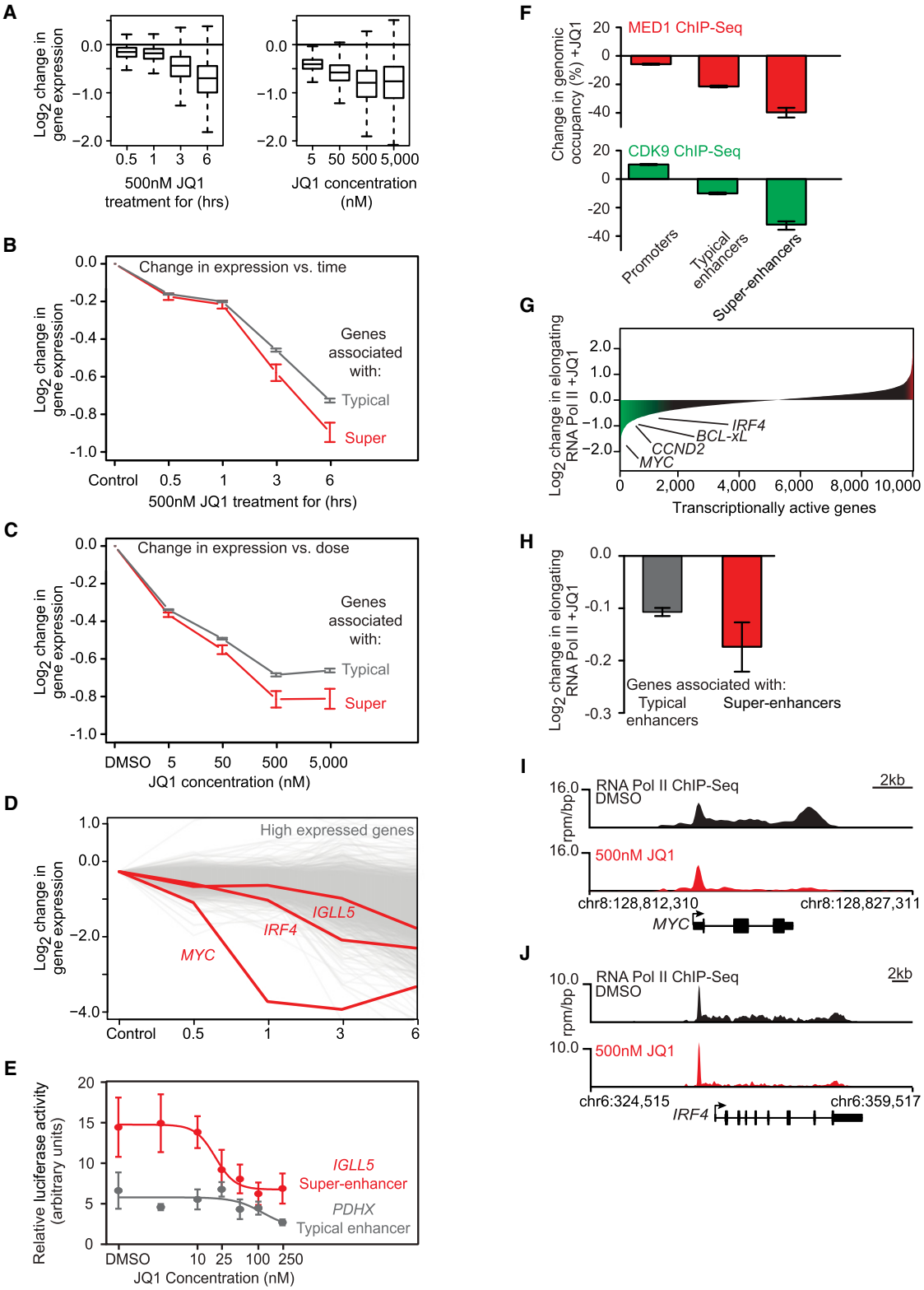

Figure 6. JQ1 Causes Disproportionate Loss of Transcription at Super-Enhancer Genes

(A) Box plots showing the Log_2 change in gene expression for all actively transcribed genes in JQ1-treated versus control cells for a time course of cells treated with 500 nM JQ1 (left) or for a concentration course of cells treated for 6 hr with varying amounts of JQ1 (right). The y axis shows the Log_2 change in gene expression versus untreated control cells (left graph) or control cells treated with DMSO for 6 hr (right graph).

(legend continued on next page)

MM1.S cells, large genomic domains were occupied by this co-activator in both GBM and SCLC (Figures 7A, 7B, 7D, and 7E). The median super-enhancer was 30 kb in GBM cells and 11 kb in SCLC cells (Figures 7B and 7E). As in MM1.S cells, these GBM and SCLC super-enhancers were an order or magnitude larger and showed a commensurate increase in MED1, BRD4, and H3K27Ac levels when compared to normal enhancers (Figures 7B and 7E).

The super-enhancers in GBM and SCLC were found to be associated with many well-known tumor-associated genes (Figures 7C and 7F and Table S5). In GBM, super-enhancers were associated with genes encoding three transcription factors (*RUNX1*, *FOSL2*, and *BHLHE40*) critical for mesenchymal transformation of brain tumors (Carro et al., 2010); the super-enhancers associated with *BHLHE40* are shown in Figure 7C. *BCL3*, which associates with NF-κB and is deregulated in many blood and solid tumor types, is associated with a super-enhancer in GBM (Figure 7C) (Maldonado and Melendez-Zajgla, 2011). In SCLC, a super-enhancer is associated with the *INSM1* gene, which encodes a transcription factor involved in neuronal development that is highly expressed in neuroendocrine tissue and tumors such as SCLC (Figure 7F) (Pedersen et al., 2003). A super-enhancer is also associated with the *ID2* gene, which is highly expressed in SCLCs and encodes a protein that interacts with the well-known retinoblastoma tumor suppressor (Figure 7F) (Pedersen et al., 2003; Perk et al., 2005). These results indicate that super-enhancers are likely to associate with critical tumor oncogenes in diverse tumor types.

DISCUSSION

Chromatin regulators have become attractive targets for cancer therapy, but many of these regulators are expressed in a broad range of healthy cells and contribute generally to gene expression. Thus, it is unclear how inhibition of a global chromatin regulator such as BRD4 might produce selective effects, such as at the *MYC* oncogene (Delmore et al., 2011). We have found that key regulators of tumor cell state in MM1.S cells are associated with large enhancer domains, characterized by disproportionately high levels of BRD4 and Mediator. These super-enhancers are more sensitive to perturbation than typical enhancers, and the expression of the genes associated with super-enhancers is preferentially affected. Thus, the preferential loss of BRD4 at super-enhancers associated with the *MYC* oncogene and other key tumor-associated genes can explain the gene-selective effects of JQ1 treatment in these cells.

BRD4 is an excellent example of a chromatin regulator that is expressed in a broad range of healthy cells and contributes generally to gene expression. Most cell types for which RNA-seq data are available express the *BRD4* gene. ChIP-seq data revealed that BRD4 generally occupies the enhancer and promoter elements of active genes with the Mediator coactivator in MM1.S cells (Figure 1). These results eliminate the model that BRD4 is exclusively associated with a small set of genes that are thereby rendered inactive by the BRD4 inhibitor JQ1 and instead suggest that the gene-specific effects of the small molecule have other causes.

We have found that ~3% of the enhancers in MM1.S cells are exceptionally large and are occupied by remarkably high amounts of BRD4 and Mediator. These super-enhancers are generally an order of magnitude larger and contain an order of magnitude more BRD4, Mediator, and histone marks associated with enhancers (H3K27Ac) than typical enhancers. Our results suggest that super-enhancers are collections of closely spaced enhancers that can collectively facilitate high levels of transcription from adjacent genes. Importantly, the super-enhancers are associated with the *MYC* oncogene and additional genes such as *IGLL5*, *IRF4*, *PRDM1/BLIMP-1*, and *XBP1* that feature prominently in MM biology.

Cooperative and synergistic binding of multiple transcription factors and coactivators occurs at enhancers. Enhancers bound by many cooperatively interacting factors can lose activity more rapidly than enhancers bound by fewer factors when the levels of enhancer-bound factors are reduced (Giniger and Ptashne, 1988; Griggs and Johnston, 1991). The presence of super-enhancers at *MYC* and other key genes associated with MM led us to test the hypothesis that super-enhancers are more sensitive to reduced levels of BRD4 than average enhancers. We

(B and C) Line graph showing the Log2 change in gene expression versus control cells after JQ1 treatment in a time- (B) or dose (C)-dependent manner for genes associated with typical enhancers (gray line) or genes associated with super-enhancers (red line). The y axis shows the Log2 change in gene expression of JQ1 treated versus untreated control cells. The x axis shows time of 500 nM JQ1 treatment (B) or JQ1 treatment concentration at 6 hr (C). Error bars represent 95% confidence intervals of the mean (95% CI).

(D) Graph showing the Log_2 change in gene expression after JQ1 treatment over time for genes ranked in the top 10% of expression in MM1.S cells. Each line represents a single gene, with the *MYC* and *IRF4* genes drawn in red. The y axis shows the Log_2 change in gene expression of JQ1-treated versus untreated control cells. The x axis shows time of 500 nM JQ1 treatment.

(E) Line graph showing luciferase activity after JQ1 treatment at various concentrations for luciferase reporter constructs containing either a fragment from the *IGLL5* super-enhancer (red line) or the *PDHX* typical enhancer (gray line). The y axis represents relative luciferase activity in arbitrary units. The x axis shows JQ1 concentrations. Error bars are SEM.

(F) Bar graphs showing the percentage loss of either MED1 (top, red) or CDK9 (bottom, green) at promoters, typical enhancers, and super-enhancers. Error bars represent 95% CI.

(G) Graph of loss of RNA Pol II density in the elongating gene body region for all transcriptionally active genes in MM1.S cells after 6 hr of 500 nM JQ1 treatment. Genes are ordered by decrease in elongating RNA Pol II in units of Log_2 fold loss. Genes with a greater than 0.5 Log_2 fold change in elongating RNA Pol II are shaded in green (loss) or red (gain). The amount of RNA Pol II loss is indicated for select genes.

(H) Bar graph showing the Log_2 fold change in RNA Pol II density in elongating gene body regions after 6 hr of 500 nM JQ1 treatment for genes with typical enhancers (left, gray) or genes with super-enhancers (red, right). Error bars represent 95% confidence intervals of the mean (95% CI).

(I and J) Gene tracks of RNA Pol II ChIP-seq occupancy after DMSO (black) or 500 nM JQ1 treatment (red) at the super-enhancer proximal *MYC* gene (I) and *IRF4* gene (J). The y axis shows signal of ChIP-seq occupancy in units of rpm/bp.

See also Figure S3.

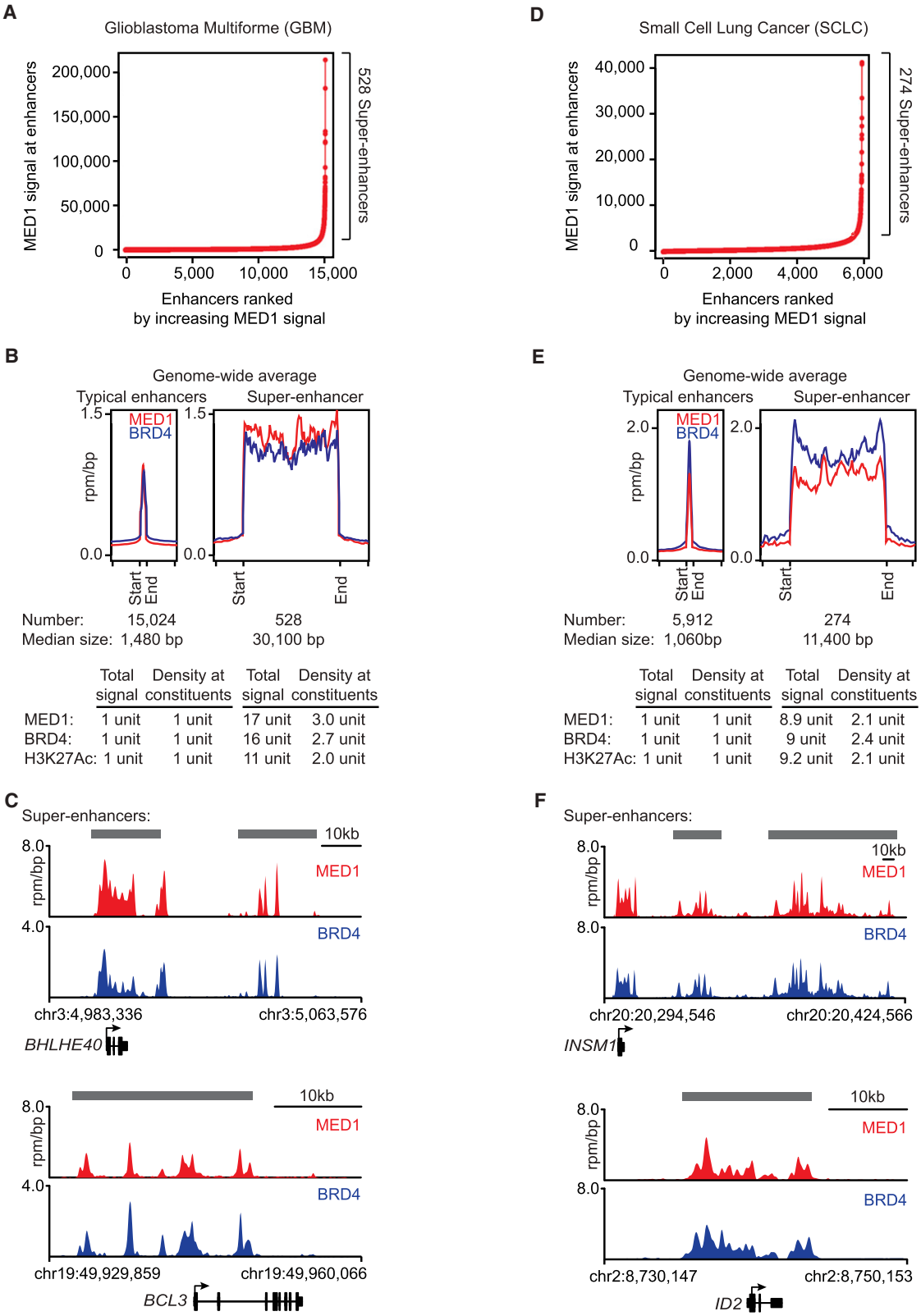

(legend on next page)

found that treatment of these tumor cells with the BET-bromodomain inhibitor JQ1 leads to preferential loss of BRD4 at super-enhancers. In addition, this decrease in BRD4 occupancy is accompanied by a corresponding loss of MED1 and CDK9 at super-enhancers. Consequent transcription elongation defects and mRNA decreases preferentially impact super-enhancer-associated genes, with an especially profound effect at the *MYC* oncogene.

Super-enhancers are not restricted to MM cells. We have identified super-enhancers in two additional tumor types, small-cell lung cancer and glioblastoma multiforme. Super-enhancers identified in these cell types have characteristics similar to those found in MM1.S; they span large genomic regions and contain exceptional amounts of Mediator and BRD4. These super-enhancers are also associated with important tumor genes in both cell types. In GBM cells, *BHLHE40* and *BCL3* are known to be important in tumor biology and are each associated with super-enhancers in this cell type. In H2171 SCLC cells, super-enhancers are associated with *INSM1* and *ID2*, which are frequently overexpressed in SCLC. In fact, super-enhancers are not restricted to tumor cells and have been identified in several additional cell types in which they similarly associate with key cell identity genes (Whyte et al., 2013 [this issue of *Cell*]).

Our results demonstrate that super-enhancers occupied by BRD4 regulate critical oncogenic drivers in MM and show that BRD4 inhibition leads to preferential disruption of these super-enhancers. This insight into the mechanism by which BRD4 inhibition causes selective loss of oncogene expression in this highly malignant blood cancer may have implications for future drug development in oncology. Tumor cells frequently become addicted to oncogenes, thus becoming unusually reliant on high-level expression of these genes (Cheung et al., 2011; Chin et al., 1999; Felsher and Bishop, 1999; Garraway and Sellers, 2006; Garraway et al., 2005; Jain et al., 2002; Weinstein, 2002). Thus, preferential disruption of super-enhancer function may be a general approach to selectively inhibiting the oncogenic drivers of many tumor cells.

EXPERIMENTAL PROCEDURES

Cell Culture

MM1.S MM cells (CRL-2974 ATCC) and U-87 MG glioblastoma cells (HTB-14 ATCC) were purchased from ATCC. H2171 small-cell lung carcinoma cells (CRL-5929 ATCC) were kindly provided by John Minna, UT Southwestern. MM1.S and H2171 cells were propagated in RPMI-1640 supplemented with 10% fetal bovine serum and 1% GlutaMAX (Invitrogen, 35050-061). U-87 MG cells were cultured in Eagle's minimum essential medium (EMEM) modified to contain Earle's Balanced Salt Solution, nonessential amino acids, 2 mM L-glutamine, 1 mM sodium pyruvate, and 1,500 mg/l sodium bicarbonate. Cells were grown at 37°C and 5% CO_2.

For JQ1 treatment experiments, cells were resuspended in fresh media containing JQ1 (5 nM, 50 nM, 500 nM, and 5,000 nM) or vehicle (DMSO, 0.05%) and treated for a duration of 6 hr, unless otherwise indicated.

ChIP-Seq

ChIP was carried out as described in Lin et al. (2012). Additional details are provided in Extended Experimental Procedures. Antibodies used are as follows: total RNA Pol II (Rpb1 N terminus), Santa Cruz sc-899 lot K0111; MED1, Bethyl Labs A300-793A lot A300-793A-2; BRD4, Bethyl Labs A301-985A lot A301-985A-1; CDK9, Santa Cruz Biotechnology sc-484, lot D1612. ChIP-seq data sets of H3K4Me3 and H3K27Ac in MM1.S and MED1 and H3K27Ac in U-87 MG and H2171 were previously published (Lin et al., 2012).

Luciferase Reporter Assays

A minimal Myc promoter was amplified from human genomic DNA and cloned into the SacI and HindIII sites of the pGL3 basic vector (Promega). Enhancer fragments were likewise amplified from human genomic DNA and cloned into the BamHI and SalI sites of the pGL3-pMyc vector. All cloning primers are listed in Table S6. Constructs were transfected into MM1.S cells using Lipofectamine 2000 (Invitrogen). The pRL-SV40 plasmid (Promega) was co-transfected as a normalization control. Cells were incubated for 24 hr, and luciferase activity was measured using the Dual-Luciferase Reporter Assay System (Promega). For the JQ1 concentration course, cells were resuspended in fresh media containing various concentrations of JQ1 24 hr after transfection and were incubated for an additional 6 hr before harvesting. Luminescence measurements were made using the Dual-Luciferase Reporter Assay System (Promega) on a Wallac EnVision (Perkin Elmer) plate reader.

Cell Viability Assays

Cell viability was measured using the CellTiterGlo assay kit (Promega, G7571). MM1.S cells were resuspended in fresh media containing JQ1 (5 nM, 50 nM, 500 nM, and 1,000 nM) or vehicle (DMSO, 0.05%) and then plated in 96-well plates at 10,000 cells/well in a volume of 100 μl. Viability was measured after 6, 24, 48, and 72 hr incubations by addition of CellTiter Glo reagent and luminescence measurement on a Tecan Safire^2 plate reader.

Western Blotting

Western blots were carried out using standard protocols. Antibodies used are as follows: c-Myc (Epitomics, category: 1472-1), BRD4 (Epitomics, category: 5716-1) or β-actin (Sigma, clone AC-15, A5441).

Data Analysis

All ChIP-seq data sets were aligned using Bowtie (version 0.12.9) (Langmead et al., 2009) to build version NCBI36/HG18 of the human genome. Individual data set GEO accession IDs and background data sets used can be found in Table S7.

ChIP-seq read densities in genomic regions were calculated as in Lin et al. (2012). We used the MACS version 1.4.2 (model-based analysis of ChIP-seq) (Zhang et al., 2008) peak finding algorithm to identify regions of ChIP-seq enrichment over background. A p value threshold of enrichment of 1×10^{-9} was used for all data sets.

Active enhancers were defined as regions of ChIP-seq enrichment for the mediator complex component MED1 outside of promoters (e.g., a region not contained within ±2.5 kb region flanking the promoter). In order to accurately capture dense clusters of enhancers, we allowed MED1 regions within 12.5 kb of one another to be stitched together. To identify super-enhancers, we first

Figure 7. Super-Enhancers Are Associated with Key Genes in Other Cancers

(A and D) Total MED1 ChIP-seq signal in units of reads per million in enhancer regions for all enhancers in (A) the GBM cell line U-87 MG or (D) the SCLC cell line H2171. Enhancers are ranked by increasing MED1 ChIP-seq signal.

(B and E) Metagene representation of global MED1 and BRD4 occupancy at (B) typical GMB enhancers and super-enhancers or (E) typical SCLC enhancers and super-enhancers. The x axis shows the start and end of the enhancer (left) or super-enhancer (right) regions flanked by ±5 kb of adjacent sequence. Enhancer and super-enhancer regions on the x axis are relatively scaled. The y axis shows the average signal in units of rpm/bp.

(C and F) Gene tracks of MED1 and BRD4 ChIP-seq occupancy at (C) super-enhancers near *BHLHE40* and *BCL3*, genes with important roles in GBM, or at (F) super-enhancers near *INSM1* and *ID2*, genes with important roles in SCLC. Super-enhancers are depicted in gray boxes over the gene tracks.

See also Figure S4.

ranked all enhancers by increasing total background subtracted ChIP-seq-occupancy of MED1 (x axis) and plotted the total background subtracted ChIP-seq occupancy of MED1 in units of total rpm (y axis). This representation revealed a clear inflection point in the distribution of MED1 at enhancers. We geometrically defined the inflection point and used it to establish the cutoff for super-enhancers (see Extended Experimental Procedures).

ACCESSION NUMBERS

The GEO accession number for the ChIP-seq and gene expression data reported in this paper is GSE44931 (http://www.ncbi.nlm.nih.gov/geo/).

SUPPLEMENTAL INFORMATION

Supplemental Information includes Extended Experimental Procedures, four figures, one data file, and seven tables and can be found with this article online at http://dx.doi.org/10.1016/j.cell.2013.03.036.

ACKNOWLEDGMENTS

We thank Zi Peng Fan for bioinformatics support; Michael R. McKeown for help with cell viability assays; Jun Qi for providing JQ1; Tom Volkert, Jennifer Love, Sumeet Gupta, and Jeong-Ah Kwon at the Whitehead Genome Technologies Core for Solexa sequencing; and members of the Young, Bradner, and Vakoc labs for helpful discussion. This work was supported by a Swedish Research Council Postdoctoral Fellowship VR-B0086301 (J.L.), the Damon-Runyon Cancer Research Foundation (J.E.B.), a Burroughs-Welcome CAMS award and NCI Cancer Center Support Grant Development Fund CA45508 (C.R.V.), and National Institutes of Health grants HG002668 (R.A.Y.) and CA146445 (R.A.Y., T.I.L.). R.A.Y. and J.E.B. are founders, J.L. and D.A.O. have become employees, and C.R.V. is a scientific advisor of Syros Pharmaceuticals.

Received: November 16, 2012
Revised: February 25, 2013
Accepted: March 25, 2013
Published: April 11, 2013

REFERENCES

Baylin, S.B., and Jones, P.A. (2011). A decade of exploring the cancer epigenome - biological and translational implications. Nat. Rev. Cancer *11*, 726–734.

Bergsagel, P.L., Kuehl, W.M., Zhan, F., Sawyer, J., Barlogie, B., and Shaughnessy, J., Jr. (2005). Cyclin D dysregulation: an early and unifying pathogenic event in multiple myeloma. Blood *106*, 296–303.

Beroukhim, R., Mermel, C.H., Porter, D., Wei, G., Raychaudhuri, S., Donovan, J., Barretina, J., Boehm, J.S., Dobson, J., Urashima, M., et al. (2010). The landscape of somatic copy-number alteration across human cancers. Nature *463*, 899–905.

Borggrefe, T., and Yue, X. (2011). Interactions between subunits of the Mediator complex with gene-specific transcription factors. Semin. Cell Dev. Biol. *22*, 759–768.

Carey, M. (1998). The enhanceosome and transcriptional synergy. Cell *92*, 5–8.

Carey, M., Leatherwood, J., and Ptashne, M. (1990). A potent GAL4 derivative activates transcription at a distance in vitro. Science *247*, 710–712.

Carrasco, D.R., Sukhdeo, K., Protopopova, M., Sinha, R., Enos, M., Carrasco, D.E., Zheng, M., Mani, M., Henderson, J., Pinkus, G.S., et al. (2007). The differentiation and stress response factor XBP-1 drives multiple myeloma pathogenesis. Cancer Cell *11*, 349–360.

Carro, M.S., Lim, W.K., Alvarez, M.J., Bollo, R.J., Zhao, X., Snyder, E.Y., Sulman, E.P., Anne, S.L., Doetsch, F., Colman, H., et al. (2010). The transcriptional network for mesenchymal transformation of brain tumours. Nature *463*, 318–325.

Chepelev, I., Wei, G., Wangsa, D., Tang, Q., and Zhao, K. (2012). Characterization of genome-wide enhancer-promoter interactions reveals co-expression of interacting genes and modes of higher order chromatin organization. Cell Res. *22*, 490–503.

Cheung, H.W., Cowley, G.S., Weir, B.A., Boehm, J.S., Rusin, S., Scott, J.A., East, A., Ali, L.D., Lizotte, P.H., Wong, T.C., et al. (2011). Systematic investigation of genetic vulnerabilities across cancer cell lines reveals lineage-specific dependencies in ovarian cancer. Proc. Natl. Acad. Sci. USA *108*, 12372–12377.

Chin, L., Tam, A., Pomerantz, J., Wong, M., Holash, J., Bardeesy, N., Shen, Q., O'Hagan, R., Pantginis, J., Zhou, H., et al. (1999). Essential role for oncogenic Ras in tumour maintenance. Nature *400*, 468–472.

Chng, W.J., Huang, G.F., Chung, T.H., Ng, S.B., Gonzalez-Paz, N., Troska-Price, T., Mulligan, G., Chesi, M., Bergsagel, P.L., and Fonseca, R. (2011). Clinical and biological implications of MYC activation: a common difference between MGUS and newly diagnosed multiple myeloma. Leukemia *25*, 1026–1035.

Claudio, J.O., Masih-Khan, E., Tang, H., Gonçalves, J., Voralia, M., Li, Z.H., Nadeem, V., Cukerman, E., Francisco-Pabalan, O., Liew, C.C., et al. (2002). A molecular compendium of genes expressed in multiple myeloma. Blood *100*, 2175–2186.

Cole, P.A. (2008). Chemical probes for histone-modifying enzymes. Nat. Chem. Biol. *4*, 590–597.

Conaway, R.C., and Conaway, J.W. (2011). Function and regulation of the Mediator complex. Curr. Opin. Genet. Dev. *21*, 225–230.

Creyghton, M.P., Cheng, A.W., Welstead, G.G., Kooistra, T., Carey, B.W., Steine, E.J., Hanna, J., Lodato, M.A., Frampton, G.M., Sharp, P.A., et al. (2010). Histone H3K27ac separates active from poised enhancers and predicts developmental state. Proc. Natl. Acad. Sci. USA *107*, 21931–21936.

Dawson, M.A., and Kouzarides, T. (2012). Cancer epigenetics: from mechanism to therapy. Cell *150*, 12–27.

Dawson, M.A., Prinjha, R.K., Dittmann, A., Giotopoulos, G., Bantscheff, M., Chan, W.I., Robson, S.C., Chung, C.W., Hopf, C., Savitski, M.M., et al. (2011). Inhibition of BET recruitment to chromatin as an effective treatment for MLL-fusion leukaemia. Nature *478*, 529–533.

Delmore, J.E., Issa, G.C., Lemieux, M.E., Rahl, P.B., Shi, J., Jacobs, H.M., Kastritis, E., Gilpatrick, T., Paranal, R.M., Qi, J., et al. (2011). BET bromodomain inhibition as a therapeutic strategy to target c-Myc. Cell *146*, 904–917.

Dey, A., Chitsaz, F., Abbasi, A., Misteli, T., and Ozato, K. (2003). The double bromodomain protein Brd4 binds to acetylated chromatin during interphase and mitosis. Proc. Natl. Acad. Sci. USA *100*, 8758–8763.

Dib, A., Gabrea, A., Glebov, O.K., Bergsagel, P.L., and Kuehl, W.M. (2008). Characterization of MYC translocations in multiple myeloma cell lines. J. Natl. Cancer Inst. Monogr. *39*, 25–31.

Dixon, J.R., Selvaraj, S., Yue, F., Kim, A., Li, Y., Shen, Y., Hu, M., Liu, J.S., and Ren, B. (2012). Topological domains in mammalian genomes identified by analysis of chromatin interactions. Nature *485*, 376–380.

Elsässer, S.J., Allis, C.D., and Lewis, P.W. (2011). Cancer. New epigenetic drivers of cancers. Science *331*, 1145–1146.

Esteller, M. (2008). Epigenetics in cancer. N. Engl. J. Med. *358*, 1148–1159.

Feinberg, A.P., and Tycko, B. (2004). The history of cancer epigenetics. Nat. Rev. Cancer *4*, 143–153.

Felsher, D.W., and Bishop, J.M. (1999). Reversible tumorigenesis by MYC in hematopoietic lineages. Mol. Cell *4*, 199–207.

Filippakopoulos, P., Qi, J., Picaud, S., Shen, Y., Smith, W.B., Fedorov, O., Morse, E.M., Keates, T., Hickman, T.T., Felletar, I., et al. (2010). Selective inhibition of BET bromodomains. Nature *468*, 1067–1073.

Garraway, L.A., and Sellers, W.R. (2006). Lineage dependency and lineage-survival oncogenes in human cancer. Nat. Rev. Cancer *6*, 593–602.

Garraway, L.A., Widlund, H.R., Rubin, M.A., Getz, G., Berger, A.J., Ramaswamy, S., Beroukhim, R., Milner, D.A., Granter, S.R., Du, J., et al. (2005).

Integrative genomic analyses identify MITF as a lineage survival oncogene amplified in malignant melanoma. Nature *436*, 117–122.

Geutjes, E.J., Bajpe, P.K., and Bernards, R. (2012). Targeting the epigenome for treatment of cancer. Oncogene *31*, 3827–3844.

Giese, K., Kingsley, C., Kirshner, J.R., and Grosschedl, R. (1995). Assembly and function of a TCR alpha enhancer complex is dependent on LEF-1-induced DNA bending and multiple protein-protein interactions. Genes Dev. *9*, 995–1008.

Giniger, E., and Ptashne, M. (1988). Cooperative DNA binding of the yeast transcriptional activator GAL4. Proc. Natl. Acad. Sci. USA *85*, 382–386.

Göndör, A., and Ohlsson, R. (2009). Chromosome crosstalk in three dimensions. Nature *461*, 212–217.

Griggs, D.W., and Johnston, M. (1991). Regulated expression of the GAL4 activator gene in yeast provides a sensitive genetic switch for glucose repression. Proc. Natl. Acad. Sci. USA *88*, 8597–8601.

Heintzman, N.D., Hon, G.C., Hawkins, R.D., Kheradpour, P., Stark, A., Harp, L.F., Ye, Z., Lee, L.K., Stuart, R.K., Ching, C.W., et al. (2009). Histone modifications at human enhancers reflect global cell-type-specific gene expression. Nature *459*, 108–112.

Holien, T., Våtsveen, T.K., Hella, H., Waage, A., and Sundan, A. (2012). Addiction to c-MYC in multiple myeloma. Blood *120*, 2450–2453.

Issa, J.P., and Kantarjian, H.M. (2009). Targeting DNA methylation. Clin. Cancer Res. *15*, 3938–3946.

Jain, M., Arvanitis, C., Chu, K., Dewey, W., Leonhardt, E., Trinh, M., Sundberg, C.D., Bishop, J.M., and Felsher, D.W. (2002). Sustained loss of a neoplastic phenotype by brief inactivation of MYC. Science *297*, 102–104.

Jang, M.K., Mochizuki, K., Zhou, M., Jeong, H.S., Brady, J.N., and Ozato, K. (2005). The bromodomain protein Brd4 is a positive regulatory component of P-TEFb and stimulates RNA polymerase II-dependent transcription. Mol. Cell *19*, 523–534.

Jiang, Y.W., Veschambre, P., Erdjument-Bromage, H., Tempst, P., Conaway, J.W., Conaway, R.C., and Kornberg, R.D. (1998). Mammalian mediator of transcriptional regulation and its possible role as an end-point of signal transduction pathways. Proc. Natl. Acad. Sci. USA *95*, 8538–8543.

Kagey, M.H., Newman, J.J., Bilodeau, S., Zhan, Y., Orlando, D.A., van Berkum, N.L., Ebmeier, C.C., Goossens, J., Rahl, P.B., Levine, S.S., et al. (2010). Mediator and cohesin connect gene expression and chromatin architecture. Nature *467*, 430–435.

Kim, T.K., and Maniatis, T. (1997). The mechanism of transcriptional synergy of an in vitro assembled interferon-beta enhanceosome. Mol. Cell *1*, 119–129.

Kornberg, R.D. (2005). Mediator and the mechanism of transcriptional activation. Trends Biochem. Sci. *30*, 235–239.

Krueger, B.J., Varzavand, K., Cooper, J.J., and Price, D.H. (2010). The mechanism of release of P-TEFb and HEXIM1 from the 7SK snRNP by viral and cellular activators includes a conformational change in 7SK. PLoS ONE *5*, e12335.

Langmead, B., Trapnell, C., Pop, M., and Salzberg, S.L. (2009). Ultrafast and memory-efficient alignment of short DNA sequences to the human genome. Genome Biol. *10*, R25.

Lelli, K.M., Slattery, M., and Mann, R.S. (2012). Disentangling the many layers of eukaryotic transcriptional regulation. Annu. Rev. Genet. *46*, 43–68.

LeRoy, G., Rickards, B., and Flint, S.J. (2008). The double bromodomain proteins Brd2 and Brd3 couple histone acetylation to transcription. Mol. Cell *30*, 51–60.

Lin, C.Y., Lovén, J., Rahl, P.B., Paranal, R.M., Burge, C.B., Bradner, J.E., Lee, T.I., and Young, R.A. (2012). Transcriptional amplification in tumor cells with elevated c-Myc. Cell *151*, 56–67.

Maldonado, V., and Melendez-Zajgla, J. (2011). Role of Bcl-3 in solid tumors. Mol. Cancer *10*, 152.

Malik, S., and Roeder, R.G. (2010). The metazoan Mediator co-activator complex as an integrative hub for transcriptional regulation. Nat. Rev. Genet. *11*, 761–772.

Marks, P.A., and Xu, W.S. (2009). Histone deacetylase inhibitors: Potential in cancer therapy. J. Cell. Biochem. *107*, 600–608.

Mertz, J.A., Conery, A.R., Bryant, B.M., Sandy, P., Balasubramanian, S., Mele, D.A., Bergeron, L., and Sims, R.J., 3rd. (2011). Targeting MYC dependence in cancer by inhibiting BET bromodomains. Proc. Natl. Acad. Sci. USA *108*, 16669–16674.

Musgrove, E.A., Caldon, C.E., Barraclough, J., Stone, A., and Sutherland, R.L. (2011). Cyclin D as a therapeutic target in cancer. Nat. Rev. Cancer *11*, 558–572.

Nicodeme, E., Jeffrey, K.L., Schaefer, U., Beinke, S., Dewell, S., Chung, C.W., Chandwani, R., Marazzi, I., Wilson, P., Coste, H., et al. (2010). Suppression of inflammation by a synthetic histone mimic. Nature *468*, 1119–1123.

Ong, C.T., and Corces, V.G. (2011). Enhancer function: new insights into the regulation of tissue-specific gene expression. Nat. Rev. Genet. *12*, 283–293.

Ott, C.J., Kopp, N., Bird, L., Paranal, R.M., Qi, J., Bowman, T., Rodig, S.J., Kung, A.L., Bradner, J.E., and Weinstock, D.M. (2012). BET bromodomain inhibition targets both c-Myc and IL7R in high-risk acute lymphoblastic leukemia. Blood *120*, 2843–2852.

Pedersen, N., Mortensen, S., Sørensen, S.B., Pedersen, M.W., Rieneck, K., Bovin, L.F., and Poulsen, H.S. (2003). Transcriptional gene expression profiling of small cell lung cancer cells. Cancer Res. *63*, 1943–1953.

Perk, J., Iavarone, A., and Benezra, R. (2005). Id family of helix-loop-helix proteins in cancer. Nat. Rev. Cancer *5*, 603–614.

Rada-Iglesias, A., Bajpai, R., Swigut, T., Brugmann, S.A., Flynn, R.A., and Wysocka, J. (2011). A unique chromatin signature uncovers early developmental enhancers in humans. Nature *470*, 279–283.

Rahman, S., Sowa, M.E., Ottinger, M., Smith, J.A., Shi, Y., Harper, J.W., and Howley, P.M. (2011). The Brd4 extraterminal domain confers transcription activation independent of pTEFb by recruiting multiple proteins, including NSD3. Mol. Cell. Biol. *31*, 2641–2652.

Reimold, A.M., Iwakoshi, N.N., Manis, J., Vallabhajosyula, P., Szomolanyi-Tsuda, E., Gravallese, E.M., Friend, D., Grusby, M.J., Alt, F., and Glimcher, L.H. (2001). Plasma cell differentiation requires the transcription factor XBP-1. Nature *412*, 300–307.

Shaffer, A.L., Emre, N.C., Lamy, L., Ngo, V.N., Wright, G., Xiao, W., Powell, J., Dave, S., Yu, X., Zhao, H., et al. (2008). IRF4 addiction in multiple myeloma. Nature *454*, 226–231.

Shah, N., Pang, B., Yeoh, K.G., Thorn, S., Chen, C.S., Lilly, M.B., and Salto-Tellez, M. (2008). Potential roles for the PIM1 kinase in human cancer - a molecular and therapeutic appraisal. Eur. J. Cancer *44*, 2144–2151.

Shapiro-Shelef, M., Lin, K.I., McHeyzer-Williams, L.J., Liao, J., McHeyzer-Williams, M.G., and Calame, K. (2003). Blimp-1 is required for the formation of immunoglobulin secreting plasma cells and pre-plasma memory B cells. Immunity *19*, 607–620.

Shou, Y., Martelli, M.L., Gabrea, A., Qi, Y., Brents, L.A., Roschke, A., Dewald, G., Kirsch, I.R., Bergsagel, P.L., and Kuehl, W.M. (2000). Diverse karyotypic abnormalities of the c-myc locus associated with c-myc dysregulation and tumor progression in multiple myeloma. Proc. Natl. Acad. Sci. USA *97*, 228–233.

Spitz, F., and Furlong, E.E. (2012). Transcription factors: from enhancer binding to developmental control. Nat. Rev. Genet. *13*, 613–626.

Taatjes, D.J. (2010). The human Mediator complex: a versatile, genome-wide regulator of transcription. Trends Biochem. Sci. *35*, 315–322.

Thanos, D., and Maniatis, T. (1995). Virus induction of human IFN beta gene expression requires the assembly of an enhanceosome. Cell *83*, 1091–1100.

Turner, C.A., Jr., Mack, D.H., and Davis, M.M. (1994). Blimp-1, a novel zinc finger-containing protein that can drive the maturation of B lymphocytes into immunoglobulin-secreting cells. Cell *77*, 297–306.

Weinstein, I.B. (2002). Cancer. Addiction to oncogenes—the Achilles heal of cancer. Science *297*, 63–64.

Whyte, W.A., Orlando, D.A., Hnisz, D., Abraham, B.J., Lin, C.Y., Kagey, M.H., Rahl, P.B., Lee, T.I., and Young, R.A. (2013). Master transcription factors and

mediator establish super-enhancers at key cell identity genes. Cell *153*, this issue, 307–319.

Wu, S.Y., and Chiang, C.M. (2007). The double bromodomain-containing chromatin adaptor Brd4 and transcriptional regulation. J. Biol. Chem. *282*, 13141–13145.

Wu, S.Y., Zhou, T., and Chiang, C.M. (2003). Human mediator enhances activator-facilitated recruitment of RNA polymerase II and promoter recognition by TATA-binding protein (TBP) independently of TBP-associated factors. Mol. Cell. Biol. *23*, 6229–6242.

Wu, S.Y., Lee, A.Y., Lai, H.T., Zhang, H., and Chiang, C.M. (2013). Phospho switch triggers brd4 chromatin binding and activator recruitment for gene-specific targeting. Mol. Cell *49*, 843–857.

Yang, Z., Yik, J.H., Chen, R., He, N., Jang, M.K., Ozato, K., and Zhou, Q. (2005). Recruitment of P-TEFb for stimulation of transcriptional elongation by the bromodomain protein Brd4. Mol. Cell *19*, 535–545.

You, J.S., and Jones, P.A. (2012). Cancer genetics and epigenetics: two sides of the same coin? Cancer Cell *22*, 9–20.

Zhang, Y., Liu, T., Meyer, C.A., Eeckhoute, J., Johnson, D.S., Bernstein, B.E., Nusbaum, C., Myers, R.M., Brown, M., Li, W., and Liu, X.S. (2008). Model-based analysis of ChIP-Seq (MACS). Genome Biol. *9*, R137.

Zhang, W., Prakash, C., Sum, C., Gong, Y., Li, Y., Kwok, J.J., Thiessen, N., Pettersson, S., Jones, S.J., Knapp, S., et al. (2012). Bromodomain-containing protein 4 (BRD4) regulates RNA polymerase II serine 2 phosphorylation in human CD4+ T cells. J. Biol. Chem. *287*, 43137–43155.

Zuber, J., Shi, J., Wang, E., Rappaport, A.R., Herrmann, H., Sison, E.A., Magoon, D., Qi, J., Blatt, K., Wunderlich, M., et al. (2011). RNAi screen identifies Brd4 as a therapeutic target in acute myeloid leukaemia. Nature *478*, 524–528.

Cell

BET Bromodomains Mediate Transcriptional Pause Release in Heart Failure

Priti Anand,[1,7] Jonathan D. Brown,[2,7] Charles Y. Lin,[3,7] Jun Qi,[3] Rongli Zhang,[1] Pedro Calderon Artero,[1] M. Amer Alaiti,[1] Jace Bullard,[1] Kareem Alazem,[1] Kenneth B. Margulies,[4] Thomas P. Cappola,[4] Madeleine Lemieux,[5] Jorge Plutzky,[2] James E. Bradner,[3,6,*] and Saptarsi M. Haldar[1,*]

[1]Case Cardiovascular Research Institute, Department of Medicine, Case Western Reserve University School of Medicine, and Harrington Heart & Vascular Institute, University Hospitals Case Medical Center, Cleveland, OH 44106, USA

[2]Cardiovascular Division, Brigham and Women's Hospital, Harvard Medical School, Boston, MA 02115, USA

[3]Department of Medical Oncology, Dana-Farber Cancer Institute, Boston, MA 02115, USA

[4]Penn Cardiovascular Institute, Perelman School of Medicine, University of Pennsylvania, Philadelphia, PA 19104, USA

[5]Bioinfo, Plantagenet, Ontario K0B 1L0, Canada

[6]Department of Medicine, Harvard Medical School, Boston, MA 02115, USA

[7]These authors contributed equally to this work

*Correspondence: james_bradner@dfci.harvard.edu (J.E.B.), saptarsi.haldar@case.edu (S.M.H.)

http://dx.doi.org/10.1016/j.cell.2013.07.013

SUMMARY

Heart failure (HF) is driven by the interplay between regulatory transcription factors and dynamic alterations in chromatin structure. Pathologic gene transactivation in HF is associated with recruitment of histone acetyl-transferases and local chromatin hyperacetylation. We therefore assessed the role of acetyl-lysine reader proteins, or bromodomains, in HF. Using a chemical genetic approach, we establish a central role for BET family bromodomain proteins in gene control during HF pathogenesis. BET inhibition potently suppresses cardiomyocyte hypertrophy in vitro and pathologic cardiac remodeling in vivo. Integrative transcriptional and epigenomic analyses reveal that BET proteins function mechanistically as pause-release factors critical to expression of genes that are central to HF pathogenesis and relevant to the pathobiology of failing human hearts. This study implicates epigenetic readers as essential effectors of transcriptional pause release during HF pathogenesis and identifies BET coactivator proteins as therapeutic targets in the heart.

INTRODUCTION

Heart failure (HF) is a leading cause of healthcare expenditures, hospitalization, and mortality in modern society (Hill and Olson, 2008; Roger et al., 2012). HF occurs when the heart is unable to maintain organ perfusion at a level sufficient to meet tissue demand and results in fatigue, breathlessness, multiorgan dysfunction, and early death. Existing pharmacotherapies for individuals afflicted with HF, such as β adrenergic receptor antagonists and inhibitors of the renin-angiotensin system, generally target neurohormonal signaling pathways. While such therapies have improved survival in HF patients, residual morbidity and mortality remain unacceptably high (Roger et al., 2012). In light of this unmet clinical need, the elucidation of novel mechanisms involved in HF pathogenesis holds the promise of identifying new therapies for this prevalent and deadly disease.

In response to diverse hemodynamic and neurohormonal insults, the heart undergoes pathologic remodeling, a process characterized by increased cardiomyocyte (CM) volume (hypertrophy), interstitial fibrosis, inflammatory pathway activation, and cellular dysfunction culminating in contractile failure (Hill and Olson, 2008; Sano et al., 2002; van Berlo et al., 2013). The pathologic nature of this process has been validated in large epidemiologic studies, which demonstrate that the presence of chronic cardiac hypertrophy is a robust predictor of subsequent HF and death (Hill and Olson, 2008; Levy et al., 1990). Although hypertrophic remodeling may provide short-term adaptation to pathologic stress, sustained activation of this process is maladaptive and drives disease progression (Hill and Olson, 2008). Studies over the past decade have clearly demonstrated that inhibition of specific prohypertrophic signaling effectors exerts cardioprotective effects even in the face of persistent stress. Together, these data provide a cogent rationale that targeting the hypertrophic process itself can be beneficial without compromising contractile performance (Hill and Olson, 2008; van Berlo et al., 2013).

Hemodynamic and neurohormonal stressors activate a network of cardiac signal transduction cascades that ultimately converge on a defined set of transcription factors (TFs), which control the cellular state of the CM (Hill and Olson, 2008; Lee and Young, 2013; van Berlo et al., 2013). Studies in animal models have implicated several master TFs that drive HF progression (e.g., NFAT, GATA4, NFκB, MEF2, c-Myc) via induction of pathologic gene expression programs that weaken cardiac

performance (Hill and Olson, 2008; Maier et al., 2012; van Berlo et al., 2011; Zhong et al., 2006). In addition to stimulus-coupled activation of DNA-binding proteins, changes in cell state occur through an interplay between these master regulatory TFs and changes in chromatin structure (Lee and Young, 2013). Notably, stress pathways activated in HF are associated with dynamic remodeling of chromatin (McKinsey and Olson, 2005; Sayed et al., 2013), including global changes in histone acetylation and DNA methylation. As alterations in higher-order chromatin structure modulate the net output of multiple, simultaneously activated transcriptional networks (Lee and Young, 2013; Schreiber and Bernstein, 2002), manipulation of cardiac gene control via targeting of chromatin-dependent signal transduction represents a potentially powerful therapeutic approach to abrogate pathologic gene expression and HF progression.

Transcriptional activation is associated with local N-ε-acetylation of lysine sidechains on the unstructured amino-terminal tail of histone proteins (Schreiber and Bernstein, 2002). Dynamic positioning of acetyl-lysine (Kac) arises from the interplay of so-called epigenetic "writers" (histone acetyltransferases or HATs) and epigenetic "erasers" (histone deacetylases or HDACs). Context-specific recognition of Kac at regions of actively transcribed euchromatin is mediated by epigenetic "reader" proteins possessing a Kac-recognition module or bromodomain (Filippakopoulos et al., 2012). Molecular recognition of Kac by bromodomain-containing proteins serves to increase the effective molarity of transcriptional complexes promoting chromatin remodeling, transcriptional initiation, and elongation (Dawson et al., 2012). Elegant studies over the past decade have implicated both epigenetic writers (e.g., EP300) (Wei et al., 2008) and erasers (e.g., HDACs) (Montgomery et al., 2007; Trivedi et al., 2007; Zhang et al., 2002) in cardiac development and disease. In contrast, little is known about epigenetic readers in cardiac biology.

Members of the bromodomain and extraterminal (BET) family of bromodomain-containing reader proteins (BRD2, BRD3, BRD4, and testis-specific BRDT) associate with acetylated chromatin and facilitate transcriptional activation by recruitment of coregulatory complexes such as mediator (Jiang et al., 1998) and the positive transcription elongation factor b (P-TEFb) (Hargreaves et al., 2009; Jang et al., 2005; Yang et al., 2005). Recently, we developed a first-in-class potent, selective bromodomain inhibitor, JQ1, which displaces BET bromodomains from chromatin resulting in suppression of downstream signaling events to RNA polymerase II (Pol II) (Delmore et al., 2011; Filippakopoulos et al., 2010). We and others have utilized this chemical genetic tool to probe BET function in a number of developmental and disease contexts, such as cancer (Delmore et al., 2011; Filippakopoulos et al., 2010), HIV infection (Banerjee et al., 2012), and spermatogenesis (Matzuk et al., 2012). The role of BET bromodomain proteins in the heart remains unknown.

In this study, we report that BETs are critical effectors of pathologic cardiac remodeling via their ability to coactivate defined stress-induced transcriptional programs in the heart. An important mechanism by which BETs drive pathologic gene induction is via their ability to promote transcriptional pause release and elongation, thereby coactivating multiple master TFs known to initiate and promote HF. The elucidation of BET function in the heart implicates epigenetic reader proteins in cardiac biology and HF pathogenesis. Moreover, use of chemical biology to specifically probe the role of BET bromodomain-containing proteins in the myocardium suggests that targeted manipulation of chromatin-based signal transduction might be harnessed for therapeutic gain in heart disease.

RESULTS

BET Bromodomains Are Cell-Autonomous Regulators of Pathologic Cardiomyocyte Hypertrophy In Vitro

Because pathologic cardiac hypertrophy features coordinate transcriptional activation of numerous master regulatory TFs, we hypothesized that BET bromodomains would function as coactivator proteins in this disease process. We first assessed the expression patterns of BETs in the heart. Analysis of neonatal rat ventricular cardiomyocytes (NRVM) and adult mouse ventricular tissue revealed that *Brd2*, *Brd3*, and *Brd4* are transcribed, with *Brd4* emerging as most highly expressed (Figures S1A and S1B available online). Western blots in NRVM, mouse heart tissue, and human heart tissue confirmed abundant BRD4 expression (Figure S1C) and immunofluorescence staining of NRVM demonstrated BRD4 to be nuclear localized (Figure S1D). First, using a chemical biology approach, we leveraged the validated small-molecule probe of BET bromodomain function, JQ1 (Figure 1A), in the established NRVM model in vitro (Simpson et al., 1982). Nanomolar doses of JQ1 significantly blocked phenylephrine (PE)-mediated cellular hypertrophy (Figure 1B) and pathologic gene induction (Figure 1C). In a similar manner, knockdown of *Brd4* in NRVM (Figure S1E) also attenuated PE-mediated hypertrophic growth (Figure 1D) and pathologic gene induction (Figure 1E). We next assessed a number of structurally dissimilar BET inhibitors (I-BET, I-BET-151, RVX-208, and PFI-1; chemical structures shown in Figure S1F) for their ability to inhibit CM hypertrophy. At equimolar doses, we found that inhibition of agonist-induced CM hypertrophy was indeed a class effect of BET inhibitors, with the relative potency of these compounds correlating with their known IC_{50} against BRD4 (Filippakopoulos et al., 2010). Together, these data implicate BET bromodomain proteins as putative cell-autonomous regulators of pathologic CM hypertrophy and identify potent antihypertrophic effects of the small-molecule BET inhibitor JQ1 in vitro.

BETs Are Required for Induction of a Pathologic Gene Expression Program in Cardiomyocytes

To determine the transcriptional effects of BET bromodomain inhibition during CM hypertrophy, we performed gene expression profiling (GEP) studies in cultured NRVM at baseline and after PE stimulation (1.5, 6, and 48 hr) in the presence or absence of JQ1. These three time points capture induction of early response genes such as *c-Myc* (Zhong et al., 2006), as well as the late hypertrophic expression program. Assessment of differentially expressed transcripts revealed three major clusters: genes that were PE inducible and suppressed by JQ1, genes that were PE inducible and unaffected by JQ1, and genes that were PE suppressed and unaffected by JQ1. A heatmap of genes selected based on the highest magnitude of PE-mediated change illustrates each of these clusters (Figure 2A; full list of

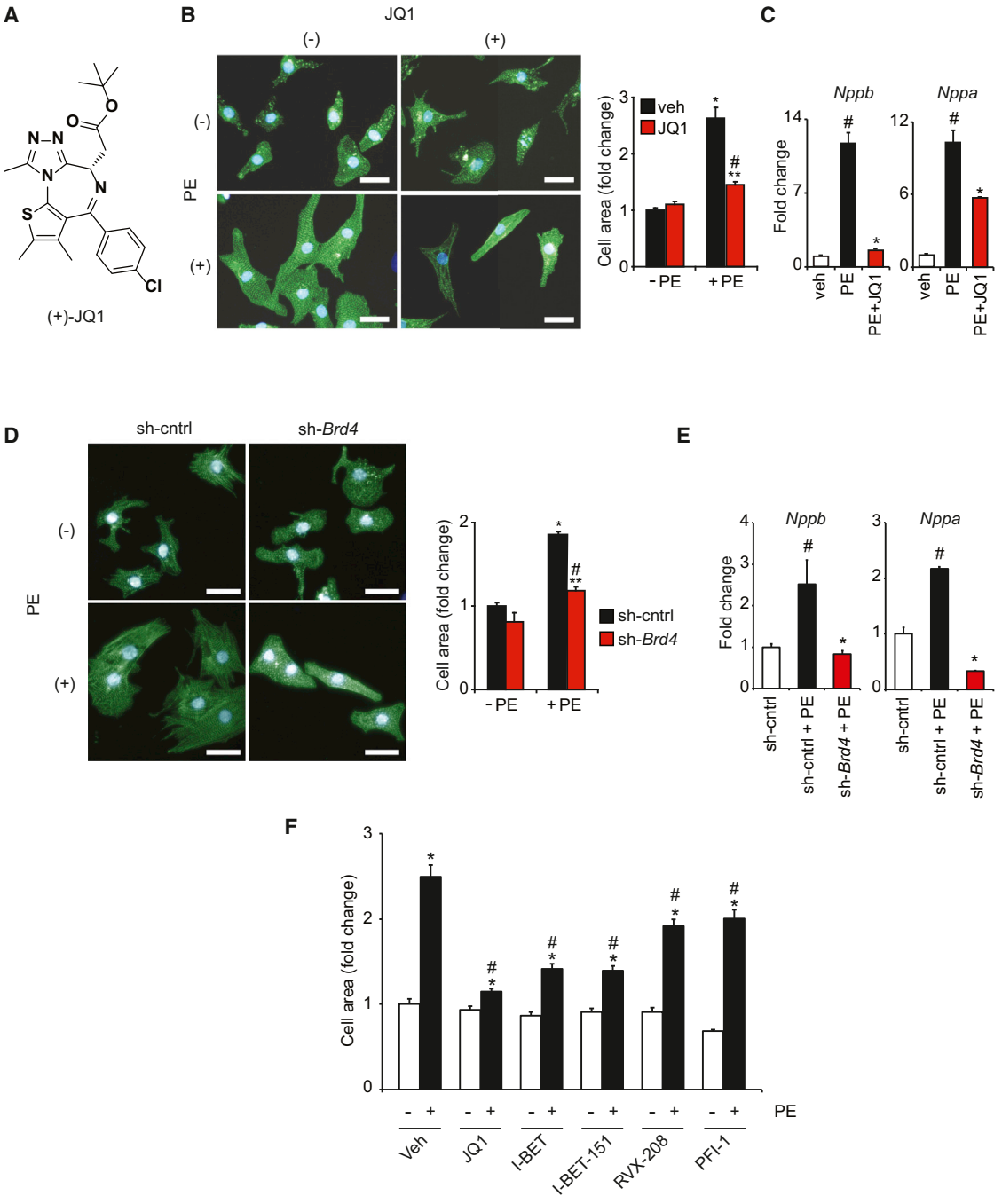

Figure 1. BET Bromodomain Inhibition Blocks CM Hypertrophy In Vitro

(A) (+)-JQ1 structure.

(B) Representative image of NRVM treated ±JQ1 (250 nM) and PE (100 μM) for 48 hr with cell area quantification. *$p < 0.05$ versus veh -PE. **$p < 0.05$ versus JQ1 -PE. #$p < 0.05$ versus veh +PE.

(C) qRT-PCR of NRVM treated with JQ1 (500 nM) and PE (100 μM, 48 hr, n = 4). #$p < 0.05$ versus veh, *$p < 0.05$ versus PE.

(D) Representative image of NRVM infected with Ad-sh-*Brd4* or sh-cntrl treated ±PE (100 μM, 48 hr) with cell area quantification. *$p < 0.05$ versus sh-cntrl -PE. **$p < 0.05$ versus sh-*Brd4* -PE. #$p < 0.05$ versus sh-cntrl +PE.

(E) qRT-PCR of NRVM during *Brd4* knockdown ±PE (100 μM, 48 hr, n = 4). #$p < 0.05$ versus sh-cntrl, *$p < 0.05$ versus sh-cntrl+PE.

(F) Cell area of NRVM treated with indicated BET inhibitors (500 nM) ±PE (100 μM, 48 hr). *$p < 0.05$ versus –PE control for indicated compound. #$p < 0.05$ versus veh +PE. Scale bar, 30 μM. Data shown as mean ± SEM.

See also Figure S1.

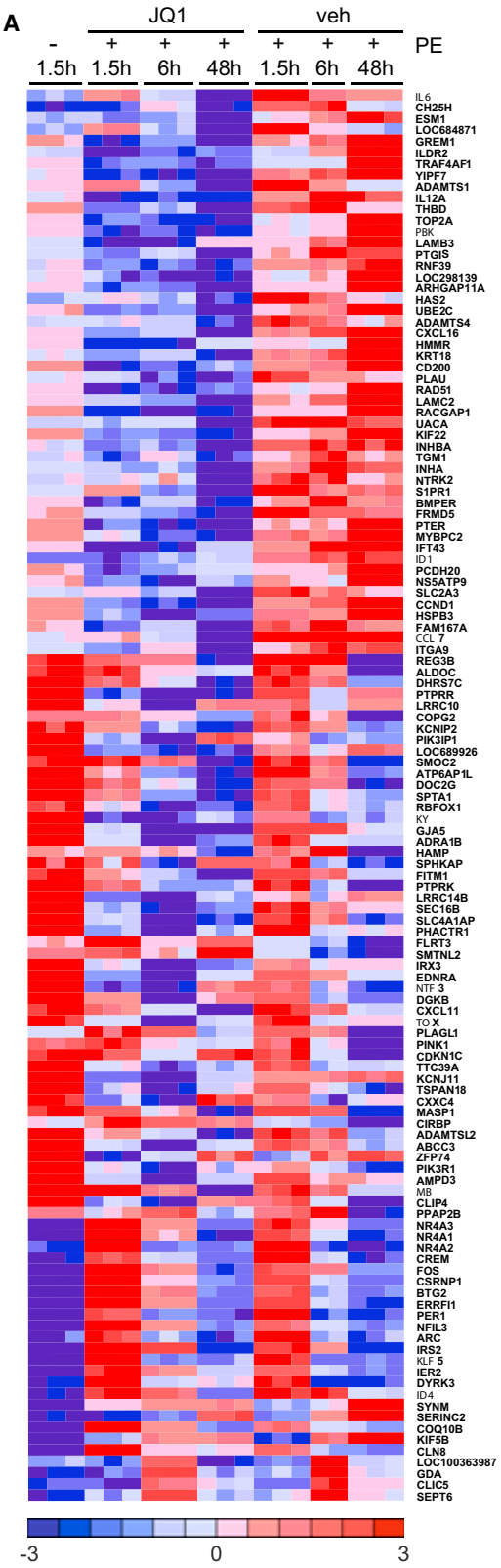

Category	Term	% List	FDR %
GOTERM_BP_FAT	GO:0007049~cell cycle	13	<0.0001
GOTERM_CC_FAT	GO:0005856~cytoskeleton	14	<0.0001
GOTERM_BP_FAT	GO:0009611~response to wounding	10	<0.0001
GOTERM_MF_FAT	GO:0005125~cytokine activity	4	<0.0001
GOTERM_BP_FAT	GO:0006954~inflammatory response	5	0.07
GOTERM_BP_FAT	GO:0006952~defense response	6	0.6
GOTERM_BP_FAT	GO:0040007~growth	4	0.2
GOTERM_CC_FAT	GO:0005576~extracellular region	16	<0.0001
GOTERM_BP_FAT	GO:0042493~response to drug	8	2.4
GOTERM_BP_FAT	GO:0010647~pos regulation cell commun	5	4.7

(legend on next page)

differential transcripts provided in Table S1). Global analysis of GEPs revealed that PE stimulation resulted in the cumulative induction of over 450 genes and that JQ1 abrogated induction of a substantial subset of PE-inducible genes. Statistically significant transcriptional effects were evident as early as 1.5 hr and increased over time (Figures 2B and 2C), consistent with the emerging role of BETs as coactivators of inducible gene expression programs (Nicodeme et al., 2010). Functional pathway analysis of PE-inducible transcripts that were suppressed by JQ1 revealed that BETs facilitate expression of a host of biological processes known to be involved in pathologic CM activation, including cytoskeletal reorganization, extracellular matrix production, cell-cycle reentry, paracrine/autocrine stimulation of cellular growth, and proinflammatory signaling (Figure 2D) (Song et al., 2012). Using the prohypertrophic cytokine *Il6* as a representative target (Figure 2C), we confirmed by qRT-PCR that JQ1 significantly attenuated PE-mediated induction (Figure 2E). Activity of BETs during pathologic stress was not due to PE-mediated increases in BET expression (Figure S2). Chromatin immunoprecipitation (ChIP) studies demonstrated BRD4 occupancy at the *Il6* locus and an increase in BRD4 enrichment after 90 min of PE stimulation that was blocked by BET inhibition (Figure 2F). Interestingly, BET bromodomain inhibition did not affect PE-mediated induction of *Myc* (Figure 2G), an established transcriptional driver of pathologic cardiac hypertrophy (Zhong et al., 2006). Prior studies from our laboratory and others have implicated BET bromodomains in neoplastic *MYC* transcription in hematopoietic tumors (Delmore et al., 2011; Zuber et al., 2011). Collectively, these in vitro data (Figures 1 and 2) demonstrate that BET bromodomain-containing proteins regulate CM hypertrophy in a cell-autonomous manner via coactivation of a broad but specific transcriptional program.

BET Bromodomain Inhibition Arrests Pathologic Hypertrophy and Heart Failure In Vivo

Given these observations in cultured CMs, we hypothesized that BETs might regulate pathologic cardiac remodeling in the intact organism. We leveraged the favorable therapeutic index of JQ1, which has previously been shown to potently inhibit BET bromodomain function in adult mice without significant toxicity when administered chronically at 50 mg/kg/day (Filippakopoulos et al., 2010). Independently, we confirmed the lack of overt toxicity by treating mice with JQ1 for 2–3 weeks, observing no effect on endurance exercise capacity (Figure S3A), a metric of global cardiometabolic health. For in vivo studies, we first used transverse aortic constriction (TAC), a thoroughly characterized model of cardiac pressure overload, which provides focal hemodynamic stress to the heart and recapitulates several cardinal aspects of pathologic hypertrophy and HF in humans (Rockman et al., 1991). In our hands, adult mice subject to TAC develop concentric left ventricular hypertrophy (LVH) by 7–10 days and progress to advanced HF after 3–4 weeks.

We performed TAC or sham surgery, followed by administration of JQ1 (50 mg/kg/day versus vehicle control) beginning 1.5 days after initiation of TAC (Figure 3A). Serial echocardiography showed that JQ1 protected against TAC-mediated LV systolic dysfunction, cavity dilation, and wall thickening, with effects that were sustained out to 4 weeks (Figures 3B–3D and S3B; Movies S1 and S2). JQ1 treatment also inhibited pathologic cardiomegaly (Figure 3E; representative photos in Figure 3F), pulmonary congestion (Figure 3G), and myocardial expression of canonical hypertrophic marker genes (Figure 3H) after TAC. JQ1 was well tolerated, as evidenced by normal activity (Movies S3 and S4) and the lack of significant mortality or weight loss compared to vehicle-treated mice (data not shown). In addition, JQ1 had no adverse effect on LV structure or function in sham-treated mice (Figures 3E, 3F, and S3B). Importantly, JQ1 does not affect systemic blood pressure (Figure S3C). Furthermore, the protective effects of JQ1 in the TAC model were not associated with differences in the pressure gradient across the aortic constriction (Figure S3D).

In addition to hemodynamic stress, excessive neurohormonal activation is also a central driver of pathologic cardiac hypertrophy (Hill and Olson, 2008; van Berlo et al., 2013). Therefore, we next assessed whether JQ1 could ameliorate pathology in a second mouse model of neurohormonally mediated cardiac hypertrophy. Mice were implanted with osmotic minipumps delivering phenylephrine (PE, 75 mg/kg/day versus saline) followed by JQ1 or vehicle administration beginning 1.5 days after minipump installation. This infusion protocol produces robust concentric LVH in 2–3 weeks but does not cause significant LV cavity dilation or depression of LV systolic function in wild-type mice. Concordant with our TAC results above, JQ1 potently suppressed the development of pathologic cardiac hypertrophy during chronic PE infusion, without any compromise in LV systolic function (Figure 3I).

In addition to favorable effects on cardiac function, we assessed whether JQ1 also ameliorated cardinal histopathologic features of HF in vivo. Analysis of mouse heart tissue demonstrated that JQ1 significantly attenuated the development of CM hypertrophy (Figure 4A), myocardial fibrosis (Figure 4B), apoptotic cell death (Figure 4C), and capillary rarefaction

Figure 2. BET Regulated Transcriptional Programs during CM Hypertrophy In Vitro

(A) Selected heatmap of differentially expressed (DE) transcripts. NRVM treated with 500 nM JQ1, 100 μM PE.

(B) Global analysis of DE transcripts showing induction of genes by PE with time (red) and progressive reversal of PE-mediated gene induction by JQ1 (blue).

(C) Volcano plot showing fold change (x axis) effect of PE+JQ1 versus PE+vehicle (shades of blue) on all genes upregulated at any time point by PE versus veh (shades of red). Progression from lighter to darker shading represents increasing time (1.5, 6, and 48 hr).

(D) Functional pathway analysis (DAVID) of PE-induced genes that were JQ1-reversed. FDR < 5% considered statistically significant.

(E) *Il6* qRT-PCR in NRVM treated with JQ1 (500 nM) and PE (100 μM, n = 4). *$p < 0.05$ versus veh, #$p < 0.05$ versus PE.

(F) BRD4 ChIP-qPCR in NRVM treated with JQ1 (500 nM) and PE (100 μM) for 90 min. Target and nontarget (−4 kb region) primers depicted. n = 3, *$p < 0.05$ versus veh, #$p < 0.05$ versus PE.

(G) *Myc* qRT-PCR in NRVM treated with JQ1 (500 nM) and PE (100 μM, n = 4). *$p < 0.05$ versus veh, #$p < 0.05$ versus PE. Data shown as mean ± SEM.

See also Figure S2 and Table S1.

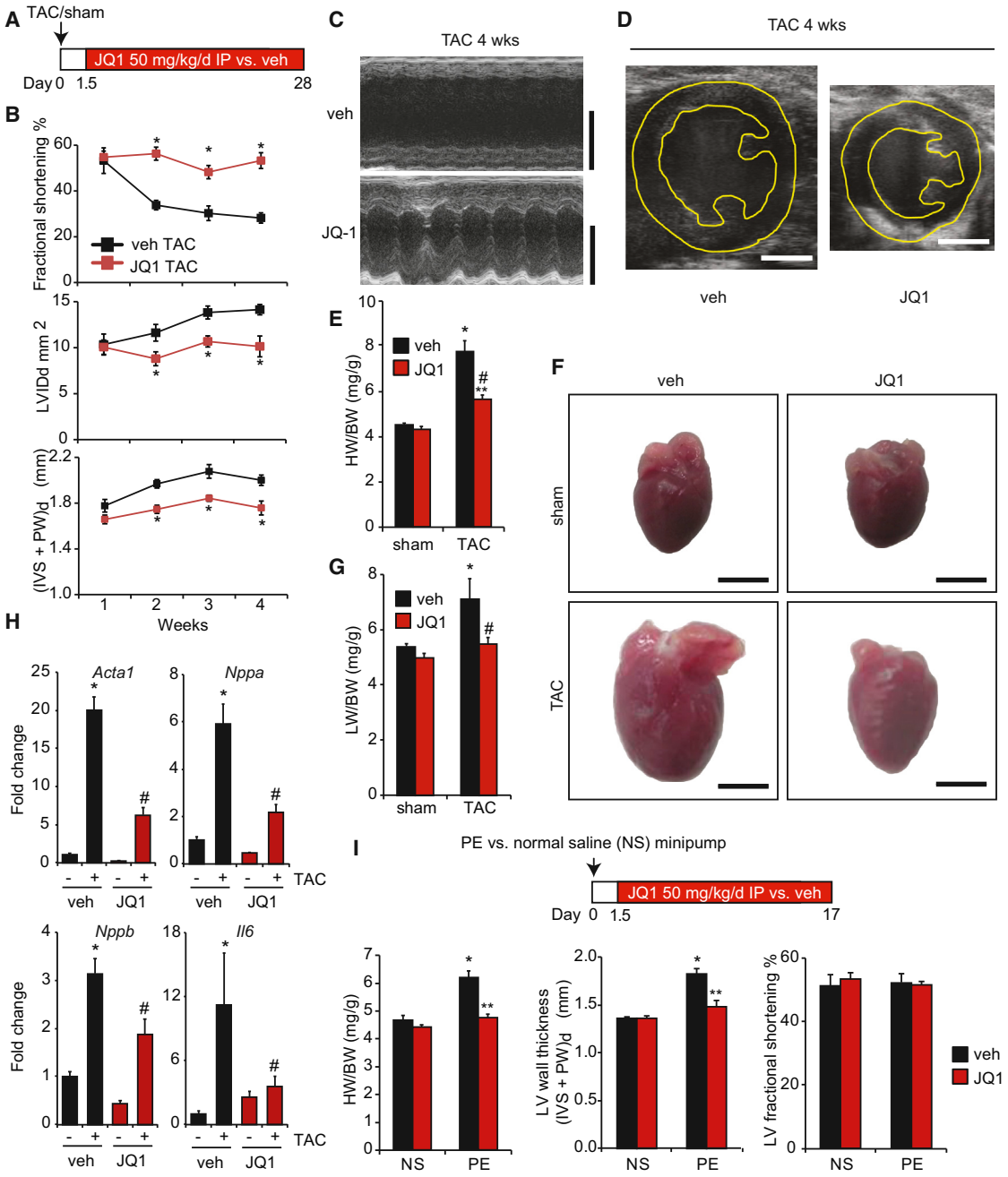

Figure 3. BET Bromodomain Inhibition with JQ1 Potently Attenuates Pathologic Cardiac Hypertrophy and HF In Vivo

(A) Experimental protocol.

(B) Echocardiographic parameters during TAC (n = 7). $LVID_d$ is LV end diastolic area, $(IVS + PW)_d$ is sum thickness of the interventricular septum and posterior LV wall at end diastole. *p < 0.05 versus veh TAC.

(C) Representative M-mode tracings and (D) end-diastolic 2D images at 4 weeks TAC. Scale bar, 3 mm.

(E) Heart/body weight (HW/BW) ratios, 4 weeks. *p < 0.05 versus sham veh. #p < 0.05 versus TAC veh. **p < 0.05 versus sham JQ1.

(F) Representative photos of freshly excised whole hearts. Scale bar, 3 mm.

(G) Lung/body weight (LW/BW) ratios, 4 weeks TAC (n = 7 TAC, n = 5 sham). *p < 0.05 versus sham veh. #p < 0.05 versus TAC veh.

(H) qRT-PCR in mouse hearts (n = 5–7). *p < 0.05 versus sham veh. #p < 0.05 versus TAC veh.

(I) PE infusion (75 mg/kg/day) and JQ1 administration (n = 7 PE, n = 5 normal saline). *p < 0.05 versus NS veh. **p < 0.05 versus PE veh. Data shown as mean ± SEM.

See also Figure S3 and Movies S1, S2, S3, and S4.

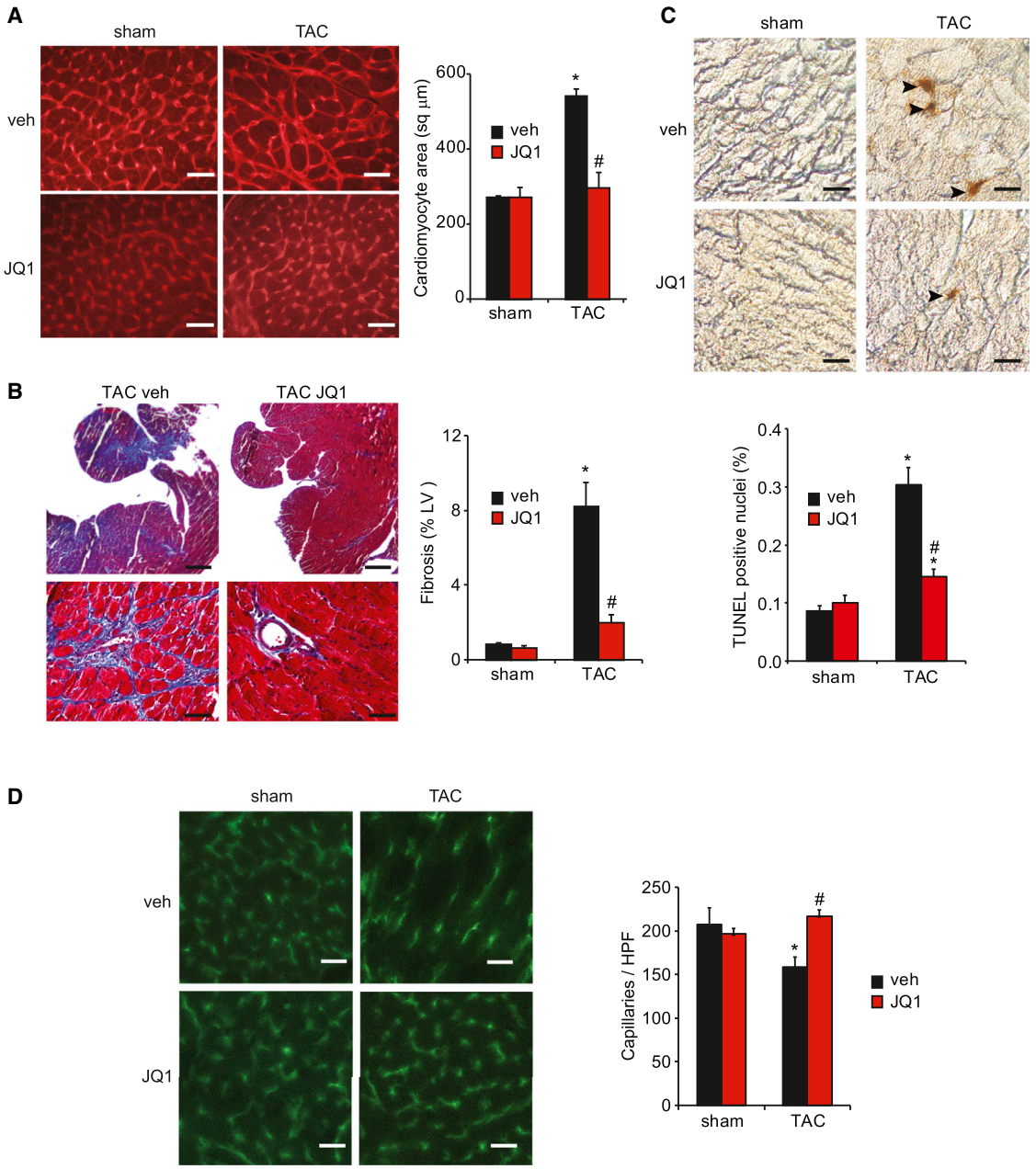

Figure 4. BET Bromodomain Inhibition Attenuates Cardinal Histopathologic Features of HF

(A) CM area quantification in LV sections. Scale bar, 30 μm.

(B) Trichrome staining and quantification of fibrotic area. Scale bar, 400 μm (top), 40 μm (bottom).

(C) TUNEL staining of heart sections with quantification of TUNEL-positive nuclei. Scale bar, 20 μm.

(D) PECAM-1 immunofluorescence staining of LV sections with quantification of myocardial capillary density. HPF, 400× high-powered field. Scale bar, 30 μm.

For (A–D) n = 3–4, 4 week time point, *p < 0.05 versus sham veh, #p < 0.05 versus TAC veh. Data shown as mean ± SEM.

(Figure 4D) typically seen after 4 weeks of TAC (Sano et al., 2007; Song et al., 2010).

BET Inhibition Suppresses a Pathologic Cardiac Gene Expression Program In Vivo

Using the TAC model, we performed detailed transcriptional analysis in three groups (sham vehicle, TAC vehicle, and TAC-JQ1) at three time points (Figure 5A): 3 days (to reflect early events that occur prior to the onset of hypertrophy), 11 days (established hypertrophy), and 28 days (advanced pathologic remodeling with signs of HF). Unsupervised hierarchical clustering revealed that the TAC-veh group had a distinct GEP signature that evolved with time when compared to the sham-veh group (Figure 5B). In contrast, TAC-JQ1 clustered with the sham group

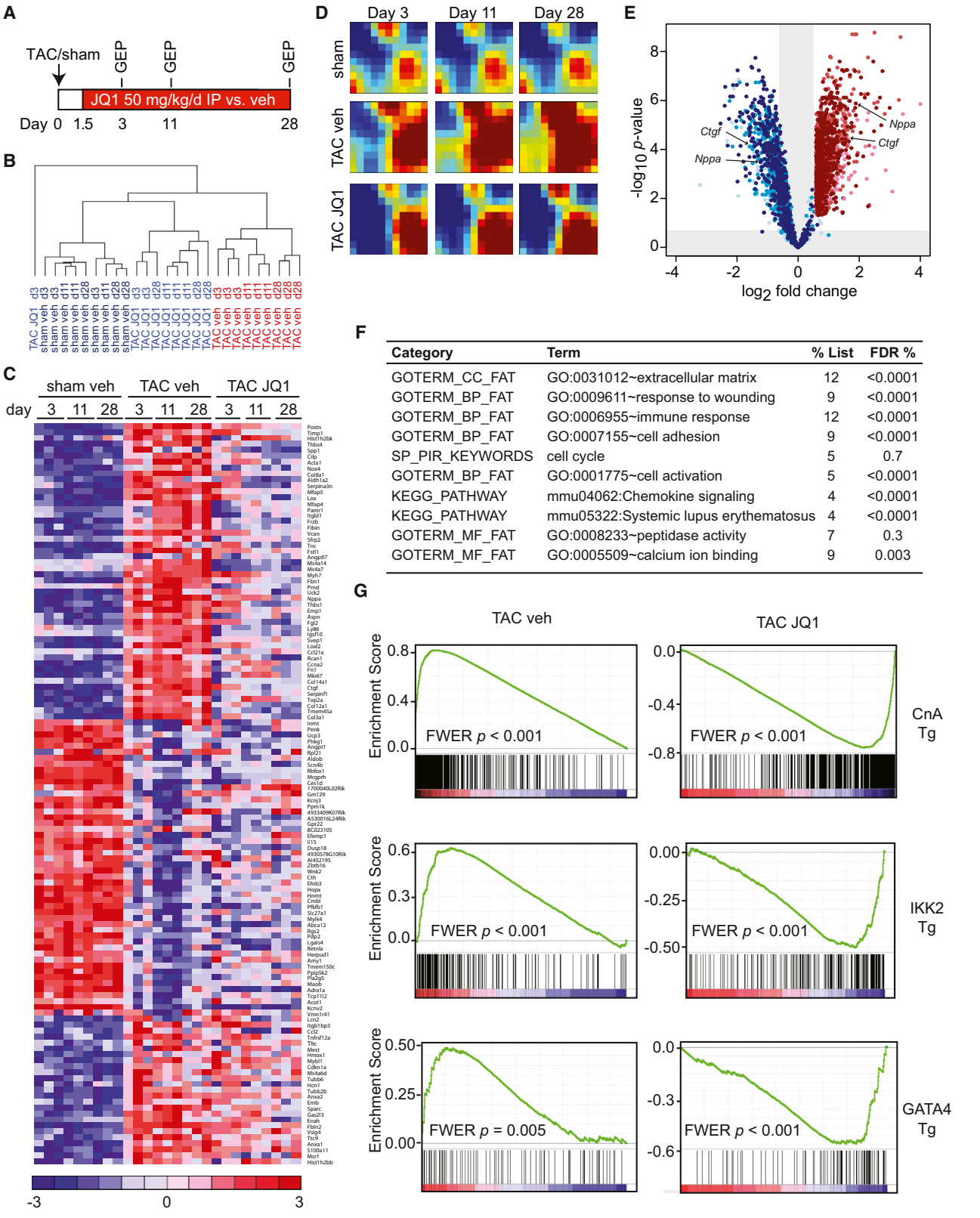

Category	Term	% List	FDR %
GOTERM_CC_FAT	GO:0031012~extracellular matrix	12	<0.0001
GOTERM_BP_FAT	GO:0009611~response to wounding	9	<0.0001
GOTERM_BP_FAT	GO:0006955~immune response	12	<0.0001
GOTERM_BP_FAT	GO:0007155~cell adhesion	9	<0.0001
SP_PIR_KEYWORDS	cell cycle	5	0.7
GOTERM_BP_FAT	GO:0001775~cell activation	5	<0.0001
KEGG_PATHWAY	mmu04062:Chemokine signaling	4	<0.0001
KEGG_PATHWAY	mmu05322:Systemic lupus erythematosus	4	<0.0001
GOTERM_MF_FAT	GO:0008233~peptidase activity	7	0.3
GOTERM_MF_FAT	GO:0005509~calcium ion binding	9	0.003

(legend on next page)

and displayed no significant temporal change despite continuous exposure to TAC (Figure 5B). Hence, JQ1 treatment suppressed the evolution of a broad pathologic gene expression program in the heart, with effects evident as early as 3 days post-TAC. Similar to our studies in isolated CMs (Figure 2), global GEP analysis revealed three major clusters: genes that were TAC inducible and suppressed by JQ1, those that were TAC inducible and unaffected by JQ1, and those that were TAC suppressed and unaffected by JQ1. A representative heatmap of genes (selected for the highest magnitude of TAC-mediated change) highlights each of these three clusters (Figure 5C; full list of differential transcripts provided in Table S2). TAC did not significantly alter myocardial expression of *Brd2*, *Brd3*, or *Brd4* (Figure S4A).

To visualize the global transcriptional effects of TAC and BET bromodomain inhibition in the model over time, we performed gene expression dynamics inspector (GEDI) analysis (Eichler et al., 2003). Although the sham mosaic remained temporally invariant, TAC resulted in progressive induction of gene clusters over time, indicated by increased signal in numerous tiles within the mosaic (Figure 5D). BET bromodomain inhibition disrupted the temporal evolution of this TAC-induced, pathologic transcriptional program with a mosaic signature that more closely resembled the sham group (Figure 5D). A volcano plot showing fold change effect of TAC-JQ1 versus TAC vehicle (shades of blue) on the set of all genes upregulated at any time point by TAC (shades of red) is shown in Figure 5E. These data illustrate the potent and statistically significant effects of JQ1 in suppressing TAC-mediated gene induction. Additionally, comparison of fold change effect of TAC-JQ1 versus sham vehicle (shades of blue) on the set of all genes upregulated at any time point by TAC (shades of red) shows that JQ1 administration reversed TAC-mediated gene induction to levels similar to those in the sham-treated hearts (Figure S4B). Functional pathway analysis of TAC-inducible transcripts that were suppressed by JQ1 showed enrichment for key biological processes involved in pathologic myocardial remodeling and HF progression in vivo (Figure 5F) (Song et al., 2012; Zhao et al., 2004). Importantly, these functional terms aligned with the data from isolated NRVM (Figure 2D) and represent pathologic processes universally observed in advanced human HF (Hannenhalli et al., 2006).

Given the broad effects on myocardial gene expression seen with JQ1, we hypothesized that BETs enable pathologic gene induction via their ability to coordinately coactivate multiple TF pathways in vivo. Using gene set enrichment analysis (GSEA) (Subramanian et al., 2005), we compared our set of TAC-inducible genes that were suppressed by BET inhibition, against compendia of TF signatures. Specifically, we studied the Broad Institute Molecular Signatures Database C3 motif gene sets (Xie et al., 2005), as well as three functional, in vivo signatures of CM-specific transcriptional effectors: Calcineurin-NFAT (Bousette et al., 2010), NFκB (Maier et al., 2012), and GATA4 (Heineke et al., 2007). These analyses revealed that the TAC-induced gene expression profile was positively enriched for IRF and ETS consensus binding motifs (family-wise error rate [FWER] $p < 0.0001$), as well as for myocardial signatures that result from Calcineurin-A, NFκB, and GATA4 activation (Figure 5G). Conversely, the effect of JQ1 demonstrated strong negative enrichment for these same TF signatures (Figure 5G; FWER $p < 0.0001$ for IRF and ETS motifs). In contrast, although TAC was strongly correlated with both c-Myc and E2F signatures, there was no significant correlation between c-Myc/E2F and JQ1 effect at any time point (Figure S4C). Consistent with our NRVM studies, we also found that JQ1 had no effect on TAC-mediated induction of *Myc* expression in vivo (Figure S4D). Hence, the GSEA data support a model in which BET bromodomains facilitate gene induction via coactivation of specific myocardial TF networks.

We next compared the set of TAC-inducible genes that were suppressed by JQ1 against validated gene expression profiles of advanced nonischemic and ischemic HF in humans (Hannenhalli et al., 2006). This analysis demonstrated that targets of BETs in the mouse TAC model overlapped in a statistically significant manner with the set of genes induced in human HF (Figure S4E; $\chi^2 < 5 \times 10^{-14}$). Interestingly, the vast majority (89%) of these targets were common to both ischemic and nonischemic human HF (Figure S4F). Thus, inasmuch as the gene expression profiles of mice subjected to TAC overlap with that of advanced HF in a human cohort, we found the principal transcriptional targets of BET bromodomains in mice were also relevant in human disease.

BET Bromodomain Inhibition Abrogates Transcriptional Pause Release Genome wide during Pathologic Hypertrophy In Vivo

To establish the mechanism by which BET bromodomain inhibition impairs global transactivation of pathologic transcriptional programs concomitantly activated during pressure overload, we performed ChIP coupled with high-throughput genome sequencing (ChIP-seq) on heart tissue from mice subjected to sham versus TAC surgery, with and without JQ1 treatment. For

Figure 5. BETs Coactivate a Broad, but Specific Transcriptional Program in the Heart during TAC

(A) Protocol for GEP experiment.

(B) Unsupervised hierarchical clustering of GEPs.

(C) Heatmap of selected genes. Full list of DE genes in Table S2.

(D) GEDI plots showing temporal evolution of gene clusters.

(E) Volcano plot showing fold change effect of TAC+JQ1 versus TAC veh (shades of blue) on all genes upregulated at any time point by TAC-veh versus sham veh (shades of red). Progression from lighter to darker shading represents increasing time (3, 11, and 28 days).

(F) DAVID analysis of genes that were TAC-induced and JQ1-reversed. FDR < 5% considered statistically significant.

(G) GSEA for TAC veh and TAC-JQ1 against three independent GEPs derived from CM-specific activation of canonical prohypertrophic transcriptional effectors in vivo: Calcineurin-NFAT (driven by a constitutively active Calcineurin-A (CnA) transgene [Bousette et al., 2010], NFκB driven by an IKK2 transgene [Maier et al., 2012] and transgenic GATA4 overexpression [Heineke et al., 2007]). FWER $p < 0.250$ represents statistically significant enrichment. Data representative for all three time points. Plots shown for 28 day time point. Data shown as mean ± SEM.

See also Figure S4 and Table S2.

heart tissue ChIP-seq, a 4 day time point was chosen to capture changes in chromatin state that occur during the initial phase of hypertrophic growth in the TAC model (~3–7 days). Experimental data obtained for BRD4 and Pol II were integrated with publicly available data from Bing Ren and colleagues, which provided epigenomic landscapes for murine cardiac euchromatin (Shen et al., 2012). Genome-wide data for Pol II enrichment in our sham operated mice demonstrated excellent statistical agreement with Pol II enrichment curated from the literature (R^2 = 0.65; Figures S5A and S5B).

First, we determined the sites of genome-wide localization of BRD4 in the murine heart. Strong enrichment was observed at promoter regions of actively transcribed genes, as identified by enrichment for histone 3 lysine 4 trimethylation (H3K4me3) and Pol II (Figure 6A). Rank ordering of all transcriptionally active promoters by Pol II occupancy identified global binding of BRD4 at sites of transcriptional initiation. Recently, BET bromodomains have also been shown to bind to enhancer elements in the eukaryotic genome (Lovén et al., 2013; Zhang et al., 2012). Binding of BRD4 to enhancer elements was assessed by rank-ordering regions of enrichment for histone 3 lysine 27 acetylation (H3K27ac) and comparing BRD4 enrichment to that of P300, a known enhancer factor of functional significance in cardiac hypertrophy (Wei et al., 2008). Importantly, BRD4 binds to the vast majority of active enhancers in the murine cardiac genome (Figure 6B).

BRD4, through its C-terminal domain (CTD), physically associates with and activates CDK9 (Bisgrove et al., 2007; Jang et al., 2005; Yang et al., 2005), a core component of the P-TEFb complex, which functions as an elongation-promoting Pol II CTD kinase (Peterlin and Price, 2006). Hyperactivation of P-TEFb and consequent increases in global transcription are considered a hallmark of pathologic cardiac hypertrophy in multiple systems (Espinoza-Derout et al., 2009; Sano et al., 2002; Yoshikawa et al., 2012). Inhibition of CDK9 function in NRVM has been shown to attenuate endothelin-1-mediated hypertrophy in vitro (Sano et al., 2002). These observations provided us with a rationale to explore the effect of BET bromodomain inhibition on transcriptional elongation in the TAC model in vivo.

BET bromodomain inhibition by JQ1 has been shown to displace BRD4 and P-TEFb from chromatin leading to a decrease in Pol II elongation at active genes (Lovén et al., 2013). Gene-specific effects on Pol II occupancy were explored at canonical mediators and effectors of pathologic cardiac remodeling. As shown for representative genes in Figures 6C and 6D, sham-treated hearts feature a pronounced Pol II enrichment peak at the TSS of *Ctgf* and *Serpine1 (SerpinE1/PAI-1)*, with only modest evidence of downstream elongation (gray wiggle plots). Following TAC, transcriptional activation (as shown in Figure 5C and Table S2) was accompanied by a shift in the distribution of gene bound Pol II toward a higher relative occupancy in the elongating gene body region (black wiggle plots; Figures 6C and 6D). BET bromodomain inhibition markedly attenuated Pol II occupancy in the elongating region, leading to higher relative Pol II occupancy at the TSS initiation site (red wiggle plots), consistent with its ability to attenuate transcription elongation. Additional representative Pol II enrichment plots for the *Ace*, *Bgn*, *Thbs1*, and *Xirp2* loci are shown in Figure S5C.

Global effects of BET bromodomain inhibition on initiation and elongation were further examined by calculating the Pol II traveling ratio at all actively transcribed genes and on the subset of genes induced by TAC. Traveling ratio is a validated measure of transcriptional pause release that compares promoter and elongating gene body occupancy levels of Pol II to quantify the ratio of paused to elongating Pol II (Lin et al., 2012; Wade and Struhl, 2008). BET bromodomain inhibition of TAC-treated hearts led to a higher ratio of promoter to elongating gene body Pol II compared to TAC at all active genes (Figure 6E) and at TAC-induced genes that were reversed by JQ1 (Figure 6F). A metagene analysis of Pol II enrichment among actively transcribed genes verified the change in the ratio of promoter to elongating gene body Pol II by JQ1 (Figure S5D). The effects of JQ1 on transcriptional elongation in the TAC model were reproduced in an independent in vivo biological replicate, as shown in Figure S5E.

Given the high variability in dynamic range between heart tissue samples ChIP-seq (Figure S5F) and the relative nature of metrics such as the traveling ratio, we examined global levels of initiating and elongating Pol II to further quantify the effects of BET bromodomain inhibition. We observed a specific decrease in the elongation-specific serine 2 Pol II phosphoform (Ser2P) upon JQ1 treatment (Figure 6G) with little change to the initiation-specific serine 5 Pol II phosphoform (Ser5P) (Figure 6H). JQ1-mediated suppression of Pol II Ser2P abundance was recapitulated in the in vitro NRVM model (Figure S5G). Interestingly, we also observed significant upregulation of the P-TEFb inhibitory protein HEXIM1 (Espinoza-Derout et al., 2009; Peterlin and Price, 2006; Yoshikawa et al., 2012) during JQ1 treatment, suggesting an additional mechanism by which BET bromodomain inhibition may inhibit transcriptional elongation (Figures S5H–S5K). We conclude that transcriptional elongation is an important mechanism by which BET bromodomain inhibition attenuates gene expression programs activated during pathologic cardiac hypertrophy.

DISCUSSION

Our current work implicates BET bromodomain reader proteins as essential transcriptional coactivators of a pathologic gene expression program that drives CM hypertrophy and HF progression. Gene-expression profiling and ChIP-seq studies reveal that BET proteins function, in part, by promoting transcriptional pause release during pathologic stress. In broadest terms, the data presented here directly implicate epigenetic readers in cardiac biology and identify BET bromodomain proteins as potential therapeutic targets in heart disease.

Pathologic cardiac hypertrophy ensues by a collaborative interplay between master regulatory TFs and dynamic changes in chromatin structure (Lee and Young, 2013). TFs including NFAT, GATA4, and NFκB (Hill and Olson, 2008; Maier et al., 2012; van Berlo et al., 2011), as well as histone modifying enzymes such as EP300 and HDAC2 (Trivedi et al., 2007; Wei et al., 2008; Zhang et al., 2002) activate a CM gene expression program that results in cellular dysfunction. Dynamic and global changes in histone 3 lysine 9 acetylation, a chromatin mark for gene promoters and enhancers, have been observed genome-wide in the adult mouse heart after pressure overload (Sayed

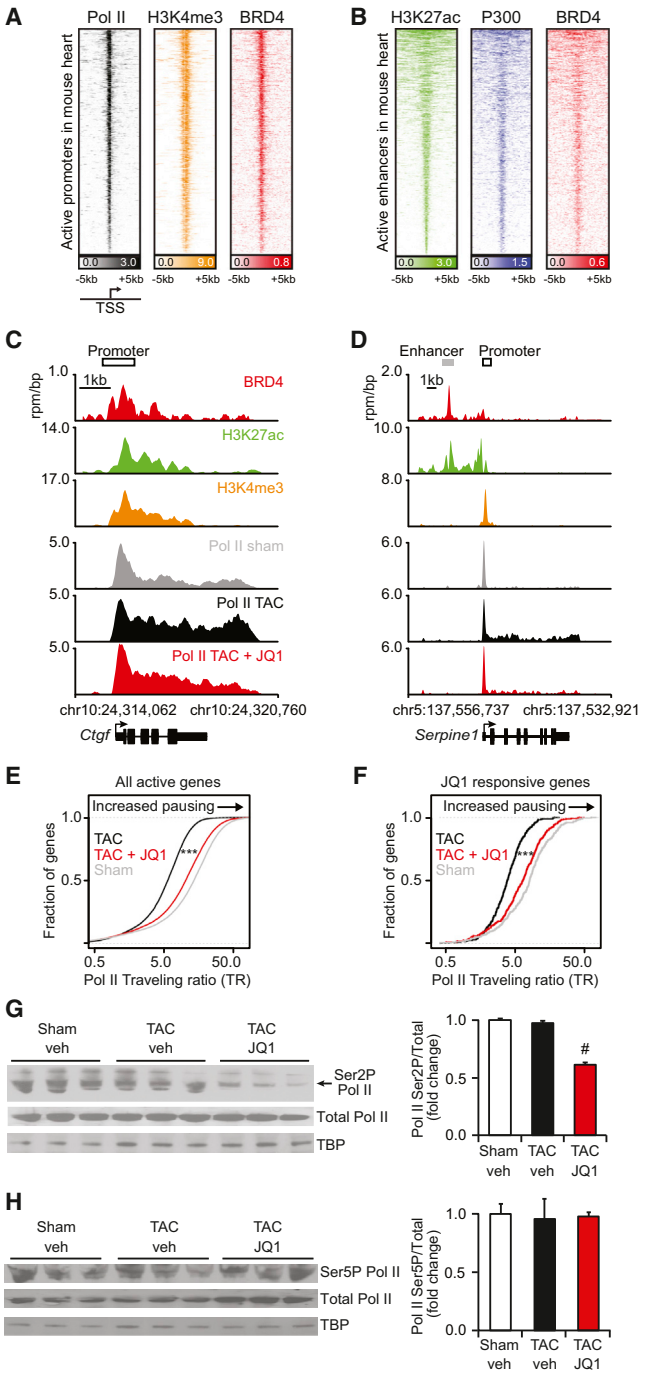

Figure 6. BET bromodomain Inhibition Abrogates Transcriptional Pause Release Genome wide in Pathologic Hypertrophy

(A) Heatmap of Pol II (black), H3K4me3 (orange), and BRD4 (red) levels at active promoters ranked by Pol II levels in sham-treated heart samples. Each row shows ±5 kb centered on H3K4me3 peak. Rows ordered by average Pol II at the promoter.

(B) Heatmap of H3K27ac (green), P300 (blue), and BRD4 (red) levels at active enhancers ranked by H3K27ac levels in adult heart. Each row shows ±5 kb centered on H3K27ac peak. Rows ordered by amount of H3K27ac at enhancer. Color scaled intensities of (A) and (B) are in units of reads per million per base pair (rpm/bp).

(C and D) Gene tracks at (C) *Ctgf* and (D) *Serpine1* gene in heart. BRD4 (red) is from sham-treated hearts. H3K27ac (green) and H3K4me3 (orange) derived from published landscapes of wild-type mouse hearts (Shen et al., 2012) that are age/sex/strain-matched to our sham-treated hearts. Pol II are from either sham (gray), TAC (black), or TAC+JQ1-treated (red) heart. x axis shows genomic position. y axis shows ChIP-seq occupancy (rpm/bp).

(E and F) Empirical cumulative distribution plots of Pol II traveling ratios (TR) (Rahl et al., 2010) for genes that are transcriptionally active in either sham or TAC-treated hearts (E) and genes that are TAC induced and reversed by JQ1 (F). Differences in TR distribution between TAC and TAC+JQ1-treated hearts are statistically significant (*** Welch's two-tailed t test, $p < 2 \times 10^{-16}$).

(G and H) Western blots with densitometry of heart tissue nuclear extracts from sham, TAC, and TAC+JQ1-treated hearts for total Pol II or indicated phosphoforms (n = 3; #p < 0.05 versus TAC veh). Data shown as mean ± SEM. See also Figure S5 and Table S3.

et al., 2013). Despite these fundamental observations, the mediators in the heart that link the activity of master regulatory TFs and histone acetylation to Pol II dynamics and global transcriptional anabolism are poorly understood.

Here, we establish that BET bromodomain reader proteins function critically in chromatin-mediated signal transduction to Pol II, coactivating pathologic gene expression in the heart. GSEA reveals that BET inhibition antagonizes multiple TF outputs known to be causal in HF pathogenesis including NFAT, NFκB, and GATA4, suggesting that BET bromodomain proteins coactivate a broad transcriptional network involving multiple TFs. Importantly, we find that BET bromodomain proteins do not directly affect *Myc* mRNA levels or function in the heart—a striking contrast to observations in hematopoietic tumors, where BETs are required for c-Myc expression and activity (Delmore et al., 2011; Zuber et al., 2011). ChIP-seq analysis reveals that BRD4 co-occupies active promoters with Pol II (as defined by H3K4me3) and active gene enhancers (as defined by H3K27ac) in the adult mouse heart and that cardiac pressure overload induces Pol II pause release and transcriptional elongation within 4 days. BET bromodomain inhibition suppresses transcriptional pause release during pressure overload in vivo and attenuates expression of the pathologic HF gene program. Together, these data demonstrate that BET bromodomain reader proteins are indispensable coactivators in pathologic gene expression in the heart that function, in part, through their ability to promote Pol II pause release and transcriptional elongation.

Activation of the P-TEFb complex, a central effector of pause release and transcriptional elongation (Lee and Young, 2013), has been observed in pathologic cardiac hypertrophy (Sano et al., 2002). Previous studies in NIH 3T3 cells and macrophages have demonstrated that BRD4 interacts with P-TEFb and facilitates stimulus-coupled recruitment of P-TEFb to target promoters (Hargreaves et al., 2009; Patel et al., 2013). Activity of CDK9, a core constituent of the P-TEFb complex, is also increased during hypertrophic stress and is required for agonist-induced hypertrophy in NRVM (Sano et al., 2002). CM-specific overexpression of the CDK9-activating protein CyclinT1 results in cardiac hypertrophy in vivo (Sano et al., 2007). In addition, deficiency of HEXIM-1, a nuclear protein that sequesters the P-TEFb in an inactive complex, has been shown to potentiate pathologic hypertrophy in vivo (Espinoza-Derout et al., 2009). In our studies, localization of BRD4 with promoter-enhancer

elements and the suppression of pause release with BET bromodomain inhibition in the TAC model (Figure 6) suggest BETs facilitate pause release at these gene loci. The robust induction of HEXIM1 expression we observed following BET bromodomain inhibition (Figures S5H–S5K) may also serve to suppress P-TEFb activity and reduce Pol II pause release. Concordant reductions in Ser2 phosphorylation of the Pol II CTD (Figure 6G and S5G), a specific target of the P-TEFb complex, both in vitro and in vivo, support these mechanisms of action. Defining the extent to which BETs alter transcriptional elongation through direct interactions with components of the P-TEFb complex (Bisgrove et al., 2007) or regulation of HEXIM-1 expression represent important avenues of future investigation.

Although evidence presented here does implicate BETs in the regulation of P-TEFb function and Pol II pause release during TAC, we cannot exclude additional effects of BET bromodomains on Pol II initiation at specific gene promoters. Consistent with our findings, other work has previously identified that Pol II pause release is a dominant mechanism for gene induction in both the developing heart and in the adult mouse heart during pressure overload, with de novo Pol II recruitment occurring at only 5% of induced genes in the TAC model (Sayed et al., 2013). Potential roles for BET bromodomain proteins in locus-specific Pol II initiation in the heart, or in other aspects of mRNA processing, are the subject of ongoing research by our group. Furthermore, the very recent discovery of asymmetrically loaded BRD4 on a critical subset of state-specific enhancers termed superenhancers (Lovén et al., 2013) raises the possibility that such superenhancers might also be active in the stressed myocardium and contribute to BET target specificity.

HF is known to progress via pathologic crosstalk between CMs and cardiac fibroblasts (van Berlo et al., 2013). Although the TAC model of HF provides a relatively focal stress to the heart, and JQ1 attenuates pathologic remodeling without effects on blood pressure or hemodynamic load (Figures S3C and S3D), we recognize that BET bromodomain inhibition in vivo may act on cardiac fibroblasts and other cell types that populate the stressed myocardium, in addition to the observed effects on CMs. We show here that BET bromodomain inhibition or *Brd4* knockdown in isolated NRVM both attenuate pathologic CM hypertrophy in vitro (Figure 1). In addition, we find that *Brd4* is the highest expressed BET gene in isolated CMs and in adult heart tissue. These data identify a cell-autonomous role for BRD4 in CMs in vitro and suggest that this protein might be an important target of BET bromodomain inhibitors in the heart in vivo. Future studies using cell type and temporally restricted gene deletion of *Brd4* and other BET family members in adult mice will help annotate their gene- and tissue-specific functions in experimental models of HF.

In conclusion, this study implicates a family of conserved epigenetic reader proteins as essential components of the transcriptional machinery that drives pathologic cardiac remodeling and HF. BET bromodomain proteins function as master regulatory TF coactivators that regulate pathologic pause release in the failing heart. The chemical biological approach leveraged here in rodent models of pathologic hypertrophy and HF provides a rationale for developing drug-like BET bromodomain inhibitors as investigational therapeutic agents in heart disease.

EXPERIMENTAL PROCEDURES

Animal Models

All protocols concerning animal use were approved by the Institutional Animal Care and Use Committee at Case Western Reserve University and conducted in accordance with the NIH Guide for the Care and Use of Laboratory Animals. All models were conducted in C57Bl/6J mice (Jackson Laboratories), which were maintained in a pathogen-free facility with standard light/dark cycling and access to food and water ad libitum.

Human Samples

LV samples from healthy human hearts were obtained as described (Hannenhalli et al., 2006; Margulies et al., 2005) in accordance with the Investigation Review Committee at the Hospital of the University of Pennsylvania, Philadelphia, PA. Nuclear protein was extracted using the NE-Per kit (Thermo Scientific, 78833) according to manufacturer's instructions. Gene expression profiles from left ventricles obtained from nonfailing versus failing human hearts were curated from a published data set (Hannenhalli et al., 2006).

Statistical Analysis

Data are reported as mean ± standard error. The statistical methods used in analysis of microarray and ChIP-seq data are detailed separately. Comparison of means between two groups was analyzed using a two-tailed Student's t test with Bonferroni correction for multiple comparisons. For all analyses, p values < 0.05 were considered significant.

ACCESSION NUMBERS

The GEO accession number for the ChIP-seq, mouse microarray, and rat microarray data is GSE48112. The GEO accession numbers for the individual GEO series corresponding to the ChIP-seq, mouse microarray, and rat microarray are GSE46668 (ChIP-seq), GSE48110 (mouse heart), and GSE48111 (NRVM).

SUPPLEMENTAL INFORMATION

Supplemental Information includes Extended Experimental Procedures, five figures, three tables, and four movies and can be found with this article online at http://dx.doi.org/10.1016/j.cell.2013.07.013.

ACKNOWLEDGMENTS

We are grateful to R. Young and P. Rahl for stimulating discussions; M. Berkeley and the late E. Fox (DFCI Microarray Core) for assistance with microarray experiments; Avery Whitlock for illustrations; and Tom Volkert, Jennifer Love, and Sumeet Gupta at the Whitehead Genome Core for assistance with genome sequencing. This research was supported by an NIH-R01 DK093821 and NIH-K08 HL086614, Individual Biomedical Research Award from The Hartwell Foundation, and the Visconsi Research Scholars Fund (S.M.H.); NIH-K08 CA128972, the Burroughs-Wellcome Fund, the Damon-Runyon Cancer Research Foundation, the Richard and Susan Smith Family Foundation, and the Next Generation Award (J.E.B.); U.S. Department of Defense (C.Y.L.); NIH-T32 HL105338 (M.A.A.); NIH-R01 HL105993 (K.B.M. and T.P.C); and NIH-K08 HL105678 (J.D.B.). Dr. Bradner is the scientific founder of Tensha Therapeutics, which is clinically translating drug-like derivatives of the JQ1 chemical probe of BET bromodomains used in this study, as cancer therapeutics. As such, the Dana-Farber Cancer Institute and Dr. Bradner have been granted minority equity in Tensha.

Received: April 30, 2013
Revised: May 30, 2013
Accepted: July 11, 2013
Published: August 1, 2013

REFERENCES

Banerjee, C., Archin, N., Michaels, D., Belkina, A.C., Denis, G.V., Bradner, J., Sebastiani, P., Margolis, D.M., and Montano, M. (2012). BET bromodomain inhibition as a novel strategy for reactivation of HIV-1. J. Leukoc. Biol. *92*, 1147–1154.

Bisgrove, D.A., Mahmoudi, T., Henklein, P., and Verdin, E. (2007). Conserved P-TEFb-interacting domain of BRD4 inhibits HIV transcription. Proc. Natl. Acad. Sci. USA *104*, 13690–13695.

Bousette, N., Chugh, S., Fong, V., Isserlin, R., Kim, K.H., Volchuk, A., Backx, P.H., Liu, P., Kislinger, T., MacLennan, D.H., et al. (2010). Constitutively active calcineurin induces cardiac endoplasmic reticulum stress and protects against apoptosis that is mediated by alpha-crystallin-B. Proc. Natl. Acad. Sci. USA *107*, 18481–18486.

Dawson, M.A., Kouzarides, T., and Huntly, B.J. (2012). Targeting epigenetic readers in cancer. N. Engl. J. Med. *367*, 647–657.

Delmore, J.E., Issa, G.C., Lemieux, M.E., Rahl, P.B., Shi, J., Jacobs, H.M., Kastritis, E., Gilpatrick, T., Paranal, R.M., Qi, J., et al. (2011). BET bromodomain inhibition as a therapeutic strategy to target c-Myc. Cell *146*, 904–917.

Eichler, G.S., Huang, S., and Ingber, D.E. (2003). Gene Expression Dynamics Inspector (GEDI): for integrative analysis of expression profiles. Bioinformatics *19*, 2321–2322.

Espinoza-Derout, J., Wagner, M., Salciccioli, L., Lazar, J.M., Bhaduri, S., Mascareno, E., Chaqour, B., and Siddiqui, M.A. (2009). Positive transcription elongation factor b activity in compensatory myocardial hypertrophy is regulated by cardiac lineage protein-1. Circ. Res. *104*, 1347–1354.

Filippakopoulos, P., Qi, J., Picaud, S., Shen, Y., Smith, W.B., Fedorov, O., Morse, E.M., Keates, T., Hickman, T.T., Felletar, I., et al. (2010). Selective inhibition of BET bromodomains. Nature *468*, 1067–1073.

Filippakopoulos, P., Picaud, S., Mangos, M., Keates, T., Lambert, J.P., Barsyte-Lovejoy, D., Felletar, I., Volkmer, R., Müller, S., Pawson, T., et al. (2012). Histone recognition and large-scale structural analysis of the human bromodomain family. Cell *149*, 214–231.

Hannenhalli, S., Putt, M.E., Gilmore, J.M., Wang, J., Parmacek, M.S., Epstein, J.A., Morrisey, E.E., Margulies, K.B., and Cappola, T.P. (2006). Transcriptional genomics associates FOX transcription factors with human heart failure. Circulation *114*, 1269–1276.

Hargreaves, D.C., Horng, T., and Medzhitov, R. (2009). Control of inducible gene expression by signal-dependent transcriptional elongation. Cell *138*, 129–145.

Heineke, J., Auger-Messier, M., Xu, J., Oka, T., Sargent, M.A., York, A., Klevitsky, R., Vaikunth, S., Duncan, S.A., Aronow, B.J., et al. (2007). Cardiomyocyte GATA4 functions as a stress-responsive regulator of angiogenesis in the murine heart. J. Clin. Invest. *117*, 3198–3210.

Hill, J.A., and Olson, E.N. (2008). Cardiac plasticity. N. Engl. J. Med. *358*, 1370–1380.

Jang, M.K., Mochizuki, K., Zhou, M., Jeong, H.S., Brady, J.N., and Ozato, K. (2005). The bromodomain protein Brd4 is a positive regulatory component of P-TEFb and stimulates RNA polymerase II-dependent transcription. Mol. Cell *19*, 523–534.

Jiang, Y.W., Veschambre, P., Erdjument-Bromage, H., Tempst, P., Conaway, J.W., Conaway, R.C., and Kornberg, R.D. (1998). Mammalian mediator of transcriptional regulation and its possible role as an end-point of signal transduction pathways. Proc. Natl. Acad. Sci. USA *95*, 8538–8543.

Lee, T.I., and Young, R.A. (2013). Transcriptional regulation and its misregulation in disease. Cell *152*, 1237–1251.

Levy, D., Garrison, R.J., Savage, D.D., Kannel, W.B., and Castelli, W.P. (1990). Prognostic implications of echocardiographically determined left ventricular mass in the Framingham Heart Study. N. Engl. J. Med. *322*, 1561–1566.

Lin, C.Y., Lovén, J., Rahl, P.B., Paranal, R.M., Burge, C.B., Bradner, J.E., Lee, T.I., and Young, R.A. (2012). Transcriptional amplification in tumor cells with elevated c-Myc. Cell *151*, 56–67.

Lovén, J., Hoke, H.A., Lin, C.Y., Lau, A., Orlando, D.A., Vakoc, C.R., Bradner, J.E., Lee, T.I., and Young, R.A. (2013). Selective inhibition of tumor oncogenes by disruption of super-enhancers. Cell *153*, 320–334.

Maier, H.J., Schips, T.G., Wietelmann, A., Krüger, M., Brunner, C., Sauter, M., Klingel, K., Böttger, T., Braun, T., and Wirth, T. (2012). Cardiomyocyte-specific IκB kinase (IKK)/NF-κB activation induces reversible inflammatory cardiomyopathy and heart failure. Proc. Natl. Acad. Sci. USA *109*, 11794–11799.

Margulies, K.B., Matiwala, S., Cornejo, C., Olsen, H., Craven, W.A., and Bednarik, D. (2005). Mixed messages: transcription patterns in failing and recovering human myocardium. Circ. Res. *96*, 592–599.

Matzuk, M.M., McKeown, M.R., Filippakopoulos, P., Li, Q., Ma, L., Agno, J.E., Lemieux, M.E., Picaud, S., Yu, R.N., Qi, J., et al. (2012). Small-molecule inhibition of BRDT for male contraception. Cell *150*, 673–684.

McKinsey, T.A., and Olson, E.N. (2005). Toward transcriptional therapies for the failing heart: chemical screens to modulate genes. J. Clin. Invest. *115*, 538–546.

Montgomery, R.L., Davis, C.A., Potthoff, M.J., Haberland, M., Fielitz, J., Qi, X., Hill, J.A., Richardson, J.A., and Olson, E.N. (2007). Histone deacetylases 1 and 2 redundantly regulate cardiac morphogenesis, growth, and contractility. Genes Dev. *21*, 1790–1802.

Nicodeme, E., Jeffrey, K.L., Schaefer, U., Beinke, S., Dewell, S., Chung, C.W., Chandwani, R., Marazzi, I., Wilson, P., Coste, H., et al. (2010). Suppression of inflammation by a synthetic histone mimic. Nature *468*, 1119–1123.

Patel, M.C., Debrosse, M., Smith, M., Dey, A., Huynh, W., Sarai, N., Heightman, T.D., Tamura, T., and Ozato, K. (2013). BRD4 coordinates recruitment of pause release factor P-TEFb and the pausing complex NELF/DSIF to regulate transcription elongation of interferon-stimulated genes. Mol. Cell. Biol. *33*, 2497–2507. http://dx.doi.org/10.1128/MCB.01180-12.

Peterlin, B.M., and Price, D.H. (2006). Controlling the elongation phase of transcription with P-TEFb. Mol. Cell *23*, 297–305.

Rahl, P.B., Lin, C.Y., Seila, A.C., Flynn, R.A., McCuine, S., Burge, C.B., Sharp, P.A., and Young, R.A. (2010). c-Myc regulates transcriptional pause release. Cell *141*, 432–445.

Rockman, H.A., Ross, R.S., Harris, A.N., Knowlton, K.U., Steinhelper, M.E., Field, L.J., Ross, J., Jr., and Chien, K.R. (1991). Segregation of atrial-specific and inducible expression of an atrial natriuretic factor transgene in an in vivo murine model of cardiac hypertrophy. Proc. Natl. Acad. Sci. USA *88*, 8277–8281.

Roger, V.L., Go, A.S., Lloyd-Jones, D.M., Benjamin, E.J., Berry, J.D., Borden, W.B., Bravata, D.M., Dai, S., Ford, E.S., Fox, C.S., et al.; American Heart Association Statistics Committee and Stroke Statistics Subcommittee. (2012). Executive summary: heart disease and stroke statistics—2012 update: a report from the American Heart Association. Circulation *125*, 188–197.

Sano, M., Abdellatif, M., Oh, H., Xie, M., Bagella, L., Giordano, A., Michael, L.H., DeMayo, F.J., and Schneider, M.D. (2002). Activation and function of cyclin T-Cdk9 (positive transcription elongation factor-b) in cardiac muscle-cell hypertrophy. Nat. Med. *8*, 1310–1317.

Sano, M., Minamino, T., Toko, H., Miyauchi, H., Orimo, M., Qin, Y., Akazawa, H., Tateno, K., Kayama, Y., Harada, M., et al. (2007). p53-induced inhibition of Hif-1 causes cardiac dysfunction during pressure overload. Nature *446*, 444–448.

Sayed, D., He, M., Yang, Z., Lin, L., and Abdellatif, M. (2013). Transcriptional regulation patterns revealed by high resolution chromatin immunoprecipitation during cardiac hypertrophy. J. Biol. Chem. *288*, 2546–2558.

Schreiber, S.L., and Bernstein, B.E. (2002). Signaling network model of chromatin. Cell *111*, 771–778.

Shen, Y., Yue, F., McCleary, D.F., Ye, Z., Edsall, L., Kuan, S., Wagner, U., Dixon, J., Lee, L., Lobanenkov, V.V., and Ren, B. (2012). A map of the cis-regulatory sequences in the mouse genome. Nature *488*, 116–120.

Simpson, P., McGrath, A., and Savion, S. (1982). Myocyte hypertrophy in neonatal rat heart cultures and its regulation by serum and by catecholamines. Circ. Res. *51*, 787–801.

Song, X., Kusakari, Y., Xiao, C.Y., Kinsella, S.D., Rosenberg, M.A., Scherrer-Crosbie, M., Hara, K., Rosenzweig, A., and Matsui, T. (2010). mTOR attenuates the inflammatory response in cardiomyocytes and prevents cardiac dysfunction in pathological hypertrophy. Am. J. Physiol. Cell Physiol. *299*, C1256–C1266.

Song, H.K., Hong, S.E., Kim, T., and Kim, H. (2012). Deep RNA sequencing reveals novel cardiac transcriptomic signatures for physiological and pathological hypertrophy. PLoS ONE *7*, e35552.

Subramanian, A., Tamayo, P., Mootha, V.K., Mukherjee, S., Ebert, B.L., Gillette, M.A., Paulovich, A., Pomeroy, S.L., Golub, T.R., Lander, E.S., and Mesirov, J.P. (2005). Gene set enrichment analysis: a knowledge-based approach for interpreting genome-wide expression profiles. Proc. Natl. Acad. Sci. USA *102*, 15545–15550.

Trivedi, C.M., Luo, Y., Yin, Z., Zhang, M., Zhu, W., Wang, T., Floss, T., Goettlicher, M., Noppinger, P.R., Wurst, W., et al. (2007). Hdac2 regulates the cardiac hypertrophic response by modulating Gsk3 beta activity. Nat. Med. *13*, 324–331.

van Berlo, J.H., Elrod, J.W., Aronow, B.J., Pu, W.T., and Molkentin, J.D. (2011). Serine 105 phosphorylation of transcription factor GATA4 is necessary for stress-induced cardiac hypertrophy in vivo. Proc. Natl. Acad. Sci. USA *108*, 12331–12336.

van Berlo, J.H., Maillet, M., and Molkentin, J.D. (2013). Signaling effectors underlying pathologic growth and remodeling of the heart. J. Clin. Invest. *123*, 37–45.

Wade, J.T., and Struhl, K. (2008). The transition from transcriptional initiation to elongation. Curr. Opin. Genet. Dev. *18*, 130–136.

Wei, J.Q., Shehadeh, L.A., Mitrani, J.M., Pessanha, M., Slepak, T.I., Webster, K.A., and Bishopric, N.H. (2008). Quantitative control of adaptive cardiac hypertrophy by acetyltransferase p300. Circulation *118*, 934–946.

Xie, X., Lu, J., Kulbokas, E.J., Golub, T.R., Mootha, V., Lindblad-Toh, K., Lander, E.S., and Kellis, M. (2005). Systematic discovery of regulatory motifs in human promoters and 3′ UTRs by comparison of several mammals. Nature *434*, 338–345.

Yang, Z., Yik, J.H., Chen, R., He, N., Jang, M.K., Ozato, K., and Zhou, Q. (2005). Recruitment of P-TEFb for stimulation of transcriptional elongation by the bromodomain protein Brd4. Mol. Cell *19*, 535–545.

Yoshikawa, N., Shimizu, N., Maruyama, T., Sano, M., Matsuhashi, T., Fukuda, K., Kataoka, M., Satoh, T., Ojima, H., Sawai, T., et al. (2012). Cardiomyocyte-specific overexpression of HEXIM1 prevents right ventricular hypertrophy in hypoxia-induced pulmonary hypertension in mice. PLoS ONE *7*, e52522.

Zhang, C.L., McKinsey, T.A., Chang, S., Antos, C.L., Hill, J.A., and Olson, E.N. (2002). Class II histone deacetylases act as signal-responsive repressors of cardiac hypertrophy. Cell *110*, 479–488.

Zhang, W., Prakash, C., Sum, C., Gong, Y., Li, Y., Kwok, J.J., Thiessen, N., Pettersson, S., Jones, S.J., Knapp, S., et al. (2012). Bromodomain-containing protein 4 (BRD4) regulates RNA polymerase II serine 2 phosphorylation in human CD4+ T cells. J. Biol. Chem. *287*, 43137–43155.

Zhao, M., Chow, A., Powers, J., Fajardo, G., and Bernstein, D. (2004). Microarray analysis of gene expression after transverse aortic constriction in mice. Physiol. Genomics *19*, 93–105.

Zhong, W., Mao, S., Tobis, S., Angelis, E., Jordan, M.C., Roos, K.P., Fishbein, M.C., de Alborán, I.M., and MacLellan, W.R. (2006). Hypertrophic growth in cardiac myocytes is mediated by Myc through a Cyclin D2-dependent pathway. EMBO J. *25*, 3869–3879.

Zuber, J., Shi, J., Wang, E., Rappaport, A.R., Herrmann, H., Sison, E.A., Magoon, D., Qi, J., Blatt, K., Wunderlich, M., et al. (2011). RNAi screen identifies Brd4 as a therapeutic target in acute myeloid leukaemia. Nature *478*, 524–528.

Cancer Cell
Article

Discovery and Characterization of Super-Enhancer-Associated Dependencies in Diffuse Large B Cell Lymphoma

Bjoern Chapuy,[1,7] Michael R. McKeown,[1,7] Charles Y. Lin,[1] Stefano Monti,[2] Margaretha G.M. Roemer,[1] Jun Qi,[1] Peter B. Rahl,[3,9] Heather H. Sun,[4] Kelly T. Yeda,[1] John G. Doench,[5] Elaine Reichert,[1] Andrew L. Kung,[6,10] Scott J. Rodig,[4] Richard A. Young,[3] Margaret A. Shipp,[1,8,*] and James E. Bradner[1,8,*]

[1]Department of Medical Oncology, Dana-Farber Cancer Institute, Boston, MA 02115, USA
[2]Section of Computational Biomedicine, Boston University School of Medicine, Boston, MA 02118, USA
[3]Whitehead Institute of Genome Research, Massachusetts Institute of Technology, Cambridge, MA 02142, USA
[4]Department of Pathology, Brigham and Women's Hospital, Boston, MA 02115, USA
[5]Broad Institute, Cambridge, MA 02142, USA
[6]Department of Pediatric Oncology, Dana-Farber Cancer Institute, Boston, MA 02215, USA
[7]These authors contributed equally to this work
[8]These authors contributed equally to this work
[9]Present address: Syros Pharmaceuticals, Watertown, MA 02472, USA
[10]Present address: Department of Pediatrics, Columbia University, New York, NY 10032, USA
*Correspondence: margaret_shipp@dfci.harvard.edu (M.A.S.), james_bradner@dfci.harvard.edu (J.E.B.)
http://dx.doi.org/10.1016/j.ccr.2013.11.003

SUMMARY

Diffuse large B cell lymphoma (DLBCL) is a biologically heterogeneous and clinically aggressive disease. Here, we explore the role of bromodomain and extra-terminal domain (BET) proteins in DLBCL, using integrative chemical genetics and functional epigenomics. We observe highly asymmetric loading of bromodomain 4 (BRD4) at enhancers, with approximately 33% of all BRD4 localizing to enhancers at 1.6% of occupied genes. These super-enhancers prove particularly sensitive to bromodomain inhibition, explaining the selective effect of BET inhibitors on oncogenic and lineage-specific transcriptional circuits. Functional study of genes marked by super-enhancers identifies DLBCLs dependent on OCA-B and suggests a strategy for discovering unrecognized cancer dependencies. Translational studies performed on a comprehensive panel of DLBCLs establish a therapeutic rationale for evaluating BET inhibitors in this disease.

INTRODUCTION

Diffuse large B cell lymphoma (DLBCL) is the most common form of non-Hodgkin's lymphoma in adults. The majority of DLBCLs arise from antigen-exposed B cells during the germinal center (GC) reaction, a process that optimizes the affinity of antibodies for antigens (Klein and Dalla-Favera, 2008). Despite significant advances in the biological understanding of DLBCL pathogenesis, current treatment regimens include empiric combination immuno/chemotherapy at induction and relapse. Mechanistic insights guiding the development of targeted therapeutic agents are urgently needed, as relapsed and refractory disease comprise significant unmet medical needs (Gisselbrecht et al., 2010).

DLBCL exhibits significant biological heterogeneity. Gene expression profiling has allowed functional classification of tumors into distinct subgroups. Presently, DLBCL is described using two transcriptional classifications, commonly referred to as the cell of origin (COO) and the consensus clustering classification (CCC). The COO classification relates subsets of DLBCL

Significance

Although oncogenic transcription factors underlie the pathophysiology and biological heterogeneity of diffuse large B cell lymphoma (DLBCL), studies of transcriptional coactivator proteins are limited in this disease. In this chemical genetic study, we demonstrate the efficacy of bromodomain and extra-terminal domain (BET) inhibition and characterize the broad function of BET bromodomains in supporting the transcriptional growth program in all subclasses of DLBCL, including coactivation of E2F and MYC target genes. We define an asymmetry in the localization of bromodomain 4 to enhancer regions nearby oncogenic and master regulatory genes and expand the finding to a representative panel of cell lines and primary samples. This finding likely explains the specific transcriptional effect of BET inhibition, which modulates the expression of master transcription factors that control B cell fate and germinal center formation.

to specific stages of normal B cell development, assigning tumors to either a germinal center-B (GCB) or activated B cell (ABC) subtype (Lenz and Staudt, 2010). The CCC classification defines three groups of DLBCLs on the basis of transcriptional heterogeneity solely within tumors. Here, DLBCL subtypes rely on B cell receptor (BCR) survival signals and glycolysis (BCR) or BCR-independent fuel utilization and oxidative phosphorylation (OxPhos), or they exhibit an increased inflammatory and immune cell infiltrate (host response) (Caro et al., 2012; Chen et al., 2013; Monti et al., 2005). Both classifications provide insights into disease pathogenesis and suggest potential tumor cell dependencies and rational therapeutic targets.

Several genome sequencing studies of DLBCL defining the mutational landscape have revealed substantial genetic heterogeneity (Lohr et al., 2012; Morin et al., 2011; Pasqualucci et al., 2011; Zhang et al., 2013). In contrast to Burkitt lymphoma (BL), another germinal center-derived tumor characterized by a hallmark t(8;14) translocation of *MYC* into the immunoglobulin heavy- or light-chain enhancer region, DLBCLs have high genotypic diversity. These tumors exhibit multiple low-frequency copy number alterations (CNAs), additional chromosomal translocations, and over 50 recurrent somatic mutations (Lohr et al., 2012; Monti et al., 2012; Morin et al., 2011; Pasqualucci et al., 2011). In DLBCL, the underlying biological and genetic heterogeneity are associated with highly variable clinical outcomes, ranging from long-term overall survival (“cure”) to rapidly progressive disease (Monti et al., 2012).

Mechanistically, the transcriptional heterogeneity of DLBCL is conferred, in part, by pathologic activation or inactivation of lineage-specific and growth-associated master regulatory transcription factors (TFs), including NF-κB (Lenz and Staudt, 2010), BCL6 (Basso and Dalla-Favera, 2012), MYC (Slack and Gascoyne, 2011), and p53 (Monti et al., 2012), and also through upstream pathway deregulation. Recently, we demonstrated that multiple, low-frequency CNAs converge functionally to deregulate p53 and cell cycle, resulting in increased proliferation and enhanced signaling from the master regulatory transcription factor E2F1 (Monti et al., 2012). In this study, deregulated cell cycle and increased expression of E2F1 target genes were associated with inferior outcome (Monti et al., 2012). In recent studies, a newly defined subset of “double-hit” DLBCLs that overexpress MYC in association with BCL2 also have an unfavorable outcome (Hu et al., 2013; Johnson et al., 2012). Together, these findings underscore the centrality of master regulatory TFs in DLBCL.

TFs control cancer cell state by binding proximal (promoter) and distal (enhancer) regulatory elements (Lee and Young, 2013). The subsequent recruitment of multiprotein complexes leads to local remodeling of chromatin, which establishes mitotic memory, and transmission of transcriptional signals to RNA polymerase II (RNA Pol II) poised at genes associated with growth and survival (Fuda et al., 2009; Schreiber and Bernstein, 2002). Chromatin associated with TF binding sites is markedly enriched in histone proteins posttranslationally modified by lysine side-chain acetylation (Marushige, 1976). This mark biophysically facilitates opening of chromatin and recruits an emerging class of coactivators that recognize ε-acetyl lysine through a specialized recognition motif or bromodomain (Owen et al., 2000).

Among the 46 known bromodomain-containing proteins (Filippakopoulos et al., 2012), the subfamily of bromodomain and extra-terminal domain (BET) coactivators (BRD2, BRD3, and BRD4) are particularly appealing targets in DLBCL. Structurally, BET proteins possess twin amino-terminal bromodomains that facilitate binding to hyperacetylated promoter/enhancer regions (Filippakopoulos et al., 2012; Zhang et al., 2012), as well as a distal carboxy-terminal binding site for the positive transcription elongation factor (P-TEFb; Bisgrove et al., 2007). In cancer, BET bromodomains promote M to G1 cell cycle progression (Yang et al., 2008) and contribute to mitotic memory (Dey et al., 2003; Zhao et al., 2011). Collaborative research from our group and others has recently identified a role for BET bromodomains in supporting the transcription of known DLBCL oncogenes (*MYC* and *BCL2*) in studies of acute leukemia, multiple myeloma, and BL (Dawson et al., 2011; Delmore et al., 2011; Mertz et al., 2011; Ott et al., 2012; Zuber et al., 2011). Interestingly, overexpression of BRD2 from an engineered immunoglobulin heavy-chain promoter-enhancer construct caused an aggressive B cell neoplasm resembling DLBCL in mice (Greenwald et al., 2004). Together, the findings establish a compelling hypothesis that BET bromodomains serve as chromatin-associated modulators of major gene regulatory pathways in DLBCL.

In an effort to study the role of BET bromodomains in cancer, we recently developed specific inhibitors of BET transcriptional coactivator proteins (Filippakopoulos et al., 2010), including a prototypical triazolo-diazepine inhibitor of the acetyl-lysine binding site, JQ1. Here, we explore the role of BET bromodomains in oncogenic transcription by master regulatory TFs and assess BRD4 as a therapeutic target in DLBCL.

RESULTS

BET Bromodomain Inhibition Exerts Pan-Subtype Growth Arrest in DLBCL and in BL

To assess the role of BET bromodomains as cancer cell dependencies in DLBCL, we first studied the effects of four structurally dissimilar BET bromodomain inhibitors on a comprehensive panel of 34 human lymphoma cell lines (21 DLBCL, capturing all transcriptionally defined subtypes, 6 BL, and 7 Hodgkin’s lymphoma [HL]; Table S1 available online) in comparative high-throughput format. In addition to the prototypical BET inhibitor JQ1 (JQ1S) (Filippakopoulos et al., 2010), we resynthesized, characterized, and tested an analogous thienodiazepine from Mitsubishi-Tanabe Pharmaceutical (Y803, OTX015; Oncoethix), which was developed for inflammatory bowel disease (Figure S1A; Miyoshi et al., 2009), a benzodiazepine inhibitor (iBET; Nicodeme et al., 2010), and a dimethylisoxazole inhibitor (iBET-151) from GlaxoSmithKline (Dawson et al., 2011). Analyses of cellular proliferation at 72 hr revealed a potent class effect of BET bromodomain inhibitors on the DLBCL and BL cell lines irrespective of subtype and the lack of effect of an inactive enantiomer, JQ1R (Figure 1A). The HL cell lines were comparatively less sensitive to BET inhibition and one HL line, L428, was resistant to all four compounds.

The effects of BET inhibition on growth over time, cell cycle progression, and apoptosis were then studied in a representative panel of nine DLBCL cell lines, using the L428 HL line as a negative control (Figures 1B, 1C, S1B, and S1C). BET inhibition with

JQ1 significantly attenuated growth in a dose-responsive manner in all tested DLBCL cell lines (Figure 1B). In three representative DLBCL cell lines, genetic depletion of BRD2 or BRD4 similarly decreased DLBCL proliferation, consistent with an on-target effect of JQ1 (Figures S1D–S1G). We observed a profound S phase and G2 peak reduction following JQ1 treatment, consistent with a G1 cell cycle arrest (Figures 1C and S1B). BET inhibition (500 nM) did not induce apoptosis in most cell lines studied, evidenced by low AnnexinV/7AAD staining (Figure S1C) and absence of a sub-G1 peak (Figure 1C). Neither enantiomeric (JQ1R) nor vehicle (DMSO) controls affected DLBCL proliferation or survival (Figures 1C, S1B, and S1C). Treatment with 500 nM JQ1 was similarly cytostatic in BL cell lines (Figure S1C). The L428 HL cell line was resistant to BET inhibition in all tested assays.

Efficacy of BET Inhibition in DLBCL Xenograft Models

We next explored the therapeutic potential of BET inhibition in two independent DLBCL xenotransplantation models (Figures 1D–1G and S1H–S1K). First, the human DLBCL cell line Ly1 was engineered to ectopically express firefly luciferase and mCherry, allowing surrogate measurement of tumor growth in vivo. Nonobese diabetic severe combined immunodeficiency IL2Rγ^{null} (NSG) mice xenotransplanted with Ly1-Luc-mCherry cells had a statistically significant reduction in tumor burden when treated with JQ1 (30 mg twice daily by intraperitoneal [IP] injection; Figure 1D). A representative cohort of animals was sacrificed on day 13 of treatment for full hematological analysis. JQ1-treated animals had significantly decreased lymphoma infiltration of the bone marrow (BM) as measured by flow cytometric assessment of mCherry$^+$ cells (Figure 1E). Morphological and immunohistochemical analyses revealed that the highly proliferative (Ki67$^+$) human CD20$^+$ lymphoma cell infiltrate (Figure 1F, upper panel) was markedly reduced in animals treated with the BET bromodomain inhibitor (Figure 1F, lower panel). In the remainder of the Ly1 xenograft cohort, the JQ1-treated mice had a significant median overall survival advantage of 9 days ($p = 0.003$; Figure 1G).

To confirm the pharmacodynamic findings, a second xenotransplantation model was established using the Toledo DLBCL cell line. NSG mice with established tumors had delayed tumor progression when treated with JQ1 (Figure S1H). Full hematological analysis revealed that JQ1-treated animals had lower spleen weights (Figure S1I) and decreased lymphomatous infiltration of bone marrow and spleen (Figure S1J). Morphological and immunohistochemical analysis of the BM revealed significantly reduced the infiltration of CD20$^+$/Ki67$^+$ human lymphoma cells following BET inhibition (Figure S1K).

BET Inhibition Downregulates Oncogenic Transcriptional Pathways

To gain insights into the transcriptional pathways regulated by BET bromodomain coactivator proteins, we performed kinetic transcriptional profiling of vehicle- and JQ1-treated DLBCL cell lines. Five human DLBCL cell lines that captured the recognized transcriptional heterogeneity (Ly1, BCR/GCB; DHL6, BCR/GCB; Ly4, OxPhos/unclassified; Toledo, OxPhos/unclassified; and HBL1, BCR/ABC) were treated with JQ1 (500 nM) or vehicle control for 0, 2, 6, 12, 24, and 48 hr. At each time point, differential analysis was performed between the vehicle- and JQ1-treated samples (24 hr comparison, fold change (FC) > 1.3, false discovery rate (FDR) < 0.01; Figure S2A). Consistent with prior studies of BET bromodomain function and inhibition, HEXIM1 was markedly upregulated by JQ1 in all DLBCL cell lines (Figure S2B; Bartholomeeusen et al., 2012; Puissant et al., 2013).

The most differentially expressed genes were assessed for pathway enrichment using a comprehensive pathway compendium (C2, CP; MSigDB 3.0), and each time point was ranked by FDR and visualized as a color-coded matrix (Figure 2A; full list in Table S2). We observed the early downregulation of MYD88/toll-like receptor (TLR) pathway components following JQ1 treatment, including TLR10 and MYD88 (Figures 2A–2C and S2C). These data are consistent with previous studies in which the anti-inflammatory effect of BET inhibition in normal B cells was attributed to TLR pathway downregulation (Nicodeme et al., 2010). In the JQ1-treated DLBCL cell lines, we also observed downregulation of multiple components of the BCR signaling pathway, E2F transcriptional targets, and additional cell cycle transition gene sets (Figures 2A and S2D). Similar results were obtained when GCB and ABC DLBCL cell lines were analyzed separately (Figures S2E and S2F).

BET Inhibition Modulates MYC and E2F Target Gene Transcription

Cell state transitions are influenced by the function of specific regulatory TFs. To identify candidate TFs associated with BET bromodomain coactivators, we assessed the effects of JQ1 on sets of genes with common TF binding motifs (C3; MSigDB 3.0). The differentially expressed genes in vehicle- versus JQ1-treated DLBCL cell lines were tested for enrichment of candidate TF targets at 2–48 hr. Results at each time point were ranked by FDR and visualized as a color-coded matrix (Figure 2D; Table S2).

It is of interest that gene sets with MYC and E2F binding motifs were significantly downregulated following JQ1 treatment (Figure 2D). To further evaluate the effects of BET bromodomain inhibition on MYC and E2F transcriptional programs, we used multiple functionally validated MYC and E2F target gene sets to perform directed pathway analyses. Following JQ1 treatment, there was highly significant early downregulation of well-defined and functionally validated MYC and E2F target gene sets (Figures 2E, 2F, S2G, and S2H). In complementary studies, we performed gene set enrichment analyses (GSEA) of multiple independent MYC and E2F target gene sets in vehicle- versus JQ1-treated samples and found that MYC and E2F targets were significantly less abundant in JQ1-treated cells (Figures 2F, S2I, and S2J).

BET bromodomain proteins may function as coactivators of the MYC and E2F proteins and/or as direct modulators of MYC and E2F expression. To distinguish between these possibilities, we assessed the transcript abundance and protein levels of MYC and E2F in vehicle- and JQ1-treated DLBCLs. BET bromodomain inhibition resulted in an apparent decrease in MYC transcripts and protein in each of the DLBCL cell lines (Figures 2G, S2K, and S2L), suggesting that BET bromodomains directly modulate MYC transcription. The consequences of MYC downregulation following BET inhibition have been characterized by our group and others in hematologic malignancies

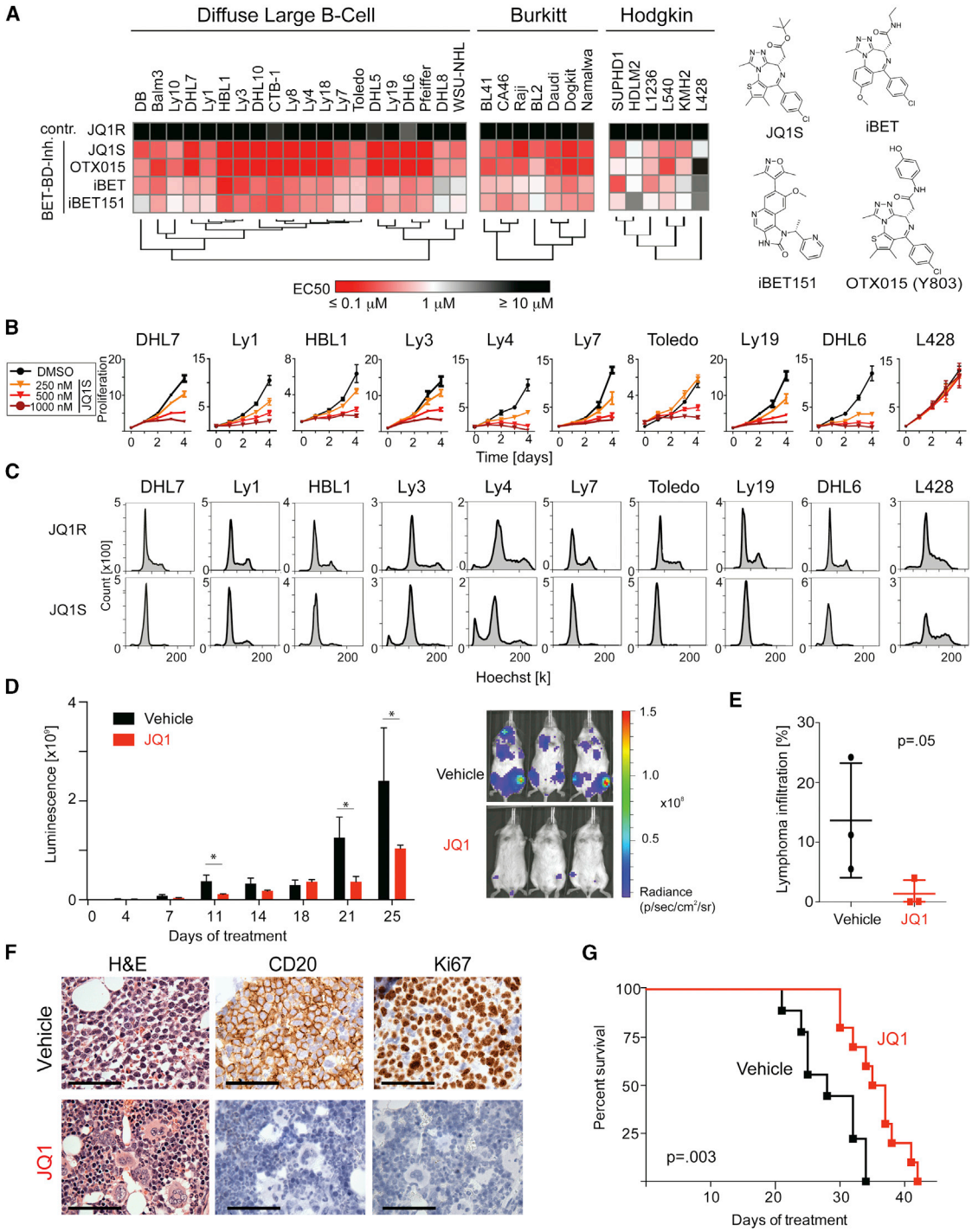

Figure 1. In Vitro Analyses of BET Bromodomain Inhibition in Various B Cell Lymphomas

(A) Hierarchical clustering of mean EC_{50}s of the four BET inhibitors (72 hr treatment) in the indicated panel of B cell lymphoma cell lines. EC_{50} values in a colorimetric scale: very sensitive ($\leq$1 μM) in red, sensitive (=1 μM) in white, to resistant ($\geq$10 μM) in black. Corresponding structures are shown.

(B) Proliferation of the indicated DLBCL and HL cell lines treated with vehicle or 250-1000 nM JQ1 for 1-4 days.

(C) Cell cycle analysis following 72 hr treatment with JQ1 (500 nM) or inactive enantiomer JQ1R (500 nM). Error bars represent the SD of triplicates.

(D) Bioluminescence of JQ1 (30 mg/kg IP twice daily) or vehicle-treated NSG mice xenotransplanted with luciferized mCherry$^+$ Ly1 cells. Asterisks indicate $p < 0.05$ using a one-sided t test. Error bars represent SEM.

(E) Lymphoma infiltration of BM in a representative set of animals was assessed by flow cytometric analysis of mCherry+ cells and visualized as scatter plots (median, line; whiskers, SEM). The p values were obtained with a one-sided Mann-Whitney U test.

(legend continued on next page)

(Dawson et al., 2011; Delmore et al., 2011; Mertz et al., 2011; Zuber et al., 2011). Notably, ectopic expression of MYC in DLBCL cell lines failed to rescue the antiproliferative effects of JQ1 (Figures S2M–S2O), also consistent with a model in which BET bromodomains function as coactivators of MYC target gene transcription. In contrast to effects on MYC expression, in four of five cell lines, JQ1 treatment did not measurably alter E2F1 transcript or protein abundance over 24 hr (Figures 2G, S2P, and S2Q). These data suggest that BET bromodomains may function at regulatory elements at E2F1 target genes, rather than by influencing the abundance of E2F1 itself.

BET Bromodomains as Promoter-Bound Coactivators of E2F1-Dependent Transcription

To explore the role of BETs as coactivators of oncogenic E2F1 transcriptional signaling, we performed chromatin immunoprecipitation with massively parallel sequencing (ChIP-seq), using a chemical genetic approach. We selected Ly1 cells for mechanistic consideration owing to the robust downregulation of E2F target genes in the transcriptional profiling (Figure S3A) and the lack of effect of JQ1 on E2F1 protein expression (Figure 2G). Changes in BET localization, chromatin structure, and RNA polymerase function were studied in Ly1 cells treated with JQ1 (500 nM) or vehicle control.

First, we established a chromatin landscape for Ly1 using H3K4me3 to identify promoters, H3K27ac to reveal enhancers, and H3K27me3 to define repressive regions of the genome. Then, we assessed the genome-wide localization of E2F1 and the representative BET protein, BRD4, also by ChIP-seq using the respective antibodies. Rank ordering of all transcriptionally active promoters based on H3K4me3 enrichment and RNA Pol II occupancy identifies pervasive binding of BRD4 and E2F1 to active promoter elements (Figure 3A). Analysis of enrichment data as a metagene of all active promoters centered on the transcription start site reveals spatial colocalization of E2F1 and BRD4 at all transcriptionally active promoters (Figure 3B).

ChIP-seq for E2F1 allowed the annotation of an E2F1 target gene set, based on the top promoter-bound genes in Ly1 cells (Table S3). Using a gene set of the top 100 ChIP-seq-defined E2F1 targets (Table S3), we performed GSEA in Ly1 and additional DLBCL cell lines DHL6, Ly4, Toledo, and HBL1. JQ1 treatment significantly decreased the transcript abundance of our functionally defined E2F1 targets at 24 hr and 48 hr in all cell lines studied (Figures 3C and S3A). The E2F1 dependency of these DLBCL cell lines as previously reported (Monti et al., 2012) was validated herein by genetic depletion in three representative cell lines (Figures 3D, 3E, S3B, and S3C). Together, these data mechanistically establish BET bromodomains as E2F1 coactivators in DLBCL.

Disproportionate Binding of BRD4 to Overloaded Enhancers

At the time this research was initiated, studies of BET bromodomains mainly focused on effects at promoter regions of the genome. Our research in multiple myeloma identified a role for BRD4 in enforcing MYC transcription from the translocated immunoglobulin H (IgH) enhancer locus (Delmore et al., 2011), where massive accumulation of BRD4 was identified by ChIP (approximately 200-fold enrichment). As oncogenic TFs may signal to RNA Pol II through distal enhancer elements, we sought to characterize the genome-wide localization of BRD4 to enhancers in DLBCL.

Rank ordering of enhancer regions by H3K27ac enrichment reveals that BRD4 binds to the vast majority of active enhancers in the Ly1 DLBCL genome (Figure 4A, blue and red tracks). Given the established role of BCL6 in the pathogenesis of DLBCL, we also documented genome-wide colocalization of BRD4 and BCL6 at H3K27ac-defined enhancers (Figure 4A, orange tracks). A metagene for active enhancers illustrates focal, superimposable enrichment for BRD4 with H3K27ac (Figure 4B). The correlation between BRD4 occupancy and H3K27 acetylation is extremely strong genome wide, with 79.1% of H3K27ac regions containing BRD4 and 92.2% of all chromatin-bound BRD4 occurring in regions marked by H3K27ac (Figure 4C). Genome-wide binding data for BRD4 reveal that BRD4 is most commonly associated with enhancer regions, defined by the presence of H3K27ac and absence of H3K4me3 (Figure 4D).

As predicted, BRD4 load is asymmetrically distributed throughout the genome at enhancer sites. Completely unexpected is the magnitude by which BRD4 load varies among active enhancer regions (Figure 4E). Only a small subset of BRD-loaded enhancers, 285/18,330 (1.6%), account for 32% of all of the BRD4 enhancer binding in the cell (Figure 4E; Table S4). The BRD4-loaded enhancers in the Ly1 DLBCL cell line are considerably larger than typical enhancer elements, resembling the super-enhancers (SEs) we recently described with Richard Young (Lovén et al., 2013).

Notably, the top two gene loci with BRD4-loaded enhancers, *POU2AF1* (which encodes the OCA-B transcriptional coactivator protein) and *BCL6,* and additional genes with disproportionally BRD4-loaded enhancers such as *PAX5* and *IRF8* (Figure 4E), are essential for B cell fate determination and germinal center formation (Basso and Dalla-Favera, 2012; Klein and Dalla-Favera, 2008; Teitell, 2003; Wang et al., 2008). In fact, mice with genetic ablation of *POU2AF1*, *BCL6*, *PAX5*, or *IRF8* lack the ability to form germinal centers, the physiological structures from which most DLBCLs arise (Cobaleda et al., 2007; Nutt et al., 2011; Teitell, 2003; Wang et al., 2008; Ye et al., 1997). Additionally, BRD4-superloaded enhancers are found adjacent to known oncogenes relevant to DLBCL biology, such as *CD79B* and *MYC* (Figures S4A and S4B).

These data indicate that BRD4 is predominantly an enhancer-associated factor, which distributes throughout DLBCL euchromatin in a highly asymmetric manner, adjacent to known oncogenes and lineage-specific transcription factors (Figure 4E). BET bromodomain inhibition selectively decreased the transcript abundance of the 285 genes with the most BRD4-loaded SEs, in contrast to the 285 genes with the least BRD4-loaded

(F) Immunohistochemical analysis of lymphoma (Ly1) BM infiltration in JQ1- and vehicle-treated mice: hematoxylin and eosin (H&E), anti-human CD20, and anti-Ki67 immunostaining. Scale bar represents 100 μm.
(G) Kaplan-Meier plot of the remainder of the Ly1 cohort (n = 21) treated with either vehicle or JQ1 30 mg/kg twice daily. The p value was obtained by log rank test. See also Figure S1 and Table S1.

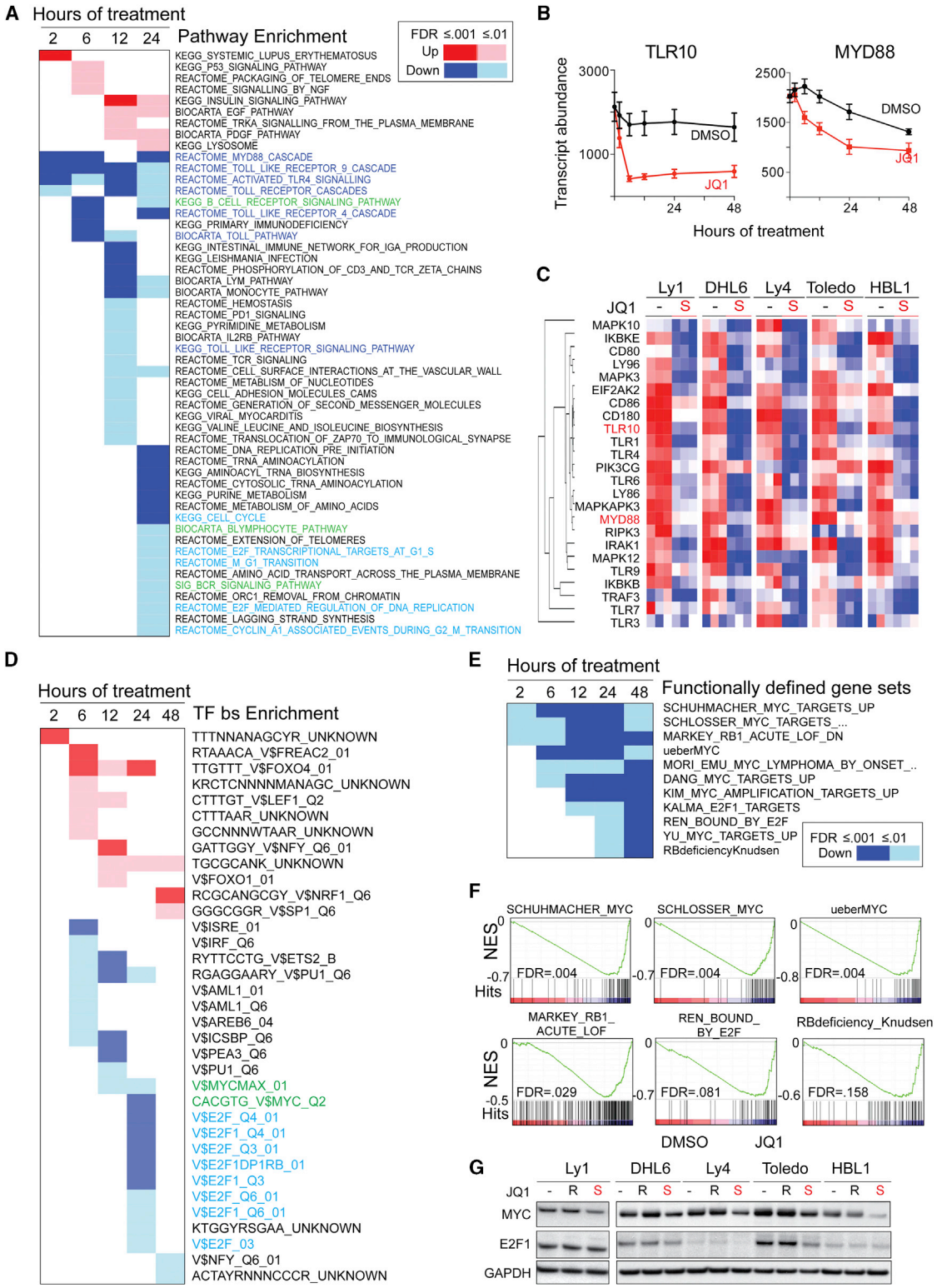

Figure 2. Transcriptional Response to BET Inhibition in Representative DLBCL Cell Lines

(A) Hyperenrichment analysis of differentially expressed genes in all five lines (FDR < 0.01; FC > 1.3) following 24 hr of treatment with 500 nM JQ1 or vehicle was performed using a pathway compendium (MSigDB, C2.CP). Results at each time point were ranked by FDR and visualized as a color-coded matrix. Upregulated pathways are in red, and downregulated pathways are in blue. Intensity of color correlates with FDR significance level. Highlighted pathways include: TLR/MYD88, blue; BCR signaling, green; and cell cycle/E2F, cyan.

(legend continued on next page)

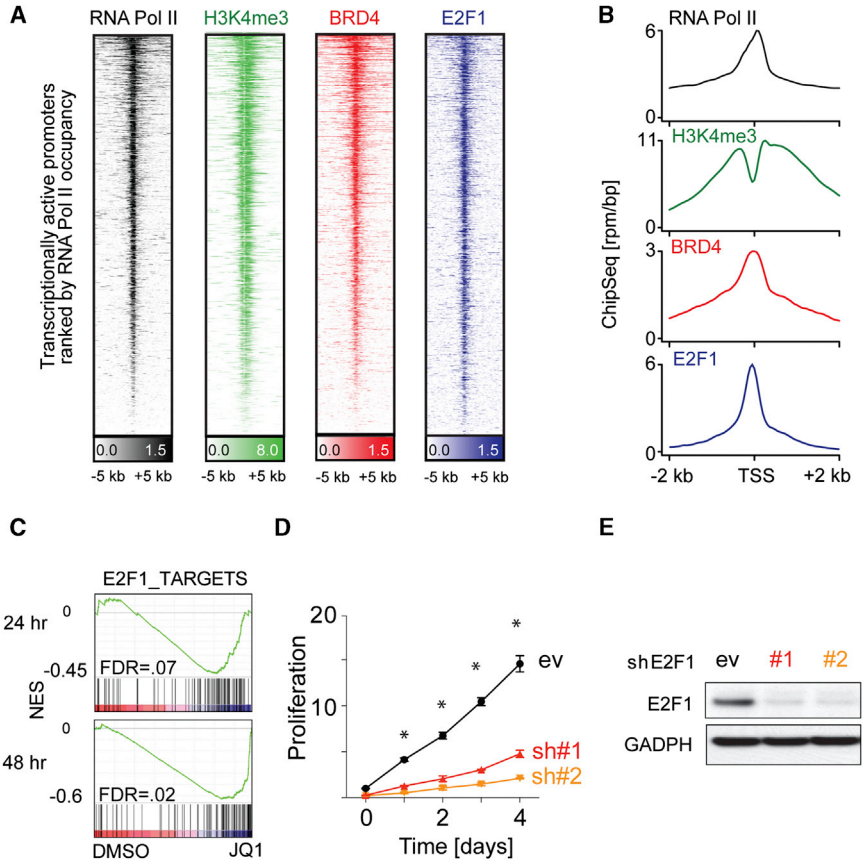

Figure 3. Colocalization and Function of BRD4 and E2F1 at Active Promoters

(A) Heatmap of ChIP-seq reads for RNA Pol II (transcriptionally active; black), H3K4me3 (green), BRD4 (red), and E2F1 (blue) rank ordered from high to low RNA Pol II occupancy centered on a ±5 kb window around the TSS of all transcriptionally active promoters. Color density reflects enrichment; white indicates no enrichment.

(B) Metagenes created from normalized genome-wide average of reads for designated factors centered on a ±2 kb window around the TSS.

(C) GSEA plots of a ChIP-seq-defined E2F1 target gene set in the five DLBCL cell lines treated with vehicle versus JQ1 for 24 and 48 hr.

(D) Assessment of proliferation in Ly1 cell line following genetic depletion of E2F1 with two independent hairpins and a control hairpin (ev). Error bars represent SD, and asterisks show $p < 0.01$ by a two-sided Student's t test.

(E) Immunoblot of E2F1 of cells in (D) to demonstrate knockdown efficiency.

See also Figure S3 and Table S3.

enhancers (Figure 4F). Similar results were obtained using H3K27ac as surrogate enhancer mark (Figure S4C). Taken together, these data suggest that BRD4 loading of select DLBCL enhancers underlies the pathway-specific transcriptional consequences of BET inhibition.

JQ1 Targets the *POU2AF1* SE and Decreases OCA-B Expression and Activity

The *POU2AF1* locus emerged as the most BRD4-overloaded enhancer in the Ly1 DLBCL cell line (Figure 4E), prompting further analysis of the effect of BET inhibition on OCA-B expression and function. OCA-B is a gene regulatory factor that interacts with the OCT1 and OCT2 TFs at octamer motifs and regulates B cell development, maturation, and GC formation (Teitell, 2003). Although OCA-B is expressed throughout B cell development, it is most abundant in normal GCB cells and GC-derived tumors, including DLBCL (Greiner et al., 2000).

POU2AF1 has a large H3K27ac-defined enhancer with strong BRD4 binding that is abolished by JQ1 treatment (Figure 5A). Consistent with this observation, BET inhibition reduced RNA Pol II elongation of *POU2AF1*, with a relative increase in promoter-paused RNA Pol II near the transcriptional start site (TSS; Figure 5B). Notably, intronic enrichment for H3K4me3 and RNA Pol II was observed in *POU2AF1*, consistent with an alternate promoter element, which was also affected by JQ1 treatment. JQ1 treatment (500 nM) decreased OCA-B transcript abundance and protein expression in Ly1 (Figure 5C), as well as additional DLBCL cell lines (Figure S5A).

We next assessed the consequences of JQ1 treatment on the OCA-B transcriptional program by performing GSEA with a well-defined series of OCA-B target genes (Table S5, modified from Teitell, 2003). OCA-B targets were downregulated in JQ1-treated DLBCLs as illustrated in Ly1 (Figure 5D) and recapitulated in the full DLBCL panel (Figures S5B and S5C). OCA-B depletion with two independent small hairpin RNAs (shRNAs) significantly decreased the proliferation of Ly1 (Figure 5E), and enforced expression of OCA-B partially rescued the JQ1-mediated antiproliferative effects (Figures S5D and S5E). Genetic depletion of either BRD2 or BRD4 phenocopied the JQ1-mediated reduction of OCA-B (Figures 5F, 5G, S5F, and S5G).

(B) Mean transcript abundance of TLR10 (left) and MYD88 (right) in all five lines. Error bars represent SEM.

(C) Heatmap of TLR pathway components in vehicle- or JQ1-treated DLBCLs (all five lines; 24 hr).

(D) The most differentially expressed genes (FDR < 0.01; FC > 1.3) were analyzed for common TF binding sites in the regulatory region using the MSigDB.C3 compendium. Results at each time point were ranked using a color-coded matrix as in (A). Genes with MYC binding sites are in green and E2F binding sites are in cyan.

(E) GSEA of multiple functionally defined MYC and E2F TF target gene sets was performed. Results are reported over time in a color-coded matrix with color intensity reflecting significance level.

(F) GSEA plots of functionally defined MYC and E2F target gene sets in vehicle- versus JQ1-treated cells at 24 hr.

(G) Protein abundance of MYC and E2F in the indicated DLBCL lines treated with vehicle or JQ1S or JQ1R (500 nM; 24 hr).

See also Figure S2 and Table S2.

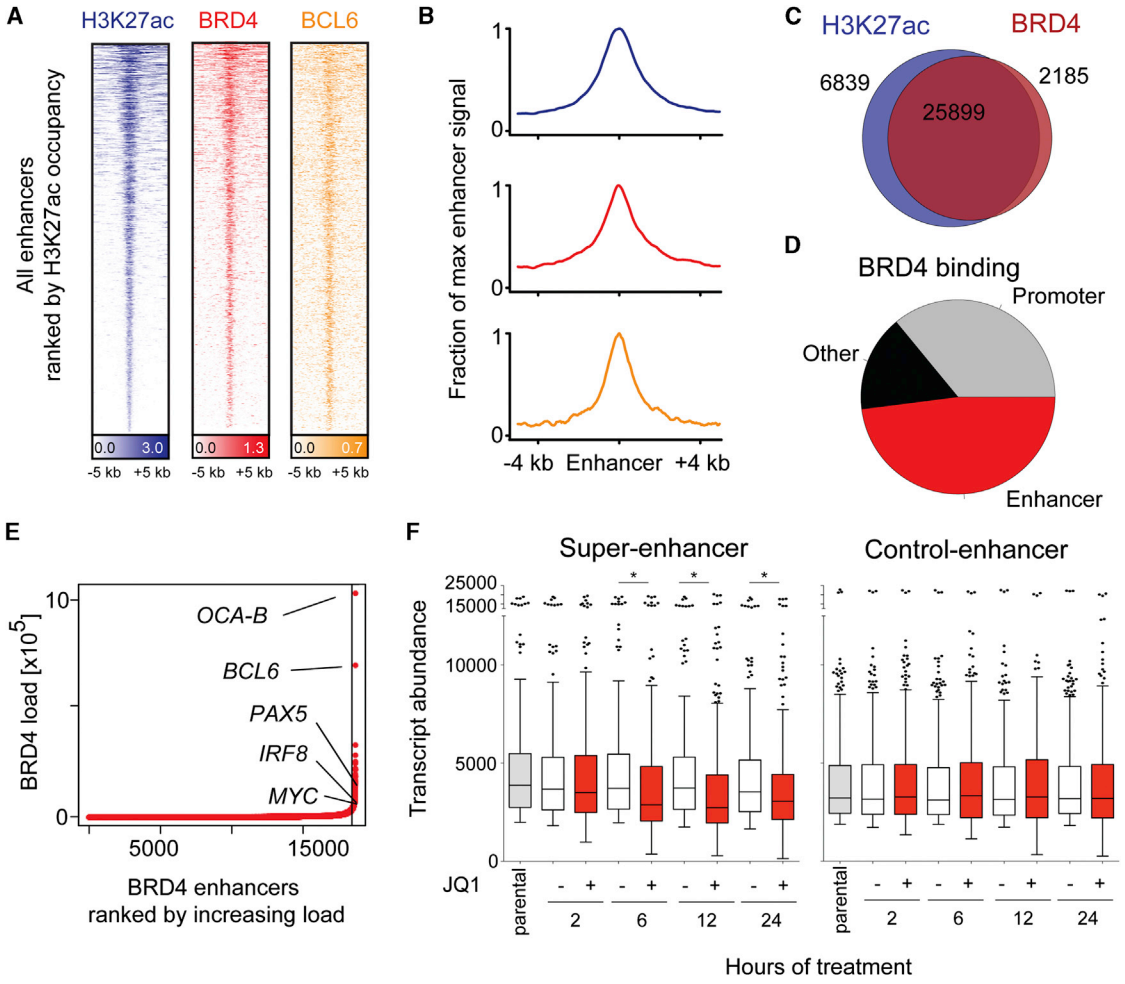

Figure 4. Asymmetric BRD4 Loading at Enhancer Elements of Actively Transcribed Genes

(A) Heatmap of ChIP-seq binding for H3K27ac (blue), BRD4 (red), and BCL6 (orange) rank ordered from high to low H3K27 occupancy centered on a ±5 kb window around enhancers. Color density reflects enrichment; white indicates no enrichment.

(B) Metagenes created from normalized genome-wide average of reads for designated factors centered on a ±4 kb window around the enhancers.

(C) Venn diagram of BRD4 binding and H3K27ac occupancy. A total of 79.1% of H3K27ac regions contain BRD4, and 92.2% of all chromatin-bound BRD4 occurs within H3K27ac regions.

(D) Pie chart of BRD4 binding to regions of the genome. BRD4 colocalization with H3K27ac without H3K4me3 defined as enhancer-bound (red); BRD4 colocalization with H3K4me3 reported as promoter-bound (gray); and remaining genomic regions in "other" (black).

(E) BRD4 loading/binding across enhancers of 18,330 genes. A total of 1.6% (285/18,330) of enhancers contain 32% of all enhancer-bound BRD4, with super-loading defined as surpassing the inflection point. Top BRD4-superloaded enhancers are indicated.

(F) Mean transcript abundance of the genes associated with the 285 most and least BRD4-loaded enhancers (left and right panel, respectively) in five DLBCL cell lines treated with vehicle or JQ1 (2–24 hr). Asterisks indicate a $p < 0.0001$ obtained using a two-sided Mann-Whitney U test.

See also Table S4 and Figure S4.

Together, these data underscore the importance of OCA-B to DLBCL growth and illustrate the use of SEs to identify cancer dependencies.

JQ1 Targets SEs of Additional Critical B Cell TFs and Modulates the GC Program

Three of the master regulatory TFs with BRD4-loaded SEs (*BCL6, IRF8*, and *PAX5*) promote and maintain the B cell gene expression program and limit differentiation into antibody-secreting plasma cells (Nutt et al., 2011). For these reasons, we further assessed the functional consequences of BET inhibition on the critical B cell TFs with BRD4-loaded SEs.

Given the known oncogenic function of deregulated BCL6 in GC B cells (Basso and Dalla-Favera, 2012) and the sensitivity of certain DLBCLs to BCL6 depletion (Polo et al., 2007), we first evaluated the consequences of BET inhibition on BCL6 expression and function. The *BCL6* locus includes a large previously defined upstream enhancer (Ramachandrareddy et al., 2010) that is severely depleted of BRD4 upon JQ1 treatment (Figure 6A). Consistent with depletion of BRD4 from the *BCL6* enhancer, the promoter reveals a suggestion of increased RNA Pol II pausing and reduced elongating RNA Pol II (Figure 6B). JQ1 treatment markedly decreased *BCL6* transcript abundance and protein expression in Ly1 (Figures 6C and 6D) and additional

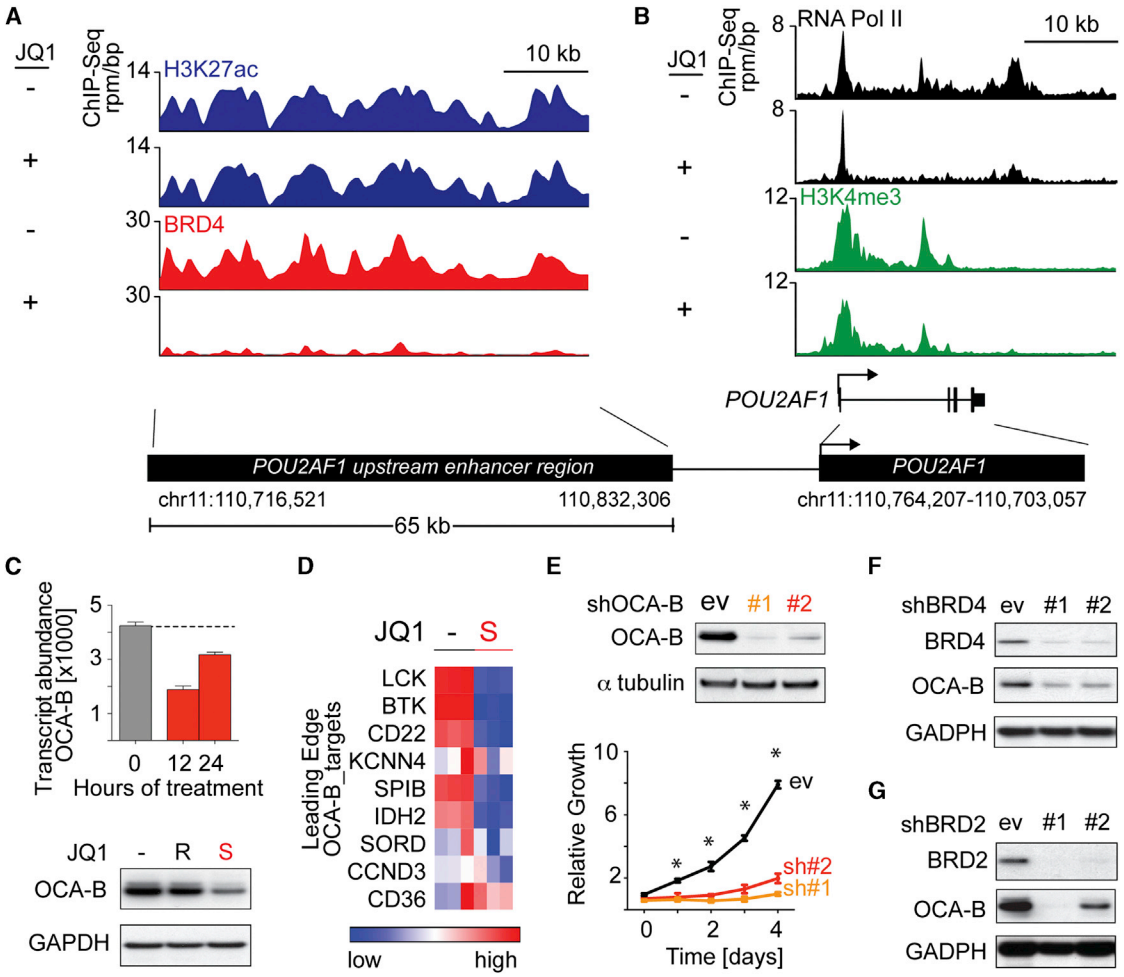

Figure 5. Identification of OCA-B as a DLBCL Dependency by SE Analysis

(A) ChIP-seq binding density for H3K27ac (blue) and BRD4 (red) at the enhancer of *POU2AF1* following JQ1 (+) or vehicle (DMSO; –) treatment.

(B) ChIP-seq reads at the *POU2AF1* promoter for RNA Pol II (black) and H3K4me3 (green) following JQ1 (+) or vehicle (–) treatment.

(C) OCA-B transcript and protein abundance in Ly1 cells treated with vehicle or 500 nM JQ1 or JQ1R (24 hr). Error bars represent SD.

(D) OCA-B target genes (leading edge, OCA-B GSEA) in Ly1 cells treated with vehicle or 500 nM JQ1 are visualized as heatmap.

(E) Knockdown efficacy of two independent OCA-B shRNAs was detected by western blot (top panel). Proliferation of OCA-B-depleted cells was measured by alamar blue. The p values for control versus each OCA-B shRNA were delineated by two-sided Student's t test; asterisks show $p < 0.01$. Error bars represent SD.

(F and G) Knockdown efficiency of two independent shRNAs against BRD4 (F) or BRD2 (G) and the associated changes in OCA-B expression were evaluated by western blot.

See also Figure S5 and Table S5.

DLBCL lines (Figure S6A). Interestingly, the observed broad localization of BCL6 to its enhancer region was reduced by JQ1 (Figures 6A and 6B), a finding we confirmed by ChIP-quantitative PCR (Figure S6B). This may reflect an influence of BET inhibition on TF binding or a consequence of downregulation of BCL6 by JQ1. Similarly, *PAX5* and *IRF8* also have BRD4-loaded SEs that are severely depleted of BRD4 following JQ1 treatment (Figure 6E). BET inhibition also decreased PAX5 and IRF8 transcript abundance and protein expression (Figures 6F and 6G).

SE Clustering Identifies Transcriptional Subtypes of DLBCL

Using the robust H3K27ac mark to identify and discriminate SEs, we conducted ChIP-seq SE analysis on five additional human DLBCL lines (DHL6, BCR/GCB; HBL1 and Ly3, BCR/ABC; Toledo and Ly4, OxPhos/unclassified; Table S7) and a normal lymphoid sample (tonsil; Table S7). Asymmetric enhancer loading was detected in all of the DLBCL cell lines (Figures 7A–7C) and the normal tonsil (Figure 7D), confirming the ubiquitous nature of this epigenomic structural element.

In all of the DLBCL cell lines and normal tonsil, large SEs were identified adjacent to genes encoding master TFs such as PAX5, OCA-B, and IRF8 (Figures 7A–7F, tracks; Table S7) that maintain the B cell program and limit plasma cell differentiation. Given the critical role of these master regulatory TFs in maintaining GC integrity and limiting GC exit (Nutt et al., 2011), we functionally assessed the consequences of BET inhibition on the GC program in all DLBCL cell lines. To that end, we

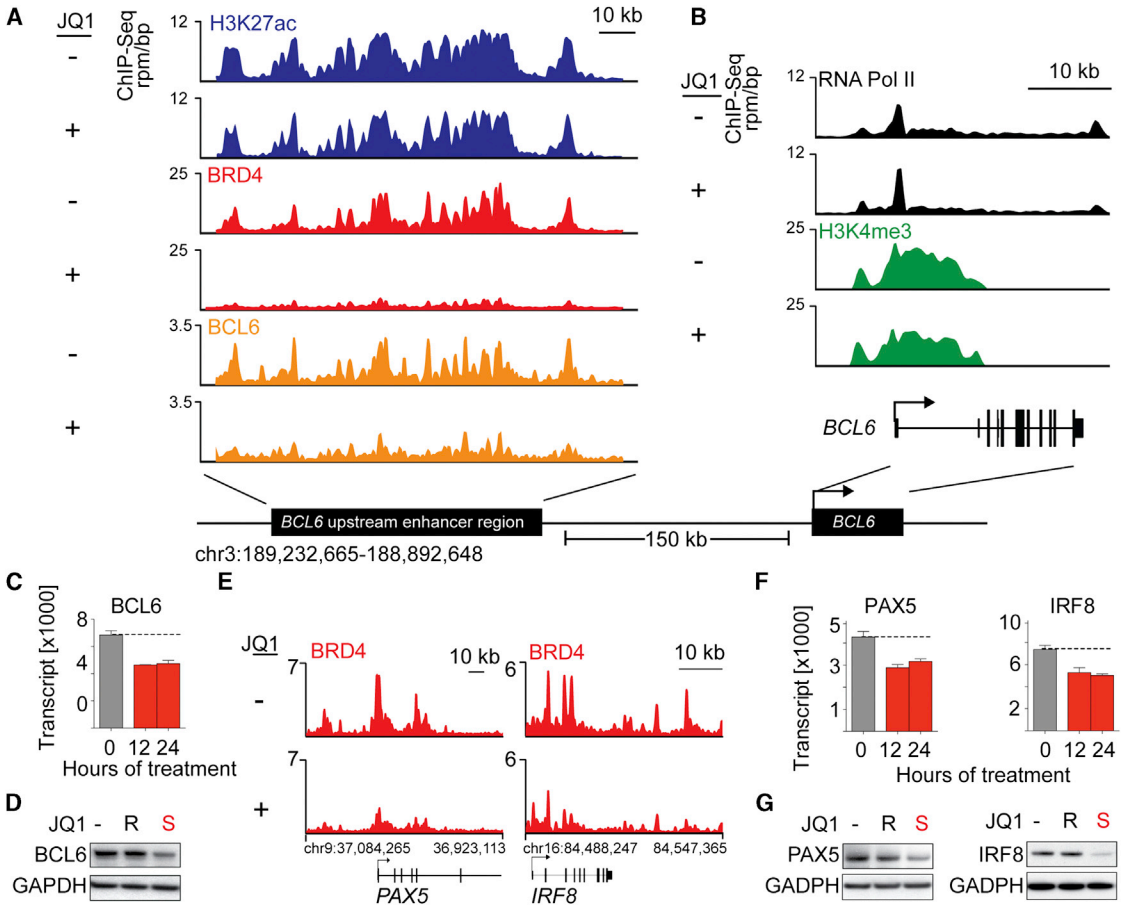

Figure 6. BET Inhibition Modulates Tissue-Specifying TF Expression by Disrupting SEs

(A) ChIP-seq binding density for H3K27ac (blue), BRD4 (red), and BCL6 (orange) at the *BCL6* enhancer following JQ1 (+) or vehicle (DMSO; −) treatment.

(B) ChIP-seq reads at the *BCL6* promoter for RNA Pol II (black) and H3K4me3 (green) following JQ1 (+) or vehicle (−) treatment.

(C) BCL6 transcript abundance in Ly1 cells 12 and 24 hr following vehicle or JQ1 treatment (derived from GEP data). Error bars represent SD.

(D) BCL6 protein abundance following treatment with vehicle or JQ1 or JQ1R (500 nM; 24 hr).

(E) ChIP-seq density of BRD4 (red) at SEs of the two additional B cell TFs, *PAX5* and *IRF8*, following treatment with JQ1 (+) or DMSO (−).

(F and G) PAX5 and IRF8 transcript (F) and protein abundance (G) in Ly1 cells following JQ1 treatment. Error bars represent SD.

See also Table S6, Figure S6, and Supplemental Experimental Procedures.

used publicly available gene expression profiles (GEP) of highly purified human B cell subsets and defined a set of genes that are significantly more abundant in GC centrocytes and centroblasts than in post-GC plasma cells (UP_IN_GCB_VS_PC). Using GSEA, we confirmed that this common GC developmental program was downregulated in Ly1 and in all five DLBCL cell lines following JQ1 treatment (Figures 7G, 7H, and S7B).

In a subset of the DLBCL cell lines, SEs were identified adjacent to differentially expressed genes validated as discriminating DLBCL subtypes by the COO classification (Figure S7C; Table S7). In the ABC DLBCL cell lines, but not the GCB lines, the subtype-specific TF locus *IRF4* had an adjacent SE (Figure 7A, GCB; Figure 7B, ABC; Figure 7F, tracks; Table S7). The *IRF4* SE was also detected in normal tonsil (Figure 7D), suggesting that it represented a developmental epigenetic mark rather than a tumor-specific feature. Additional genes associated with the developmental ABC signature, including *PIM1* and *CCND2*, featured adjacent SEs in ABC, but not GCB, cell lines (Figure S7C; Table S7). Observing lineage-specifying genes flanked by SEs, we explored whether SE analysis could independently discriminate DLBCL subtypes. Indeed, unsupervised bidirectional hierarchical clustering of DLBCL cell lines by SEs distinguished ABC from GCB cell lines (Figures 7I and S7C).

To evaluate the clinical significance of these findings, we performed SE analysis on primary patient samples by genome-wide ChIP-seq for H3K27ac on four primary DLBCLs that were previously subtyped as either GCB or ABC (Monti et al., 2012). All primary DLBCLs exhibited the same characteristic asymmetry in H3K27ac enrichment, with readily identified regulatory regions consistent with SEs (Figures 8A and 8B; Table S8). Again, SEs were found adjacent to lineage-specifying TFs, such as *PAX5*, and subtype-associated TFs, such as *IRF4* (Figures 8A and 8B; tracks in Figures 8C and 8D; Table S8). Importantly, aggregate unsupervised hierarchical clustering of all SE data principally segregated cell lines from primary samples (malignant or nonmalignant), whereas isolated unsupervised clustering of primary tissue segregated DLBCL samples in

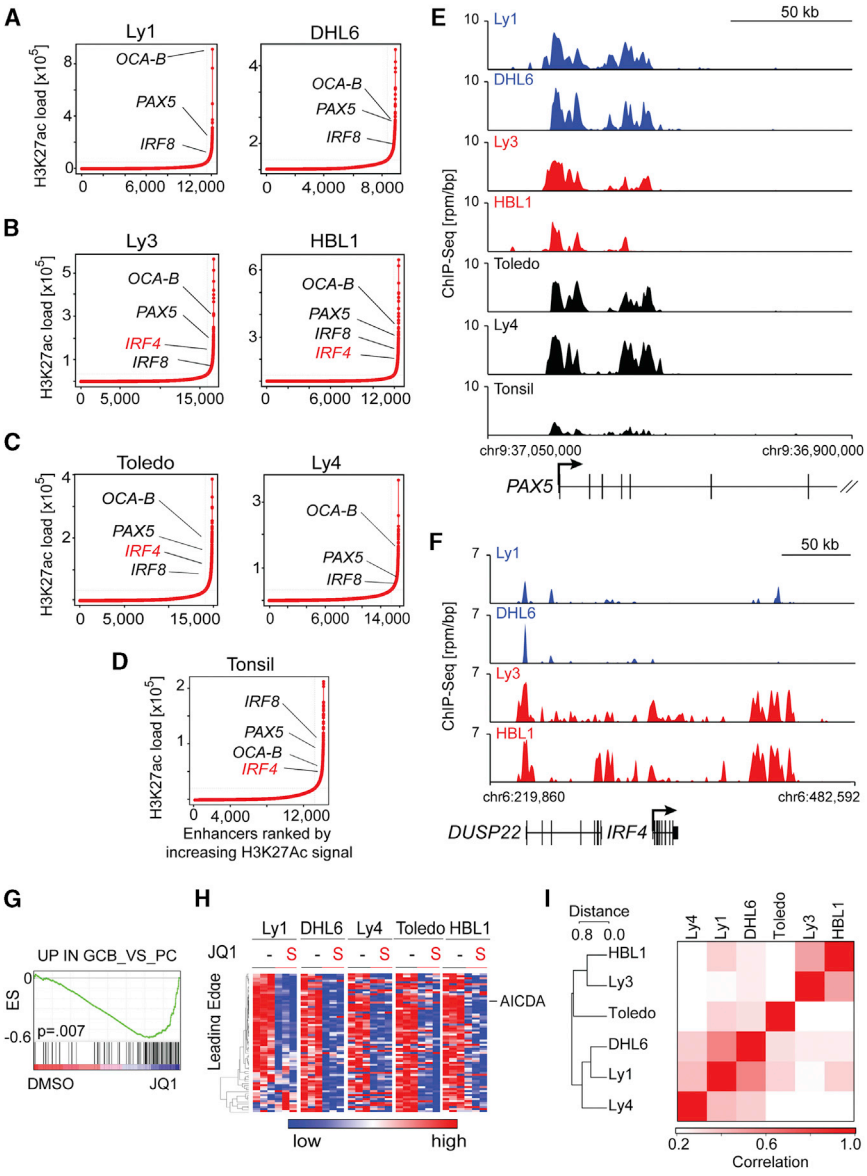

Figure 7. Comparative SE Analysis of DLBCL Cell Lines and Normal Lymphoid Tissue

(A–D) Rank order of increasing integrated H3K27ac fold enrichment at enhancer loci in DLBCL cell lines GCB (A), ABC (B), unclassified (C), and normal tonsil (D).

(E) H3K27ac ChIP-seq fold enrichment at the *PAX5* locus showing the SE region.

(F) H3K27ac ChIP-seq reads at *IRF4* locus in the two GCB and two ABC cell lines.

(G) GSEA plot of the "UP_IN GCB_VS_PC" signature in five DLBCL cell lines following JQ1 treatment.

(H) The leading edge genes of the GSEA in (G) were visualized as heatmap.

(I) Similarity matrix from unsupervised hierarchical clustering of each cell line by location of SEs.

See also Table S7 and Figure S7.

agreement with transcriptional developmental distinctions (Figures 8E and S8; Table S8).

DISCUSSION

Here, we provide mechanistic evidence of BET bromodomains as transcriptional coactivators at large enhancers and E2F1-driven promoters and contribute data supporting the study of BET inhibitors in all recognized subtypes of DLBCL. BET inhibition caused a profound G1 cell cycle arrest in a panel of DLBCL cell lines representing all transcriptionally defined subtypes and significantly delayed tumor growth in two independent DLBCL xenograft models. Gene expression profiling of multiple JQ1-treated DLBCL cell lines revealed downregulation of MYD88/TLR and BCR signaling components, which are important for certain subtypes of DLBCL (Chen et al., 2013; Ngo et al., 2011; Nicodeme et al., 2010). More broadly relevant for all subtypes of DLBCLs, we identified highly significant transcriptional downregulation of MYC and E2F1 target genes and the selective depletion of BRD4-loaded promoters and enhancers.

BET inhibition decreased the abundance of multiple functionally defined E2F target genes, but did not measurably alter E2F1 protein levels. Epigenomic analyses confirmed the colocalization of BRD4 and E2F1 at active promoters. The selective decrease in BRD4 loading of E2F1-driven genes following JQ1 treatment is consistent with studies suggesting a role of BET proteins in E2F1-mediated transcription (Peng et al., 2007; Sinha et al., 2005). Genome-wide assessment of effects of BRD4 on transcriptional elongation at E2F1 target genes was statistically significant but subtle on an individual gene level (data not shown), leaving open the possibility that BRD4-mediated effects on elongation are most apparent on SE-associated genes. Given the recently identified structural genetic signature of deregulated cell cycle and increased E2F activity in poor-prognosis DLBCLs (Monti et al., 2012), BET inhibition may represent a promising targeted treatment strategy.

Studies from our lab and others have highlighted the important role of BRD4 as a coactivator of MYC-mediated transcription (Delmore et al., 2011; Mertz et al., 2011; Ott et al., 2012). In multiple myeloma cell lines with *Ig/MYC* translocations, BRD4 was postulated to function via long-range interactions with the distal *IgH* enhancer (Delmore et al., 2011). However, emerging data indicate that BET inhibitors suppress MYC transcription in the context of translocated, amplified, or wild-type *MYC* alleles and that BRD4 localizes to *MYC* promoter and enhancer elements (Delmore et al., 2011; Lovén et al., 2013; Mertz et al., 2011; Ott et al., 2012). In the current studies, we identify a BRD4-loaded *MYC* enhancer and find that BET inhibition

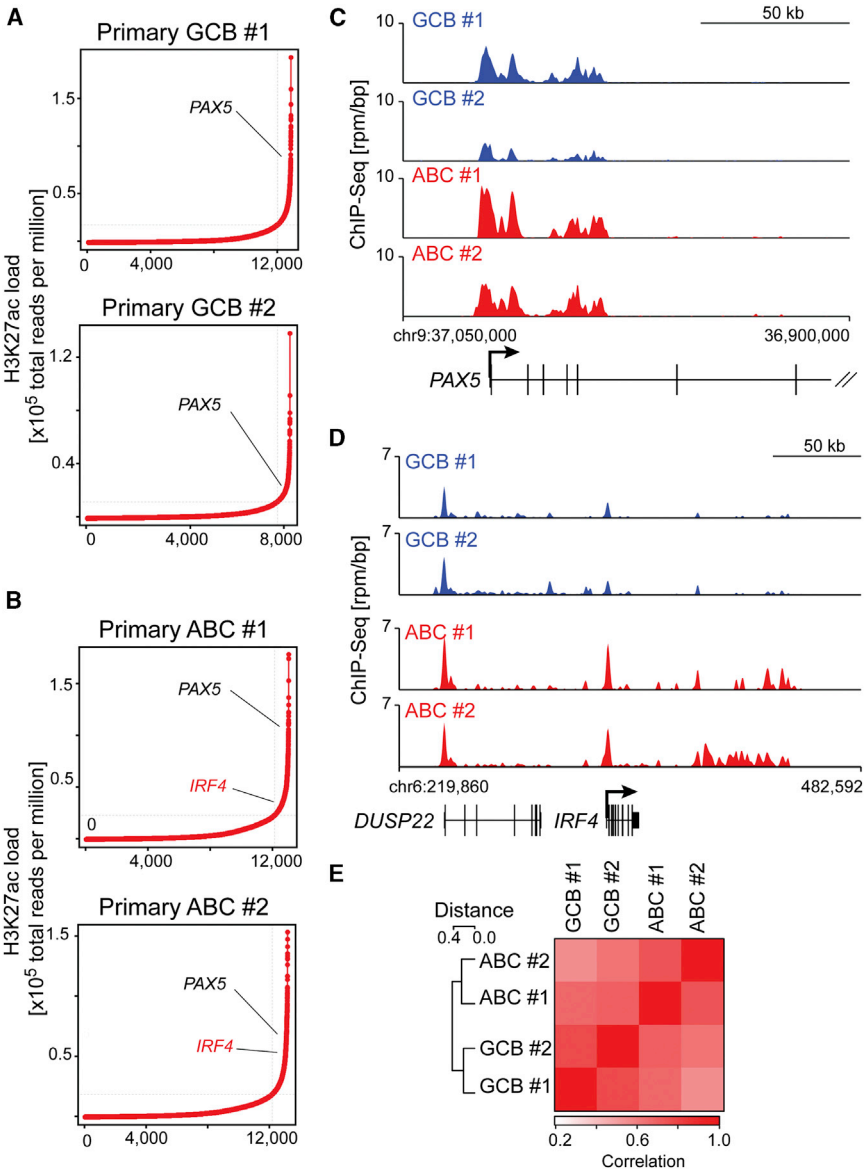

Figure 8. SE Analysis of Primary DLBCLs

(A and B) Rank order of increased H3K27ac fold enrichment at enhancer loci in primary DLBCLs: GCB#1 and #2 (A); ABC#1 and #2 (B).

(C) Gene tracks showing H3K27ac enrichment at the *PAX5* locus in all four primary DLBCLs.

(D) Tracks as in (C) comparing the H3K27 enrichment at the *IRF4* locus in primary GCB versus ABC DLBCLs.

(E) Unsupervised hierarchical clustering of primary DLBCLs using the genomic locations of all SEs in Figure S7I.

See also Table S8 and Figure S8.

decreases MYC transcription and expression in DLBCL cell lines with translocated, amplified, or wild-type MYC alleles. In this extensive DLBCL cell line panel, the functional consequences of BET inhibition—cell cycle arrest and decreased cellular proliferation—were largely comparable. Although JQ1 treatment broadly downregulated the transcriptional targets of MYC and E2F, we sought additional bases for the effect of BET inhibition across multiple DLBCL subtypes.

We observed that a small subset of genes had a disproportionately high BRD4 load at their proximal enhancers. These unusual regulatory elements were approximately 12-fold larger than typical enhancer regions. Integrated epigenomic and transcriptional studies established that such SE-marked genes were particularly sensitive to BET inhibition. As SEs were found adjacent to genes encoding known lineage factors and DLBCL oncoproteins, we surmised that SE analysis might identify previously unrecognized tumor dependencies. The functional exploration of OCA-B, encoded by SE-marked *POU2AF1*, validates this factor as a cancer dependency in DLBCL. Mechanistic research has established OCA-B as a coactivator protein that binds into the OCT1-OCT2 transcriptional complex, enhancing IgH promoter-enhancer communication (Luo and Roeder, 1995; Ren et al., 2011). Mice lacking OCA-B expression due to germline knockout of *POU2AF1* are developmentally normal, even capable of early transcription from immunoglobulin promoters; however, they lack an apparent GC reaction to antigen (Kim et al., 1996; Teitell, 2003). Collectively, the earlier studies and the current research support a putative therapeutic window to targeting OCA-B, potentially by protein-protein inhibition via the POU domain. More generally, these studies establish a rationale to systematically explore SEs for unrecognized tumor dependencies, and potentially to use SEs as biomarkers for targeted therapeutic development.

In this comparative epigenomic analysis of human DLBCL cell lines, primary tumor specimens, and normal lymphoid samples, we analyzed patterns of H3K27ac enrichment to understand the relevance of enhancer variation and function. These studies reveal SEs as characteristic features of human lymphoid tissues, both benign and malignant. Preservation of tissue-specific SEs is observed, comparing nonmalignant nodal tissue to primary DLBCL samples, as well as patient-derived human DLBCL cell lines.

In summary, our data suggest that BET inhibition limits the growth of DLBCLs by at least two complementary activities: a specific effect on genes that define a given cell type by high BRD4 loading at enhancers and a more general suppression of transcription at E2F- and MYC-driven target genes. Thus, an E2F/MYC pathway effect is combined with massive depletion of proteins driven by BRD4-overloaded enhancers, preventing cell cycle progression and leading to growth arrest. The majority of DLBCLs have a structural basis for increased E2F1-mediated

cell cycle progression; however, these tumors may differ in BRD4 super-loading of cell-fate-determining enhancers, including *MYC*, depending on their molecular context. This framework of BET inhibition explains its broad subclass- and tumor-type-independent mechanism of action and reconciles the apparent pleiotropic effects and cell type-specific outcomes. Importantly, these data provide a compelling rationale for further human clinical investigation.

EXPERIMENTAL PROCEDURES

High-Throughput Screening of BET Bromodomain Inhibitors in B Cell Lymphoma Cell Line Panel

Using a semiautomated screen, we tested the indicated compounds in 34 human lymphoma lines in a 384-well format. Cell viability at 72 hr was evaluated using ATPlite (Perkin Elmer). The means of absolute effective concentration of 50% impact (EC_{50}) from two independent screens were visualized and clustered using GENE-E (http://www.broadinstitute.org/cancer/software/GENE-E/index.html).

Human Samples

Frozen biopsy specimens of newly diagnosed, previously untreated primary DLBCLs with >80% tumor involvement and known transcriptional subtyping (Monti et al., 2012) were obtained according to Institutional Review Board (IRB)-approved protocols (Brigham and Women's Hospital and Dana-Farber Cancer Institute). A waiver to obtain informed consent was granted by the local IRBs because only coded, deidentified, discarded tissue was used.

Animal Studies

All animal studies were performed according to Dana-Farber Cancer Institute Institutional Animal Care and Use Committee-approved protocols, as previously described (Monti et al., 2012), and Supplemental Experimental Procedures.

Analyses of Cellular Proliferation and Apoptosis, Immunohistochemistry, Immunoblotting, Transcriptional Profiling, GSEA and Lentiviral-Mediated shRNA, ChIP-Seq, and Analysis of ChIP-Seq Data

A full description of these methods is listed in Supplemental Experimental Procedures.

ACCESSION NUMBERS

The Gene Expression Omnibus accession numbers for the gene expression and ChIP-seq data reported in this paper are GSE45630 and GSE46663, respectively.

SUPPLEMENTAL INFORMATION

Supplemental Information includes Supplemental Experimental Procedures, eight figures, and eight tables and can be found with this article online at http://dx.doi.org/10.1016/j.ccr.2013.11.003.

ACKNOWLEDGMENTS

The authors acknowledge support from the National Institutes of Health and the Leukemia & Lymphoma Society (to M.A.S. and J.E.B.); the Damon-Runyon Cancer Research Foundation, the Broad New Idea Award, the William Lawrence and Blanche Hughes Foundation; and the American Society of Hematology (to J.E.B.); the Department of Defense (CDMRP CA120184 to C.Y.L.); the American Cancer Society (PF-11-042-01-DMC to P.B.R.); and the German Research Foundation (DFG Ch 735/1-1 to B.C.). Drug-like derivities of JQ1 have been licensed to Tensha Therapuetics for clinical development by DFCI. J.E.B. is a Scientific Founder of Tensha. J.E.B. and R.A.Y. are Scientific Founders of Syros Pharmacueticals. C.Y.L. and P.B.R. were paid consultants for Syros Pharmaceuticals.

Received: May 24, 2013
Revised: September 17, 2013
Accepted: November 6, 2013
Published: December 9, 2013

REFERENCES

Bartholomeeusen, K., Xiang, Y., Fujinaga, K., and Peterlin, B.M. (2012). Bromodomain and extra-terminal (BET) bromodomain inhibition activate transcription via transient release of positive transcription elongation factor b (P-TEFb) from 7SK small nuclear ribonucleoprotein. J. Biol. Chem. *287*, 36609–36616.

Basso, K., and Dalla-Favera, R. (2012). Roles of BCL6 in normal and transformed germinal center B cells. Immunol. Rev. *247*, 172–183.

Bisgrove, D.A., Mahmoudi, T., Henklein, P., and Verdin, E. (2007). Conserved P-TEFb-interacting domain of BRD4 inhibits HIV transcription. Proc. Natl. Acad. Sci. USA *104*, 13690–13695.

Caro, P., Kishan, A.U., Norberg, E., Stanley, I.A., Chapuy, B., Ficarro, S.B., Polak, K., Tondera, D., Gounarides, J., Yin, H., et al. (2012). Metabolic signatures uncover distinct targets in molecular subsets of diffuse large B cell lymphoma. Cancer Cell *22*, 547–560.

Chen, L., Monti, S., Juszczynski, P., Ouyang, J., Chapuy, B., Neuberg, D., Doench, J.G., Bogusz, A.M., Habermann, T.M., Dogan, A., et al. (2013). SYK inhibition modulates distinct PI3K/AKT-dependent survival pathways and cholesterol biosynthesis in diffuse large B cell lymphomas. Cancer Cell *23*, 826–838.

Cobaleda, C., Schebesta, A., Delogu, A., and Busslinger, M. (2007). Pax5: the guardian of B cell identity and function. Nat. Immunol. *8*, 463–470.

Dawson, M.A., Prinjha, R.K., Dittmann, A., Giotopoulos, G., Bantscheff, M., Chan, W.I., Robson, S.C., Chung, C.W., Hopf, C., Savitski, M.M., et al. (2011). Inhibition of BET recruitment to chromatin as an effective treatment for MLL-fusion leukaemia. Nature *478*, 529–533.

Delmore, J.E., Issa, G.C., Lemieux, M.E., Rahl, P.B., Shi, J., Jacobs, H.M., Kastritis, E., Gilpatrick, T., Paranal, R.M., Qi, J., et al. (2011). BET bromodomain inhibition as a therapeutic strategy to target c-Myc. Cell *146*, 904–917.

Dey, A., Chitsaz, F., Abbasi, A., Misteli, T., and Ozato, K. (2003). The double bromodomain protein Brd4 binds to acetylated chromatin during interphase and mitosis. Proc. Natl. Acad. Sci. USA *100*, 8758–8763.

Filippakopoulos, P., Qi, J., Picaud, S., Shen, Y., Smith, W.B., Fedorov, O., Morse, E.M., Keates, T., Hickman, T.T., Felletar, I., et al. (2010). Selective inhibition of BET bromodomains. Nature *468*, 1067–1073.

Filippakopoulos, P., Picaud, S., Mangos, M., Keates, T., Lambert, J.P., Barsyte-Lovejoy, D., Felletar, I., Volkmer, R., Müller, S., Pawson, T., et al. (2012). Histone recognition and large-scale structural analysis of the human bromodomain family. Cell *149*, 214–231.

Fuda, N.J., Ardehali, M.B., and Lis, J.T. (2009). Defining mechanisms that regulate RNA polymerase II transcription in vivo. Nature *461*, 186–192.

Gisselbrecht, C., Glass, B., Mounier, N., Singh Gill, D., Linch, D.C., Trneny, M., Bosly, A., Ketterer, N., Shpilberg, O., Hagberg, H., et al. (2010). Salvage regimens with autologous transplantation for relapsed large B-cell lymphoma in the rituximab era. J. Clin. Oncol. *28*, 4184–4190.

Greenwald, R.J., Tumang, J.R., Sinha, A., Currier, N., Cardiff, R.D., Rothstein, T.L., Faller, D.V., and Denis, G.V. (2004). E mu-BRD2 transgenic mice develop B-cell lymphoma and leukemia. Blood *103*, 1475–1484.

Greiner, A., Müller, K.B., Hess, J., Pfeffer, K., Müller-Hermelink, H.K., and Wirth, T. (2000). Up-regulation of BOB.1/OBF.1 expression in normal germinal center B cells and germinal center-derived lymphomas. Am. J. Pathol. *156*, 501–507.

Hu, S., Xu-Monette, Z.Y., Tzankov, A., Green, T., Wu, L., Balasubramanyam, A., Liu, W.M., Visco, C., Li, Y., Miranda, R.N., et al. (2013). MYC/BCL2 protein coexpression contributes to the inferior survival of activated B-cell subtype of diffuse large B-cell lymphoma and demonstrates high-risk gene expression signatures: a report from The International DLBCL Rituximab-CHOP Consortium Program. Blood *121*, 4021–4031, quiz 4250.

Johnson, N.A., Slack, G.W., Savage, K.J., Connors, J.M., Ben-Neriah, S., Rogic, S., Scott, D.W., Tan, K.L., Steidl, C., Sehn, L.H., et al. (2012). Concurrent expression of MYC and BCL2 in diffuse large B-cell lymphoma treated with rituximab plus cyclophosphamide, doxorubicin, vincristine, and prednisone. J. Clin. Oncol. *30*, 3452–3459.

Kim, U., Qin, X.F., Gong, S., Stevens, S., Luo, Y., Nussenzweig, M., and Roeder, R.G. (1996). The B-cell-specific transcription coactivator OCA-B/OBF-1/Bob-1 is essential for normal production of immunoglobulin isotypes. Nature *383*, 542–547.

Klein, U., and Dalla-Favera, R. (2008). Germinal centres: role in B-cell physiology and malignancy. Nat. Rev. Immunol. *8*, 22–33.

Lee, T.I., and Young, R.A. (2013). Transcriptional regulation and its misregulation in disease. Cell *152*, 1237–1251.

Lenz, G., and Staudt, L.M. (2010). Aggressive lymphomas. N. Engl. J. Med. *362*, 1417–1429.

Lohr, J.G., Stojanov, P., Lawrence, M.S., Auclair, D., Chapuy, B., Sougnez, C., Cruz-Gordillo, P., Knoechel, B., Asmann, Y.W., Slager, S.L., et al. (2012). Discovery and prioritization of somatic mutations in diffuse large B-cell lymphoma (DLBCL) by whole-exome sequencing. Proc. Natl. Acad. Sci. USA *109*, 3879–3884.

Lovén, J., Hoke, H.A., Lin, C.Y., Lau, A., Orlando, D.A., Vakoc, C.R., Bradner, J.E., Lee, T.I., and Young, R.A. (2013). Selective inhibition of tumor oncogenes by disruption of super-enhancers. Cell *153*, 320–334.

Luo, Y., and Roeder, R.G. (1995). Cloning, functional characterization, and mechanism of action of the B-cell-specific transcriptional coactivator OCA-B. Mol. Cell. Biol. *15*, 4115–4124.

Marushige, K. (1976). Activation of chromatin by acetylation of histone side chains. Proc. Natl. Acad. Sci. USA *73*, 3937–3941.

Mertz, J.A., Conery, A.R., Bryant, B.M., Sandy, P., Balasubramanian, S., Mele, D.A., Bergeron, L., and Sims, R.J., 3rd. (2011). Targeting MYC dependence in cancer by inhibiting BET bromodomains. Proc. Natl. Acad. Sci. USA *108*, 16669–16674.

Miyoshi, S., Ooike, S., Iwata, K., Hikawa, H., and Sugaraha, K. September 2009. Antitumor agent. International patent PCT/JP2008/073864 (WO/2009/084693).

Monti, S., Savage, K.J., Kutok, J.L., Feuerhake, F., Kurtin, P., Mihm, M., Wu, B., Pasqualucci, L., Neuberg, D., Aguiar, R.C., et al. (2005). Molecular profiling of diffuse large B-cell lymphoma identifies robust subtypes including one characterized by host inflammatory response. Blood *105*, 1851–1861.

Monti, S., Chapuy, B., Takeyama, K., Rodig, S.J., Hao, Y., Yeda, K.T., Inguilizian, H., Mermel, C., Currie, T., Dogan, A., et al. (2012). Integrative analysis reveals an outcome-associated and targetable pattern of p53 and cell cycle deregulation in diffuse large B cell lymphoma. Cancer Cell *22*, 359–372.

Morin, R.D., Mendez-Lago, M., Mungall, A.J., Goya, R., Mungall, K.L., Corbett, R.D., Johnson, N.A., Severson, T.M., Chiu, R., Field, M., et al. (2011). Frequent mutation of histone-modifying genes in non-Hodgkin lymphoma. Nature *476*, 298–303.

Ngo, V.N., Young, R.M., Schmitz, R., Jhavar, S., Xiao, W., Lim, K.H., Kohlhammer, H., Xu, W., Yang, Y., Zhao, H., et al. (2011). Oncogenically active MYD88 mutations in human lymphoma. Nature *470*, 115–119.

Nicodeme, E., Jeffrey, K.L., Schaefer, U., Beinke, S., Dewell, S., Chung, C.W., Chandwani, R., Marazzi, I., Wilson, P., Coste, H., et al. (2010). Suppression of inflammation by a synthetic histone mimic. Nature *468*, 1119–1123.

Nutt, S.L., Taubenheim, N., Hasbold, J., Corcoran, L.M., and Hodgkin, P.D. (2011). The genetic network controlling plasma cell differentiation. Semin. Immunol. *23*, 341–349.

Ott, C.J., Kopp, N., Bird, L., Paranal, R.M., Qi, J., Bowman, T., Rodig, S.J., Kung, A.L., Bradner, J.E., and Weinstock, D.M. (2012). BET bromodomain inhibition targets both c-Myc and IL7R in high-risk acute lymphoblastic leukemia. Blood *120*, 2843–2852.

Owen, D.J., Ornaghi, P., Yang, J.C., Lowe, N., Evans, P.R., Ballario, P., Neuhaus, D., Filetici, P., and Travers, A.A. (2000). The structural basis for the recognition of acetylated histone H4 by the bromodomain of histone acetyltransferase gcn5p. EMBO J. *19*, 6141–6149.

Pasqualucci, L., Trifonov, V., Fabbri, G., Ma, J., Rossi, D., Chiarenza, A., Wells, V.A., Grunn, A., Messina, M., Elliot, O., et al. (2011). Analysis of the coding genome of diffuse large B-cell lymphoma. Nat. Genet. *43*, 830–837.

Peng, J., Dong, W., Chen, L., Zou, T., Qi, Y., and Liu, Y. (2007). Brd2 is a TBP-associated protein and recruits TBP into E2F-1 transcriptional complex in response to serum stimulation. Mol. Cell. Biochem. *294*, 45–54.

Polo, J.M., Juszczynski, P., Monti, S., Cerchietti, L., Ye, K., Greally, J.M., Shipp, M., and Melnick, A. (2007). Transcriptional signature with differential expression of BCL6 target genes accurately identifies BCL6-dependent diffuse large B cell lymphomas. Proc. Natl. Acad. Sci. USA *104*, 3207–3212.

Puissant, A., Frumm, S.M., Alexe, G., Bassil, C.F., Qi, J., Chanthery, Y.H., Nekritz, E.A., Zeid, R., Gustafson, W.C., Greninger, P., et al. (2013). Targeting MYCN in neuroblastoma by BET bromodomain inhibition. Cancer Discov. *3*, 308–323.

Ramachandrareddy, H., Bouska, A., Shen, Y., Ji, M., Rizzino, A., Chan, W.C., and McKeithan, T.W. (2010). BCL6 promoter interacts with far upstream sequences with greatly enhanced activating histone modifications in germinal center B cells. Proc. Natl. Acad. Sci. USA *107*, 11930–11935.

Ren, X., Siegel, R., Kim, U., and Roeder, R.G. (2011). Direct interactions of OCA-B and TFII-I regulate immunoglobulin heavy-chain gene transcription by facilitating enhancer-promoter communication. Mol. Cell *42*, 342–355.

Schreiber, S.L., and Bernstein, B.E. (2002). Signaling network model of chromatin. Cell *111*, 771–778.

Sinha, A., Faller, D.V., and Denis, G.V. (2005). Bromodomain analysis of Brd2-dependent transcriptional activation of cyclin A. Biochem. J. *387*, 257–269.

Slack, G.W., and Gascoyne, R.D. (2011). MYC and aggressive B-cell lymphomas. Adv. Anat. Pathol. *18*, 219–228.

Teitell, M.A. (2003). OCA-B regulation of B-cell development and function. Trends Immunol. *24*, 546–553.

Wang, H., Lee, C.H., Qi, C., Tailor, P., Feng, J., Abbasi, S., Atsumi, T., and Morse, H.C., 3rd. (2008). IRF8 regulates B-cell lineage specification, commitment, and differentiation. Blood *112*, 4028–4038.

Yang, Z., He, N., and Zhou, Q. (2008). Brd4 recruits P-TEFb to chromosomes at late mitosis to promote G1 gene expression and cell cycle progression. Mol. Cell. Biol. *28*, 967–976.

Ye, B.H., Cattoretti, G., Shen, Q., Zhang, J., Hawe, N., de Waard, R., Leung, C., Nouri-Shirazi, M., Orazi, A., Chaganti, R.S., et al. (1997). The BCL-6 proto-oncogene controls germinal-centre formation and Th2-type inflammation. Nat. Genet. *16*, 161–170.

Zhang, W., Prakash, C., Sum, C., Gong, Y., Li, Y., Kwok, J.J., Thiessen, N., Pettersson, S., Jones, S.J., Knapp, S., et al. (2012). Bromodomain-containing protein 4 (BRD4) regulates RNA polymerase II serine 2 phosphorylation in human CD4+ T cells. J. Biol. Chem. *287*, 43137–43155.

Zhang, J., Grubor, V., Love, C.L., Banerjee, A., Richards, K.L., Mieczkowski, P.A., Dunphy, C., Choi, W., Au, W.Y., Srivastava, G., et al. (2013). Genetic heterogeneity of diffuse large B-cell lymphoma. Proc. Natl. Acad. Sci. USA *110*, 1398–1403.

Zhao, R., Nakamura, T., Fu, Y., Lazar, Z., and Spector, D.L. (2011). Gene bookmarking accelerates the kinetics of post-mitotic transcriptional re-activation. Nat. Cell Biol. *13*, 1295–1304.

Zuber, J., Shi, J., Wang, E., Rappaport, A.R., Herrmann, H., Sison, E.A., Magoon, D., Qi, J., Blatt, K., Wunderlich, M., et al. (2011). RNAi screen identifies Brd4 as a therapeutic target in acute myeloid leukaemia. Nature *478*, 524–528.

Triplication of a 21q22 region contributes to B cell transformation through HMGN1 overexpression and loss of histone H3 Lys27 trimethylation

Andrew A Lane[1], Bjoern Chapuy[1], Charles Y Lin[1], Trevor Tivey[1], Hubo Li[2], Elizabeth C Townsend[1], Diederik van Bodegom[1], Tovah A Day[1], Shuo-Chieh Wu[1], Huiyun Liu[1], Akinori Yoda[1], Gabriela Alexe[2], Anna C Schinzel[1,3], Timothy J Sullivan[4], Sébastien Malinge[5], Jordan E Taylor[3], Kimberly Stegmaier[2,3], Jacob D Jaffe[3], Michael Bustin[6], Geertruy te Kronnie[7], Shai Izraeli[8,9], Marian H Harris[10], Kristen E Stevenson[11], Donna Neuberg[11], Lewis B Silverman[2], Stephen E Sallan[2], James E Bradner[1], William C Hahn[1,3], John D Crispino[12], David Pellman[2,13] & David M Weinstock[1,3]

Down syndrome confers a 20-fold increased risk of B cell acute lymphoblastic leukemia (B-ALL)[1], and polysomy 21 is the most frequent somatic aneuploidy among all B-ALLs[2]. Yet the mechanistic links between chromosome 21 triplication and B-ALL remain undefined. Here we show that germline triplication of only 31 genes orthologous to human chromosome 21q22 confers mouse progenitor B cell self renewal *in vitro*, maturation defects *in vivo* and B-ALL with either the BCR-ABL fusion protein or CRLF2 with activated JAK2. Chromosome 21q22 triplication suppresses histone H3 Lys27 trimethylation (H3K27me3) in progenitor B cells and B-ALLs, and 'bivalent' genes with both H3K27me3 and H3K4me3 at their promoters in wild-type progenitor B cells are preferentially overexpressed in triplicated cells. Human B-ALLs with polysomy 21 are distinguished by their overexpression of genes marked with H3K27me3 in multiple cell types. Overexpression of HMGN1, a nucleosome remodeling protein encoded on chromosome 21q22 (refs. 3–5), suppresses H3K27me3 and promotes both B cell proliferation *in vitro* and B-ALL *in vivo*.

To interrogate the effects of polysomy 21 directly, we assayed B cell development in Ts1Rhr mice (**Fig. 1a**), which harbor a triplication of 31 genes and one noncoding RNA on mouse chromosome 16 orthologous to a segment of human chromosome 21q22 (ref. 6). The triplicated genes also overlap with a region of recurrent intrachromosomal amplification of chromosome 21q22 (iAMP21) in human B-ALL[7]. Bone marrow from 6-week-old Ts1Rhr mice had fewer total progenitor B ($B220^+CD43^+$) cells than that from wild-type littermates (**Fig. 1b**). Within the $B220^+CD43^+$ compartment, the Hardy B and C fractions but not the Hardy A fraction were reduced compared with wild-type littermates (**Fig. 1b** and **Supplementary Fig. 1a**)[8]. C57BL/6 Ts1Rhr, FVB × C57BL/6 F1 Ts1Rhr and Ts65Dn mice[9], which harbor a larger triplication (**Fig. 1a**), all had similar reductions in progenitor B cell fractions (**Supplementary Fig. 1b**). This differentiation defect essentially phenocopies human fetal livers with trisomy 21, which have reduced numbers of pre-pro-B ($CD34^+CD19^+CD10^-$) and pro-B ($CD34^+CD19^+CD10^+$) cells[10].

We performed competitive transplantation using equal mixtures of congenic $CD45.1^+$ wild-type bone marrow and $CD45.1^+CD45.2^+$ bone marrow from either Ts1Rhr or wild-type mice (**Supplementary Fig. 1c**). After 16 weeks, recipients of wild-type $CD45.1^+$ bone marrow mixed with wild-type $CD45.1^+CD45.2^+$ bone marrow had equal representations of both populations in the Hardy A, B and C fractions, as well as in whole bone marrow (**Fig. 1c** and **Supplementary Fig. 1d**). In contrast, mice that received wild-type $CD45.1^+$ bone marrow mixed with Ts1Rhr $CD45.1^+CD45.2^+$ bone marrow recapitulated the Ts1Rhr defect, with significant reductions in the $CD45.1^+CD45.2^+$ population in the Hardy B and C fractions (**Fig. 1c** and **Supplementary Fig. 1d**). Thus, the differentiation effect is independent of nonhematopoietic cells.

To address whether chromosome 21q22 triplication directly confers transformed phenotypes *in vitro*, we generated progenitor B cell colonies from unselected Ts1Rhr and wild-type bone marrow

[1]Department of Medical Oncology, Dana-Farber Cancer Institute, Harvard Medical School, Boston, Massachusetts, USA. [2]Department of Pediatric Oncology, Dana-Farber Cancer Institute, Harvard Medical School, Boston, Massachusetts, USA. [3]Broad Institute, Cambridge, Massachusetts, USA. [4]Microarray Core, Dana-Farber Cancer Institute, Harvard Medical School, Boston, Massachusetts, USA. [5]Institut National de la Santé et de la Recherche Médicale (INSERM) U985, Institut Gustave Roussy, Villejuif, France. [6]Laboratory of Metabolism, National Cancer Institute, National Institutes of Health, Bethesda, Maryland, USA. [7]Department of Pediatrics, University of Padova, Padova, Italy. [8]Department of Pediatric Hemato-Oncology, Sheba Medical Center, Tel Hashomer, Ramat Gan, Israel. [9]Department of Human Molecular Genetics and Biochemsitry, Tel Aviv University, Tel Aviv, Israel. [10]Department of Pathology, Children's Hospital Boston, Boston, Massachusetts, USA. [11]Biostatistics and Computational Biology, Dana-Farber Cancer Institute, Harvard Medical School, Boston, Massachusetts, USA. [12]Division of Hematology/Oncology, Northwestern University, Chicago, Illinois, USA. [13]Howard Hughes Medical Institute, Chevy Chase, Maryland, USA. Correspondence should be addressed to A.A.L. (andrew_lane@dfci.harvard.edu) or D.M.W. (dweinstock@partners.org).

Received 13 January; accepted 13 March; published online 20 April 2014; doi:10.1038/ng.2949

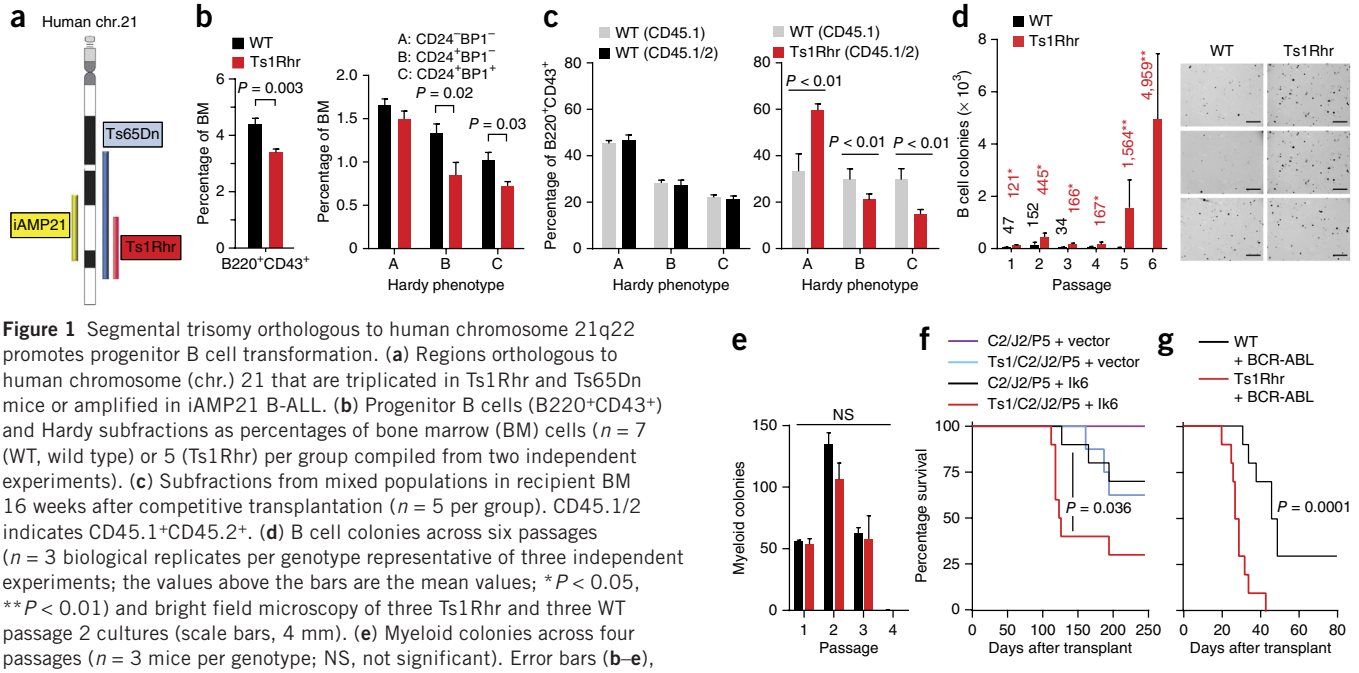

Figure 1 Segmental trisomy orthologous to human chromosome 21q22 promotes progenitor B cell transformation. (**a**) Regions orthologous to human chromosome (chr.) 21 that are triplicated in Ts1Rhr and Ts65Dn mice or amplified in iAMP21 B-ALL. (**b**) Progenitor B cells ($B220^+CD43^+$) and Hardy subfractions as percentages of bone marrow (BM) cells ($n = 7$ (WT, wild type) or 5 (Ts1Rhr) per group compiled from two independent experiments). (**c**) Subfractions from mixed populations in recipient BM 16 weeks after competitive transplantation ($n = 5$ per group). CD45.1/2 indicates $CD45.1^+CD45.2^+$. (**d**) B cell colonies across six passages ($n = 3$ biological replicates per genotype representative of three independent experiments; the values above the bars are the mean values; $^*P < 0.05$, $^{**}P < 0.01$) and bright field microscopy of three Ts1Rhr and three WT passage 2 cultures (scale bars, 4 mm). (**e**) Myeloid colonies across four passages ($n = 3$ mice per genotype; NS, not significant). Error bars (**b**–**e**), s.e.m. Groups (**b**–**e**) were compared by *t*-test. (**f**) Leukemia-free survival of recipient mice after transplantation of C2/J2/*Pax5*$^{+/-}$ (C2/J2/P5) with or without Ts1Rhr (Ts1) BM transduced with vector or Ik6 ($n = 8$ (C2/J2/P5 + vector), 8 (Ts1/C2/J2/P5 + vector), 10 (C2/J2/P5 + Ik6) or 10 (Ts1/C2/J2/P5 + Ik6) mice per group; curves compared by log-rank test). (**g**) Leukemia-free survival of recipient mice after transplantation of BM transduced with BCR-ABL ($n = 10$ mice per group, curves compared by log-rank test).

in three-dimensional cultures with IL-7 (**Supplementary Fig. 1e**,**f**). Wild-type bone marrow formed colonies (termed 'passage 1') that replated to form new colonies for two to three additional passages. In contrast, Ts1Rhr bone marrow generated more colonies in early passages and serially replated indefinitely (**Fig. 1d**), which indicates self-renewal capacity. There were no differences between Ts1Rhr and wild-type bone marrow in the number or repassaging potential of myeloid colonies (**Fig. 1e**).

Sixty percent of Down syndrome–associated B-ALLs harbor *CRLF2* rearrangements that commonly co-occur with activating JAK2 alterations[11–13]. To model this co-occurrence, we generated Eμ-CRLF2 (hereafter called 'C2') and Eμ-JAK2 p.Arg683Gly ('J2') transgenic mice, in which transgene expression is restricted to B cells. Mice harboring C2 and J2 (C2/J2) and *Pax5*$^{+/-}$ mice harboring C2 and J2 (C2/J2/*Pax5*$^{+/-}$) mice did not develop B-ALL by 18 months of age (data not shown). Transduction of C2/J2/*Pax5*$^{+/-}$ bone marrow with dominant-negative *IKZF1* (Ik6)[14] and transplantation into wild-type recipients resulted in CRLF2-positive B-ALL in all mice by 120 days after transplantation (**Supplementary Fig. 2a**,**b**). Control mice lacking C2, J2 or *Pax5* heterozygosity did not develop B-ALL with Ik6 (**Supplementary Fig. 2b**), establishing this transgenic combination as the first model of CRLF2- and JAK2-driven B-ALL. Mice transplanted with Ts1Rhr/C2/J2/*Pax5*$^{+/-}$ bone marrow transduced with a lower titer of Ik6-encoding virus developed B-ALL with greater penetrance and reduced latency compared to mice transplanted with C2/J2/*Pax5*$^{+/-}$ bone marrow alone (**Fig. 1f**). The same genotypes (C2/J2/*Pax5*$^{+/-}$/Ik6 with or without polysomy 21) occur in high-risk cases of human B-ALL[15], supporting the validity of the model.

Although BCR-ABL–rearranged ALL is uncommon in children with Down syndrome, polysomy 21 is the most common somatic aneuploidy in BCR-ABL–rearranged non-Down syndrome–associated B-ALLs[16]. Ts1Rhr and wild-type bone marrow had similar transduction efficiencies with p210 BCR-ABL[17] (**Supplementary Fig. 2c**), but mice (C57BL/6 and FVB × C57BL/6 F1 backgrounds) that received transduced Ts1Rhr bone marrow succumbed to B-ALL with shorter latency and increased penetrance (**Fig. 1g** and **Supplementary Fig. 2d**–**f**). Transplantation of BCR-ABL–transduced sorted Hardy B cells from Ts1Rhr or wild-type mice recapitulated the same effect (**Supplementary Fig. 2g**), indicating that chromosome 21q22 triplication confers leukemogenic effects that are progenitor B-cell autonomous.

Previous reports suggested that polysomy 21 contributes to leukemogenesis by promoting aberrant DNA double-strand break repair (DSBR)[18,19]. To address this possibility, we generated otherwise isogenic retinal pigment epithelial (RPE) cells with three or four copies of human chromosome 21 (**Supplementary Fig. 3a**–**c**). Using targeted DSBR reporters[20,21], we found that polysomy 21 had no effect on either homology-directed repair frequency or junction characteristics formed by nonhomologous end joining, whether DSBs were induced by the I-SceI meganuclease or the V(D)J recombinase (**Supplementary Fig. 3d**–**j**). Although a subtle defect or a defect specific to B cells remains possible, these results indicate that in an isogenic system, polysomy 21 does not drastically affect DSBR phenotype.

We next performed whole-transcriptome sequencing (RNA-seq) of passage 1 B cells. As expected, triplicated loci in Ts1Rhr cells were expressed at approximately 1.5-fold higher levels compared to wild-type cells (**Supplementary Fig. 4**). We defined a transcriptional Ts1Rhr gene set of the 150 most differentially expressed genes compared to wild type (**Supplementary Table 1a**,**b**). As expected, this signature was highly enriched by gene set enrichment analysis (GSEA)[22] for human chromosome 21q22 genes but not other human chromosomal segments (**Supplementary Table 1c**). The Ts1Rhr B cell signature was enriched among human Down syndrome–associated ALLs by GSEA (**Fig. 2a**,**b**; false discovery rate (FDR) = 0.019) in a data set of pediatric B-ALLs (Associazione Italiana Ematologia Oncologia Pediatrica (AIEOP))[19]. By hierarchical clustering, we defined a core Ts1Rhr set of 50 genes (**Fig. 2a** and **Supplementary Table 1a**) that contained none of the triplicated genes in Ts1Rhr cells but was highly enriched among Down syndrome–associated ALLs in

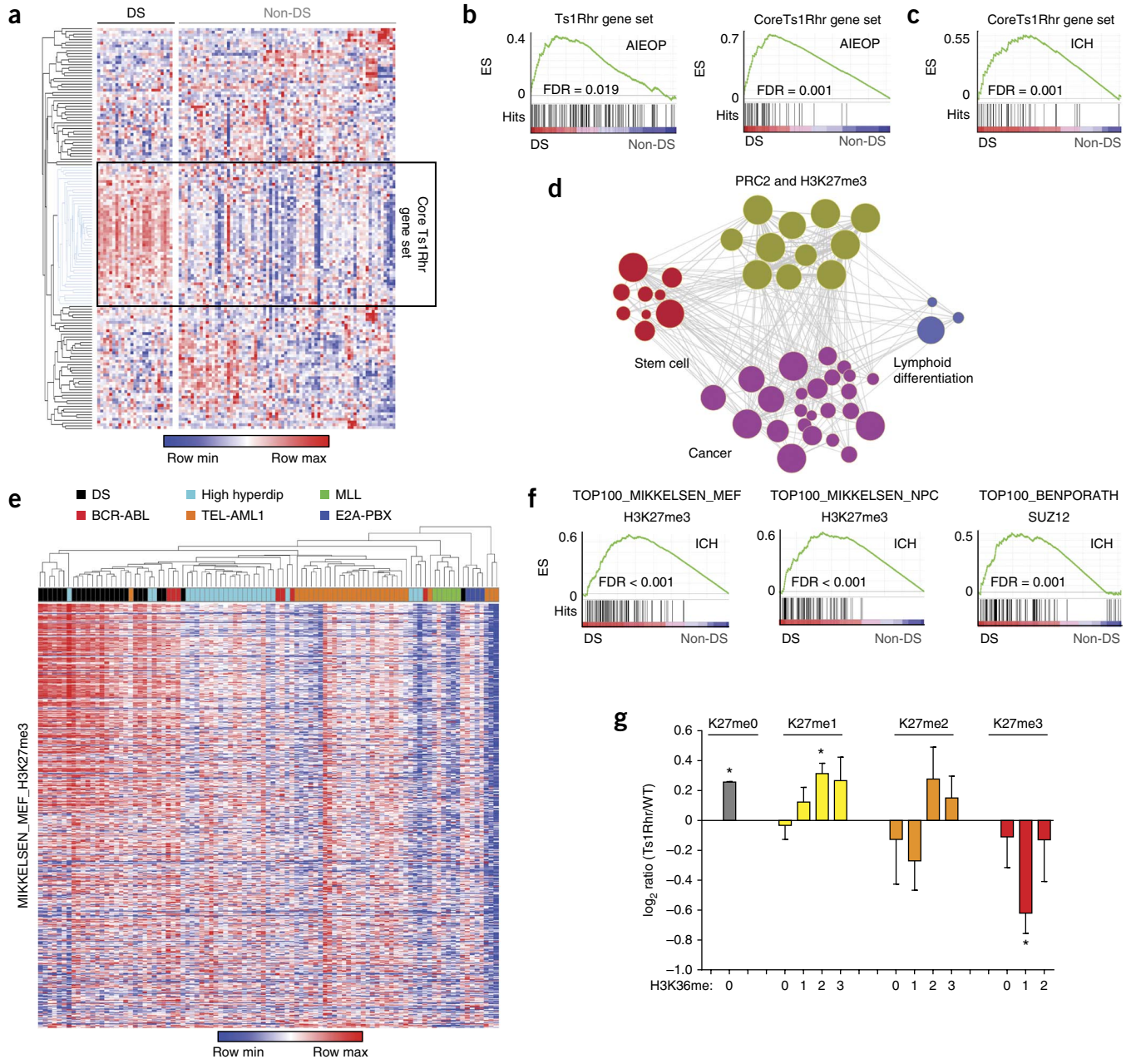

Figure 2 Polysomy 21 B-ALL is associated with the overexpression of PRC2 targets. (**a**) Heat map of human genes orthologous to the 150 most upregulated genes from Ts1Rhr B cells in primary human pediatric B-ALLs (DS indicates Down syndrome–associated ALL; non-DS indicates non–Down syndrome–associated ALL). Unsupervised hierarchical clustering by gene revealed the core Ts1Rhr gene set (boxed). (**b**) GSEA plots for the full and core Ts1Rhr gene sets in the AIEOP data set. ES, enrichment score. (**c**) GSEA plot of the core Ts1Rhr gene set in an independent ICH validation cohort. (**d**) Network enrichment map of MSigDB gene sets enriched (FDR < 0.05) in the Ts1Rhr expression signature. (**e**) Unsupervised hierarchical clustering of H3K27me3-marked genes from the MIKKELSEN_MEF_H3K27me3 gene set in the AIEOP pediatric B-ALL cohort (karyotype shown). High hyperdip, high hyperdiploid. (**f**) GSEA plots of the top 100 genes from three PRC2 and H3K27me3 gene sets (as defined in the AIEOP patient cohort) in the ICH validation cohort. (**g**) Quantitative histone mass spectrometry for H3K27–H3K36 peptides (*$P < 0.05$; $n = 3$ samples per group per genotype; each group compared to $\log_2$ ratio of zero by *t*-test). Error bars, s.e.m.

both the AIEOP data set (**Fig. 2c**; FDR = 0.001) and an independent validation data set (Institute of Child Health, London (ICH)) (**Fig. 2c**; FDR = 0.001).

To identify pathways perturbed by chromosome 21q22 triplication, we queried the Ts1Rhr gene set against over 3,000 functionally defined gene sets in the MSigDB 'c2' chemical and genetic perturbations and 'c6' oncogenic signatures repositories[22]. Arranging the significant gene sets in a network enrichment map[23] defined four clusters (**Fig. 2d**). The most highly enriched cluster consisted of polycomb repressor complex 2 (PRC2) targets and sites of H3K27me3, the repressive mark added by PRC2, that were defined across multiple lineages (**Supplementary Table 1d**,**e**). The additional clusters consisted of gene sets that distinguish stem cells from lineage-matched differentiated cells, cancer cells from nonmalignant cells or less differentiated from more differentiated lymphoid cells (**Supplementary Table 1d**).

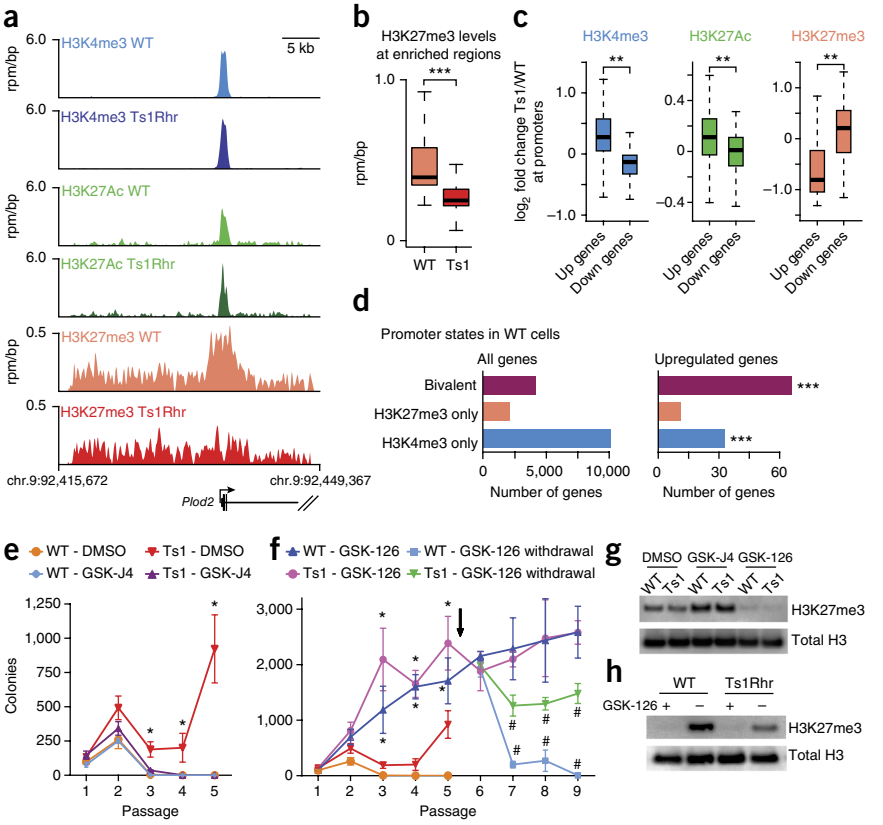

Figure 3 Ts1Rhr B cells have reduced H3K27me3 that results in overexpression of bivalently marked genes. (**a**) Gene tracks showing occupancy of histone marks at the *Plod2* promoter (1 of the 50 core Ts1Rhr genes) in reads per million per base pair (rpm/bp). (**b**) Levels of H3K27me3 in Ts1Rhr and WT B cells at regions enriched for H3K27me3 in WT cells (***$P < 1 \times 10^{-16}$; $n = 15{,}323$ loci per group; groups compared by *t*-test) (**c**) Histone marks at the promoters of genes that are upregulated (Up) or downregulated (Down) in Ts1Rhr compared to WT (Ts1/WT) cells (**$P < 1 \times 10^{-5}$; $n = 132$ (Up) or 163 (Down) genes; groups compared by *t*-test). The box plots in **b** and **c** show the median (horizontal line), 1 s.d. (box) and 2 s.d. (whiskers). (**d**) Chromatin marks in WT B cells present at promoters of all genes (left) or genes that are upregulated in Ts1Rhr B cells (right; ***$P < 0.0001$ compared to all genes by χ^2 with Yates' correction). (**e**) Colony counts in the presence of dimethyl sulfoxide (DMSO) or GSK-J4 ($n = 6$ (WT – DMSO), 6 (Ts1 – DMSO), 3 (WT – GSK-J4) or 3 (Ts1 – GSK-J4) biological replicates per genotype; *$P < 0.05$ compared to GSK-J4 for the same genotype; groups compared by *t*-test). (**f**) Colony counts in the presence of GSK-126 or after withdrawal at passage 5 ($n = 6$ (WT – DMSO), 6 (Ts1 – DMSO), 3 (WT – GSK-126), 3 (Ts1 – GSK-126), 3 (WT – GSK-126 withdrawal) or 3 (Ts1 – GSK-126 withdrawal) biological replicates per genotype; *$P < 0.05$ compared to DMSO for the same genotype, #$P < 0.05$ compared to the other genotype or no withdrawal; groups compared by *t*-test). The arrow indicates GSK-126 withdrawal. Error bars (**e**,**f**), s.e.m. (**g**) Western blotting of passage 2 colonies after 14 total days in culture with DMSO, 1 μM GSK-J4 or 1 μM GSK-126. (**h**) Western blotting of colonies one passage (7 days) after continuation (+) or removal (–) of GSK-126.

We next asked whether differential expression of PRC2- and H3K27me3-classified genes would distinguish Down syndrome–associated ALLs from other B-ALLs. A previous effort using genome-wide expression in the AIEOP cohort failed to define a transcriptional signature that was specific to Down syndrome–associated ALL[19]. Strikingly, expression of H3K27me3-marked genes defined in mouse embryonic fibroblasts[24] distinguished Down syndrome–associated ALLs from non–Down syndrome–associated ALLs (**Fig. 2e**). To validate these findings, we determined the 100 most differentially expressed genes between Down syndrome–associated ALLs and non–Down syndrome–associated ALLs in the AIEOP cohort across three different PRC2 and H3K27me3 signatures (**Supplementary Fig. 5a** and **Supplementary Table 1e**)[24,25]. All three signatures were significantly enriched (FDR ≤ 0.001) among Down syndrome–associated ALLs in the ICH validation cohort (**Fig. 2f**). In a third cohort of non–Down syndrome–associated ALLs (AIEOP-2), leukemias with either polysomy 21 or iAMP21 clustered on the basis of expression of PRC2 targets (**Supplementary Fig. 5b**; $P = 0.001$ by Fisher's exact test), and the Ts1Rhr and H3K27me3 gene sets were enriched among cases with polysomy 21 or iAMP21 by GSEA (**Supplementary Fig. 5c**).

Genes from PRC2 and H3K27me3 gene sets that distinguish Down syndrome–associated ALLs are predominantly overexpressed in Down syndrome–associated ALL (**Fig. 2e** and **Supplementary Fig. 5a**), suggesting that Down syndrome–associated ALL is associated with PRC2 target derepression through reduced H3K27me3. Histone H3 mass spectrometry confirmed a global reduction in H3K27me3 peptides in passage 1 Ts1Rhr B cells compared to wild-type cells (**Fig. 2g**). BCR-ABL B-ALLs from Ts1Rhr bone marrow also had reduced H3K27me3 by both mass spectrometry and immunoblotting (**Supplementary Fig. 5d**,**e**). Thus, triplication of only 31 genes orthologous to chromosome 21q22 is sufficient to suppress H3K27me3.

Chromatin immunoprecipitation sequencing (ChIP-seq) of passage 1 Ts1Rhr B cells demonstrated a genome-wide reduction of H3K27me3 at regions enriched for this mark in wild-type cells (**Fig. 3a**,**b**) that was confirmed at multiple loci by ChIP quantitative PCR (ChIP-qPCR) (**Supplementary Fig. 6a**). Within Ts1Rhr B cells, H3K27me3 was present almost exclusively at regions enriched for H3K27me3 in wild-type cells, suggesting little or no redistribution but rather a global reduction in H3K27me3 density (**Supplementary Fig. 6b–d**). As expected, we observed reciprocal changes in activating (H3K4me3 and acetylation of H3 Lys27 (H3K27ac)) and repressive (H3K27me3) marks at promoters of genes differentially expressed in Ts1Rhr B cells (**Fig. 3c**).

Of note, genes bivalently marked with both H3K27me3 and H3K4me3 in wild-type cells were highly enriched among those overexpressed in Ts1Rhr B cells (**Fig. 3d**; $P < 0.0001$). Bivalent marks may indicate genes that are modulated during lineage-specific differentiation[26]. Thus, global loss of H3K27me3 from chromosome 21q22 triplication could selectively drive a progenitor B cell–specific developmental program. In support of this hypothesis, the Ts1Rhr, PRC2 and H3K27me3 gene sets were highly enriched for predicted binding sites of the master B cell transcription factors E2A (also called TCF3) and LEF1 (**Supplementary Fig. 6e**). Genes within the Ts1Rhr gene set had increased proximal occupancy by E2A (**Supplementary Fig. 6f**) based on a previous data set from wild-type and E2A-deficient mouse B cell progenitors[27]. In addition, the expression of genes within both the Ts1Rhr gene set

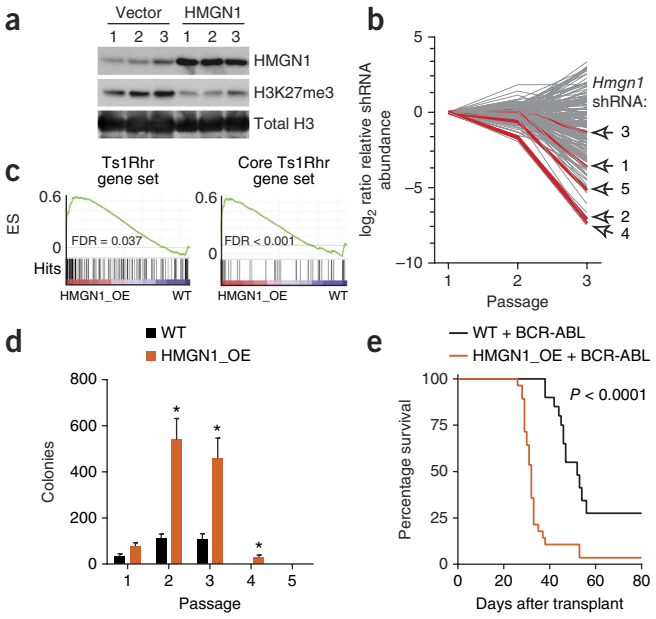

Figure 4 HMGN1 overexpression decreases H3K27me3 and promotes transformed B cell phenotypes. (**a**) Western blotting of Ba/F3 cells transduced with empty virus or mouse HMGN1 ($n = 3$ independent biological replicates). (**b**) Relative shRNA representation over passages 1–3. Each line represents an individual shRNA ($n = 155$ total). The five shRNAs targeting *Hmgn1* are indicated. (**c**) GSEA plots for the full and core Ts1Rhr gene sets in HMGN1_OE transgenic B cells. (**d**) B cell colonies during repassaging of WT and HMGN1_OE BM ($n = 4$ (WT) or 5 (HMGN1_OE) biological replicates per genotype compiled from two independent experiments; $^*P < 0.05$; groups compared by *t*-test). Error bars, s.e.m. (**e**) Leukemia-free survival of recipient mice after transplantation of WT or HMGN1_OE BM transduced with BCR-ABL (aggregate of three independent experiments (**Supplementary Fig. 8**), $n = 20$ (WT) or $n = 28$ (HMGN1_OE) per group, curves compared by log-rank test).

and the core Ts1Rhr set was preferentially increased in the presence of E2A (**Supplementary Fig. 6g**).

We hypothesized that pharmacologic restoration of H3K27me3 with GSK-J4 (ref. 28), a selective inhibitor of H3K27 demethylases, would block Ts1Rhr B cell repassaging. GSK-J4 increased H3K27me3 in Ts1Rhr B cells, decreased colony-forming activity and blocked indefinite repassaging (**Fig. 3e**,**g**). Previous studies demonstrated that 10 μM GSK-J4 reduces lipopolysaccharide-induced proinflammatory cytokine production by human primary macrophages[28]. In comparison, half-maximum inhibitory (IC_{50}) values for GSK-J4 across a panel of Down syndrome–associated ALLs ranged from only 1.4 to 2.5 μM (**Supplementary Fig. 6h**). Strikingly, treatment with GSK-126 (ref. 29), a selective inhibitor of the PRC2 catalytic subunit EZH2, decreased H3K27me3 and was sufficient to confer indefinite repassaging in wild-type B cells that was reversible by drug withdrawal (**Fig. 3f**–**h**).

Among the 31 triplicated genes in Ts1Rhr cells is *Hmgn1*, which encodes a nucleosome binding protein that modulates transcription and promotes chromatin decompaction[3,5]. Modest increases in HMGN1 expression induce changes in histone H3 modifications and gene expression[4,30]. Overexpression of HMGN1 in mouse Ba/F3 B cells suppressed H3K27me3 in a dose-dependent fashion (**Fig. 4a** and **Supplementary Fig. 7a**). By RNA-seq, *Hmgn1* was one of only seven triplicated genes that maintained >70% of its passage 1 expression level at passages 3 and 6 in all Ts1Rhr replicates (**Supplementary Fig. 7b**), suggesting it may be necessary for serial repassaging. To address this possibility, we transduced five short hairpin RNAs (shRNAs) targeting each of the 31 triplicated genes and controls individually into Ts1Rhr and wild-type passage 1 B cells (**Supplementary Fig. 7c**), pooled and serially passaged the transduced cells.

As expected, positive control shRNAs were equally depleted at later passages from Ts1Rhr and wild-type backgrounds (**Supplementary Fig. 7d** and **Supplementary Table 1g**). Among shRNAs against triplicated genes, two of the top four that most selectively depleted Ts1Rhr B cells targeted *Hmgn1* (**Fig. 4b** and **Supplementary Table 1h**). The remaining three shRNAs targeting *Hmgn1* were also preferentially depleted in Ts1Rhr B cells. By passage 6, all five shRNAs against *Hmgn1* were depleted >99%, averaged across replicates of Ts1Rhr B cells (data not shown). All five shRNAs also reduced HMGN1 protein in Ba/F3 cells (**Supplementary Fig. 7e**).

We then analyzed mice with transgenic overexpression of human HMGN1 (HMGN1_OE) at levels comparable to mouse HMGN1 (**Supplementary Fig. 7f**)[31]. HMGN1_OE passage 1 B cells had a gene expression signature that was highly enriched for the Ts1Rhr and core Ts1Rhr gene sets (**Fig. 4c**). Compared to control bone marrow, HMGN1_OE bone marrow had reduced numbers of Hardy C cells *in vivo* (**Supplementary Fig. 7g**), generated more B cell colonies in passages 1–4 *in vitro* (**Fig. 4d**) and resulted in greater penetrance and shorter latency of BCR-ABL–induced B-ALL (**Fig. 4e**). Thus, HMGN1 overexpression recapitulates many transcriptional and phenotypic alterations observed from triplication of all 31 Ts1Rhr genes.

In conclusion, we have shown that triplication of chromosome 21q22 genes confers cell-autonomous differentiation and transformation phenotypes in progenitor B cells. By first delineating these biologic consequences of chromosome 21q22 triplication, we were able to more effectively interrogate human B-ALL data sets and demonstrate that Down syndrome–associated ALLs are distinguished by overexpression of H3K27me3-marked genes. Our data also highlight the therapeutic potential of H3K27 demethylase inhibitors for B-ALLs with extra copies of chromosome 21q22. At the same time, EZH2 inhibitors may be useful for *in vitro* or *in vivo* expansion of precursor B cells. We also provide evidence that overexpression of HMGN1 suppresses global H3K27me3 and promotes B-ALL *in vivo*. Further studies will be needed to determine how HMGN1 modulates transcription at differentially expressed loci in cells with polysomy 21, as well as the contributions from other triplicated chromosome 21q22 loci.

METHODS

Methods and any associated references are available in the online version of the paper.

Accession codes. RNA-seq, ChIP-seq and microarray expression data are available through Gene Expression Omnibus (GEO) accession code GSE48555.

Note: Any Supplementary Information and Source Data files are available in the online version of the paper.

ACKNOWLEDGMENTS

We thank N. Kopp and A. Schlauch for technical assistance, M. Busslinger (Research Institute of Molecular Pathology, Vienna) for the *Pax5*$^{+/-}$ mice and M. Oshimura (Tottori University) for A9 cells carrying human chromosome 21. This research was supported by the Conquer Cancer Foundation (A.A.L.), the Lauri Strauss Leukemia Foundation (A.A.L.), the Leukemia and Lymphoma Society (A.A.L.), the Alex Lemonade Stand Foundation (A.A.L., H. Li and D.P.), the US Department of Defense (C.Y.L.), the Israel Science Foundation (S.I.), the US Israel Binational Foundation (J.D.C. and S.I.), the Stellato Fund (D.M.W.),

US National Institutes of Health/National Cancer Institute R01 awards CA15198-01 and CA172387-A01 (D.M.W.) and a Translational Research Award from the Leukemia and Lymphoma Society (J.D.C. and D.M.W.).

AUTHOR CONTRIBUTIONS

A.A.L., T.T., H. Li, E.C.T., D.v.B., T.A.D., S.-C.W., H. Liu, A.Y., S.M., J.E.T., J.D.J. and G.t.K. designed and performed experiments. A.A.L., B.C., C.Y.L., G.A., T.J.S., K.S., K.E.S., D.N., J.D.J., S.I., J.D.C., D.P. and D.M.W. analyzed data. A.C.S., J.E.B., W.C.H. and J.D.J. developed analytical tools. M.B., M.H.H., L.B.S., S.E.S. and D.P. provided essential reagents. A.A.L. and D.M.W. wrote the paper.

COMPETING FINANCIAL INTERESTS

The authors declare no competing financial interests.

1. Rabin, K.R. & Whitlock, J.A. Malignancy in children with trisomy 21. *Oncologist* **14**, 164–173 (2009).
2. Heerema, N.A. *et al.* Specific extra chromosomes occur in a modal number dependent pattern in pediatric acute lymphoblastic leukemia. *Genes Chromosom. Cancer* **46**, 684–693 (2007).
3. Catez, F., Brown, D.T., Misteli, T. & Bustin, M. Competition between histone H1 and HMGN proteins for chromatin binding sites. *EMBO Rep.* **3**, 760–766 (2002).
4. Lim, J.H. *et al.* Chromosomal protein HMGN1 enhances the acetylation of lysine 14 in histone H3. *EMBO J.* **24**, 3038–3048 (2005).
5. Rattner, B.P., Yusufzai, T. & Kadonaga, J.T. HMGN proteins act in opposition to ATP-dependent chromatin remodeling factors to restrict nucleosome mobility. *Mol. Cell* **34**, 620–626 (2009).
6. Olson, L.E., Richtsmeier, J.T., Leszl, J. & Reeves, R.H. A chromosome 21 critical region does not cause specific Down syndrome phenotypes. *Science* **306**, 687–690 (2004).
7. Moorman, A.V. *et al.* Prognostic effect of chromosomal abnormalities in childhood B-cell precursor acute lymphoblastic leukaemia: results from the UK Medical Research Council ALL97/99 randomised trial. *Lancet Oncol.* **11**, 429–438 (2010).
8. Hardy, R.R., Carmack, C.E., Shinton, S.A., Kemp, J.D. & Hayakawa, K. Resolution and characterization of pro-B and pre-pro-B cell stages in normal mouse bone marrow. *J. Exp. Med.* **173**, 1213–1225 (1991).
9. Reeves, R.H. *et al.* A mouse model for Down syndrome exhibits learning and behaviour deficits. *Nat. Genet.* **11**, 177–184 (1995).
10. Roy, A. *et al.* Perturbation of fetal liver hematopoietic stem and progenitor cell development by trisomy 21. *Proc. Natl. Acad. Sci. USA* **109**, 17579–17584 (2012).
11. Mullighan, C.G. *et al.* Rearrangement of CRLF2 in B-progenitor– and Down syndrome–associated acute lymphoblastic leukemia. *Nat. Genet.* **41**, 1243–1246 (2009).
12. Russell, L.J. *et al.* Deregulated expression of cytokine receptor gene, *CRLF2*, is involved in lymphoid transformation in B-cell precursor acute lymphoblastic leukemia. *Blood* **114**, 2688–2698 (2009).
13. Yoda, A. *et al.* Functional screening identifies CRLF2 in precursor B-cell acute lymphoblastic leukemia. *Proc. Natl. Acad. Sci. USA* **107**, 252–257 (2010).
14. Iacobucci, I. *et al.* Expression of spliced oncogenic Ikaros isoforms in Philadelphia-positive acute lymphoblastic leukemia patients treated with tyrosine kinase inhibitors: implications for a new mechanism of resistance. *Blood* **112**, 3847–3855 (2008).
15. Mullighan, C.G. *et al.* JAK mutations in high-risk childhood acute lymphoblastic leukemia. *Proc. Natl. Acad. Sci. USA* **106**, 9414–9418 (2009).
16. Wetzler, M. *et al.* Additional cytogenetic abnormalities in adults with Philadelphia chromosome-positive acute lymphoblastic leukaemia: a study of the Cancer and Leukaemia Group B. *Br. J. Haematol.* **124**, 275–288 (2004).
17. Krause, D.S., Lazarides, K., von Andrian, U.H. & Van Etten, R.A. Requirement for CD44 in homing and engraftment of BCR-ABL–expressing leukemic stem cells. *Nat. Med.* **12**, 1175–1180 (2006).
18. Cabelof, D.C. *et al.* Mutational spectrum at *GATA1* provides insights into mutagenesis and leukemogenesis in Down syndrome. *Blood* **114**, 2753–2763 (2009).
19. Hertzberg, L. *et al.* Down syndrome acute lymphoblastic leukemia, a highly heterogeneous disease in which aberrant expression of CRLF2 is associated with mutated JAK2: a report from the International BFM Study Group. *Blood* **115**, 1006–1017 (2010).
20. Smith, J.R. *et al.* Robust, persistent transgene expression in human embryonic stem cells is achieved with AAVS1-targeted integration. *Stem Cells* **26**, 496–504 (2008).
21. Weinstock, D.M. & Jasin, M. Alternative pathways for the repair of RAG-induced DNA breaks. *Mol. Cell. Biol.* **26**, 131–139 (2006).
22. Subramanian, A. *et al.* Gene set enrichment analysis: a knowledge-based approach for interpreting genome-wide expression profiles. *Proc. Natl. Acad. Sci. USA* **102**, 15545–15550 (2005).
23. Merico, D., Isserlin, R., Stueker, O., Emili, A. & Bader, G.D. Enrichment map: a network-based method for gene-set enrichment visualization and interpretation. *PLoS ONE* **5**, e13984 (2010).
24. Mikkelsen, T.S. *et al.* Genome-wide maps of chromatin state in pluripotent and lineage-committed cells. *Nature* **448**, 553–560 (2007).
25. Ben-Porath, I. *et al.* An embryonic stem cell–like gene expression signature in poorly differentiated aggressive human tumors. *Nat. Genet.* **40**, 499–507 (2008).
26. Bernstein, B.E. *et al.* A bivalent chromatin structure marks key developmental genes in embryonic stem cells. *Cell* **125**, 315–326 (2006).
27. Lin, Y.C. *et al.* A global network of transcription factors, involving E2A, EBF1 and Foxo1, that orchestrates B cell fate. *Nat. Immunol.* **11**, 635–643 (2010).
28. Kruidenier, L. *et al.* A selective jumonji H3K27 demethylase inhibitor modulates the proinflammatory macrophage response. *Nature* **488**, 404–408 (2012).
29. McCabe, M.T. *et al.* EZH2 inhibition as a therapeutic strategy for lymphoma with EZH2-activating mutations. *Nature* **492**, 108–112 (2012).
30. Rochman, M. *et al.* Effects of HMGN variants on the cellular transcription profile. *Nucleic Acids Res.* **39**, 4076–4087 (2011).
31. Bustin, M. *et al.* Characterization of transgenic mice with an increased content of chromosomal protein HMG-14 in their chromatin. *DNA Cell Biol.* **14**, 997–1005 (1995).

ONLINE METHODS

Mice. All animal experiments were performed with approval of the Dana-Farber Cancer Institute (DFCI) Institutional Animal Care and Use Committee. All experiments were performed in an FVB × C57BL/6 F1 background unless otherwise specified. Ts1Rhr (B6.129S6-Dp(16Cbr1-ORF9)1Rhr/J; #005838) and Ts65Dn (B6EiC3Sn.BLiA-Ts(17^{16})65Dn/DnJ; #005252) mice were from Jackson Laboratories. HMGN1_OE mice were previously described[31]. *Pax5*$^{+/-}$ mice[32] backcrossed to C57BL/6 mice were obtained from M. Busslinger (Research Institute of Molecular Pathology, Vienna, Austria). Eμ-CRLF2 and Eμ-JAK2 p.Arg683Gly mice were generated by subcloing cDNAs expressing human CRLF2 or mouse JAK2 p.Arg683Gly[11,13] downstream of the immunoglobulin heavy chain enhancer (Eμ) and generating transgenic founders in FVB fertilized eggs as previously described[33]. Controls for Ts1Rhr mice were wild-type littermates from crosses with either C57BL/6 (Jackson; #000664) or FVB (Jackson; #001800) mice as indicated. Controls for Ts65Dn mice were littermates from the colony (B6EiC3Sn.BLiAF1/J; Jackson #003647). HMGN1_OE mice[31] had been backcrossed over ten generations to C57BL/6 mice[34]. Controls for HMGN1_OE were wild-type littermates after crossing with FVB mice. Donors for competitive transplantation were congenic CD45.1$^+$ B6.SJL-*Ptprc*^{a}*Pepc*^{b}/BoyJ mice (Jackson; stock #002014) crossed with FVB mice (CD45.1$^+$), C57BL/6 × FVB F1 (CD45.1$^+$CD45.2$^+$) mice or Ts1Rhr (C57BL/6) mice crossed with FVB F1 (CD45.1$^+$CD45.2$^+$) mice. Recipients for competitive transplant and for BCR-ABL and Ik6 bone marrow transplants were C57BL/6 × FVB F1 female mice. No randomization was performed for experiments involving mice or samples collected from animals.

Antibodies. Western blotting antibodies were to HMGN1 (Aviva Systems Biology, #ARP38532_P050 and Abcam, #ab5212; both at 1:1,000), mouse HMGN1 (affinity purified rabbit polyclonal; 1:1,000)[35,36], H3K27me3 (Cell Signaling Technologies, #9733, rabbit polyclonal; 1:1,000), total H3 (Cell Signaling Technologies, #9715, rabbit polyclonal; 1:2,000) and α-tubulin (Sigma, #T9026, mouse monoclonal; 1:2,000). Flow cytometry antibodies were B220-Pacific Blue (BD Pharmingen, #558108, clone RA3-6B2; 1:100), CD43-allophycocyanin (APC) (BD, #560663, clone S7; 1:200) or CD43-FITC (BD, #561856, clone S7; 1:200), CD24-phycoerythrin (PE)-Cy7 (BD, #560536, clone M1/69; 1:200), BP1-PE (eBiosciences, 12-5891, clone 6C3; 1:50) or BP1-FITC (eBiosciences, 11-5891, clone 6C3; 1:50), CD45.1-PE-Cy7 (eBiosciences, 25-0453, clone A20; 1:200) and CD45.2-APC (eBiosciences, 17-0454, clone 104; 1:200). ChIP-seq antibodies were to H3K27me3 (Cell Signaling Technologies, #9733; 10 μg/ChIP), H3K4me3 (Abcam, #ab8580; 5 μg/ChIP) and H3K27ac (Abcam, #ab4729; 5 μg/ChIP).

Flow cytometry for bone marrow B cells. Whole bone marrow was harvested from femurs and tibias of 6- to 8-week-old mice. After red blood cell lysis (Qiagen, #158904), B cell progenitors were stained using antibodies, and flow cytometry was performed as previously described[8]. Analysis was performed on a BD FACSCanto II.

Competitive bone marrow transplantation. Whole bone marrow was pooled from femurs and tibias of 8-week-old donor mice. Donor cells were wild-type or Ts1Rhr CD45.1$^+$CD45.2$^+$ C57BL/6 × FVB F1 (test) and CD45.1$^+$ B6.SJL × FVB F1 (competitor) and were mixed 1:1. Recipients were lethally irradiated (550 cGy twice, >4 h apart). B6.SJL × FVB F1 mice received 10^6 total cells by lateral tail vein injection. Bone marrow was harvested 16 weeks after transplantation and analyzed by flow cytometry.

Methylcellulose colony-forming assays. Whole bone marrow was harvested from 6-to 8-week-old mice, and red blood cells were lysed. Cells were plated in B cell (Methocult M3630, Stem Cell Technologies) or myeloid (Methocult M3434) methylcelluose medium in gridded 35-mm dishes. Myeloid colonies were plated at 2×10^4 cells/ml per passage. B cell colonies were plated at 2×10^5 cells/ml in passage 1 and at 5×10^4 cells/ml per subsequent passage. Colonies were counted at 7 d, and colonies were then pooled and replated in the same manner.

Bone marrow transplantation models. For BCR-ABL transplantations[17], 10^5 transduced cells were transplanted with 10^6 wild-type untransduced bone marrow cells for radioprotection. For generation of BCR-ABL B-ALLs derived from Hardy B cells, 5×10^4 Hardy B cells from 6-week-old mice were sorted on a BD FACSAria II SORP, spinoculation was performed as described above, and 10^3 cells were transplanted into lethally irradiated wild-type recipients with 10^6 bone marrow cells for radioprotection. Dominant-negative Ikaros experiments were performed similarly, except that 10^6 cells spinfected with a murine stem cell virus (MSCV) retrovirus either expressing GFP alone or coexpressing GFP and Ik6 (refs. 14,37) were transplanted. Mice were followed daily for clinical signs of leukemia and were euthanized when moribund. Investigators were not blinded to the experimental groups. Ten mice were used per arm for 80% power to detect a 60% difference in survival at a specific time point with α of 0.05. No animals were excluded from analysis.

Cell culture. Ba/F3 cell experiments were performed as previously described[13]. shRNAs targeting *Hmgn1* are described below (competitive shRNA assay section), and cDNA expressing HMGN1 was described previously[30]. One week after selection in puromycin, retroviral cDNA or lentiviral shRNA-transduced cells were harvested for western blotting. hTERT-RPE1 cells were cultured in DMEM/F-12. Mouse A9 cells containing a single human chromosome 21 tagged with a neomycin resistance gene (a gift from M. Oshimura, Tottori University, Japan) were cultured in DMEM. All media were supplemented with 10% FBS, 100 IU/ml penicillin and 100 μg/ml streptomycin.

Immunoblotting and quantification. Western blotting was performed as previously described[13]. ImageJ (http://imagej.nih.gov/ij) was used for quantification of immunoblots, with band intensities normalized to total H3.

Microcell-mediated chromosome transfer. Microcell-mediated chromosome transfer was performed as described previously[38] with modifications. A9 cells were cultured to ~70% confluence and treated with 75 ng/ml colcemid for 48 h. Cells were collected and resuspended in 1:1 DMEM:Percoll (GE Healthcare Biosciences) with 10 μg/ml cytochalasin B (Sigma-Aldrich) and spun at 17,000 r.p.m. for 75 min in a Beckman JA17 rotor. Supernatant was collected and filtered through 10- and 5-μm filters. Approximately 2×10^6 RPE1 cells were collected and mixed with filtered microcells, treated with 100 μg/ml PHA-P (Sigma-Aldrich) for 30 min and fused by PEG 1500 (Sigma-Aldrich) in solution. Hybrid cells were plated and cultured for 48 h and selected with 500 μg/ml Geneticin (Life Technologies) for 12–14 d. Standard G-band analysis was performed at Karyologic, Inc. SNP array was performed at the DFCI microarray core using the Human Mapping 250k-Nsp platform. Fluorescent *in situ* hybridization was performed with the Vysis LSI 21 SpectrumOrange probe (Abbott Molecular) according to the manufacturer's instructions.

DR-GFP and DR-GFP-CE reporter targeting. Generating and screening of targeted clones were performed as described[39] with the following modifications. 10^6 RPE1 cells with two, three or four copies of chromosome 21 were nucleofected with 2 μg pAAVS1-DR-GFP or pAAVS1-DR-GFP-CE plasmid together with 2 μg pZFN-AAVS1 using program X-001 of the Amaxa nucleofector II (Lonza). Targeting of individual clones was confirmed by PCR using the Accuprime GC-rich DNA polymerase (Life Technologies). The presence of a single integrant was determined by qPCR (data not shown).

DNA repair assays using DR-GFP reporter cell lines. Assays for homologous recombination and imprecise nonhomologous end joining were performed as described previously[40] with the following modifications. Transfections were performed with the Neon transfection system (Life Technologies) using 1,600 V, 20 ms and 1 pulse. 4×10^5 DR-GFP cells were transfected with 10 μg I-SceI expression vector (pCBASce) or empty vector (pCAGGS) and plated in six-well plates. pmCherry-C1 vector (Clontech) was transfected in parallel to confirm equal transfection efficiency. Cells were cultured for 7 d and analyzed by fluorescence-activated cell sorting (FACS) using FACSCalibur (BD Biosciences) for homology-directed repair. The remaining cells were used to extract genomic DNA. 1 μg DNA was digested with 20 U I-SceI (Roche) overnight, purified and amplified with a two-step PCR protocol. Accuprime GC-rich polymerase was used for the first-step PCR (20 cycles), and Taq polymerase (Qiagen) was used for the second-step PCR (20 cycles).

doi:10.1038/ng.2949

PCR products were cloned with the TOPO TA cloning kit for sequencing (Life Technologies). For DR-GFP-CE cells, pCAGGS-RAG1 and pCAGGS-RAG2 vectors were co-transfected. 1 µg genomic DNA was digested with 10 U MfeI and 10 U NdeI (NEB) overnight to exclude templates that had not been cleaved by RAG-1 and RAG-2 before PCR amplification. The primer sequences are available in **Supplementary Table 2**.

Competitive shRNA assay in primary B cells. shRNAs targeting triplicated Ts1Rhr genes and controls were obtained from The RNAi Consortium (http://www.broadinstitute.org/rnai/trc) as pLKO lentiviral supernatants[41] ($n = 185$; see **Supplementary Table 1** for clone ID numbers and target sequences). Wild-type or Ts1Rhr passage 1 B cell colonies were collected and plated at 5×10^4 cells per well of a 96-well plate in 100 µl of RPMI with 20% fetal bovine serum (FBS) and 10 ng/mL each of mouse IL-7, stem cell factor and FLT3 ligand (all from R&D Systems) with 8 µg/ml polybrene. 10 µl of lentiviral supernatant was added, and the plate was centrifuged at 1,000*g* for 30 min and then placed in a 37 °C incubator for 24 h. Wells were pooled, 10^6 cells were saved for input shRNA analysis and 2×10^6 cells were plated in 6 ml M3630 methylcellulose with 0.05 µg/ml puromycin in a 10 cm non–tissue culture treated dish. At this density of plating, after 7 d of growth there were at least 4×10^4 colonies per plate, which would represent >200 colonies per individual shRNA on average. After each passage, genomic DNA was harvested from 10^6 cells (Qiagen QIAmp kit), and 2×10^6 cells were replated in the same manner. Repassaging continued until cultures stopped forming new colonies (three to four passages for wild type) or until six passages were completed. The entire assay was repeated in $n = 3$ (wild type) or $n = 4$ (Ts1Rhr) independent biological replicates.

The shRNA encoded in the genomic DNA was amplified using two rounds of PCR. Primary PCR reactions were performed using up to 10 µg of genomic DNA in 100 µl reactions consisting of 10 µl Takara Ex Taq buffer, 8 µl dNTPs (2.5 mM each), 10 µl of 5 µM primary PCR primer mix (**Supplementary Table 2**) and 1.5 µl Takara ExTaq. For the secondary PCR amplification, the reaction was performed as described previously[41] using modified forward primers, which incorporated Illumina adaptors and 6-nucleotide barcodes. Secondary PCR reactions were pooled and run on a 2% agarose gel. The bands were normalized and pooled on the basis of relative intensity. An equal amount of sample was run on a 2% agarose gel and gel purified. Samples were sequenced using a custom sequencing primer on an Illumina Hi-Seq and quantified as previously described[41]. The primary, secondary and sequencing primers are listed in **Supplementary Table 2**.

RNA sequencing and data processing. Total RNA was harvested from B cell colonies ($n = 3$ independent biologic replicates per genotype per passage). RNA sequencing was performed at the DFCI Center for Cancer Computational Biology. Quality control of total RNA was performed using the RNA Qubit Assay (Invitrogen) and the Bioanalyzer RNA Nano 6000 Chip Kit (Agilent). At least 100 ng of total RNA and a Bioanalyzer RNA Integrity Number of >7.0 were required. Library construction was performed using the TruSeq RNA Library Prep Kit (Illumina). Final library quality control was performed using the DNA High Sensitivity Qubit Kit (Invitrogen), the Bioanalyzer High Sensitivity Chip Kit (Agilent) and the 7900HT Fast qPCR machine (Applied Biosystems). qPCR was performed using the Illumina Universal Library Quantification Kit from KAPA Biosystems. RNASeq libraries were normalized to 2 nM, pooled for multiplexing in equal volumes and sequenced at 10 pM on the Illumina HiSeq 2000. Sequencing was performed as 2×50 paired-end reads using the 100 cycles per lane Sanger/Illumina 1.9 deep sequencing protocol. The raw sequence data were subjected to data quality control checks based on per-base sequence quality scores, per-sequence quality scores, per-sequence GC content, sequence length distribution and over-represented sequences, which are implemented in the FastQC tool (http://www.bioinformatics.babraham.ac.uk/projects/fastqc/). Reads that passed quality control filters were aligned against the mouse reference genome by using the ultra high-throughput long read aligner Bowtie2 (ref. 42) available through TopHat 2.0.7 (http://tophat.cbcb.umd.edu)[43]. Mapping results were further analyzed with TopHat to identify splice junctions between exons. Genomic annotations in gene transfer format (GTF) were obtained from Ensembl mouse genome GRCm38 (http://useast.ensembl.org/Mus_musculus/Info/Index). Gene-level expression measurements for 23,021 Ensembl mouse genes were reported in fragments per kilobase per million reads (FPKM) by Cufflinks 2.0.0 (http://cufflinks.cbcb.umd.edu/)[44]. An FPKM filtering cutoff of 1 in at least one sample was used to determine expressed transcripts.

Differential analysis for RNA-seq transcript expression. Differential analysis was performed by applying the EdgeR method[45] implemented in Bioconductor v2.11 (http://www.bioconductor.org/). EdgeR uses empirical Bayes estimation and exact tests based on the negative binomial distribution model of the genome-scale count data. EdgeR estimates the genewise dispersions by conditional maximum likelihood, conditioning on the total count for that gene. The genewise dispersion is 'normalized' by shrinking toward a consensus value based on an empirical Bayes procedure[46]. The differential expression is estimated separately for each gene on the basis of an exact test analogous to Fisher's exact test adopted for overdispersed data[47].

Gene expression profiling and GSEA. The series matrix files for two DS ALL data sets (AIEOP and ICH) were downloaded from GEO (GSE17459)[19], as were those for the *Rag1*$^{-/-}$ and *E2A* (*Tcf3*)$^{-/-}$ B cell progenitors (GSE21978)[27]. RNA from HMGN1 transgenic (HMGN1_OE) or wild-type littermate B cell colonies was processed and hybridized to the Affymetrix Mouse Gene 2.0 ST array at the DFCI Microarray Core per the manufacturer's instructions. Raw probe-level data from the AIEOP-2 non-DS ALL cohort and the mouse HMGN1_OE gene expression profiling were summarized using the Robust Multiarray Average (RMA)[48] and Brainarray custom chip identification files based on Entrez IDs (version 17)[49] using the ExpressionFileCreator module in Gene Pattern[50]. For GSEA, the expression file was converted to human gene orthologs using BioMart[51]. GSEA of the Ts1Rhr, the core Ts1Rhr and the PRC2 gene sets was performed as described previously using GSEA v2.0.10 (http://www.broadinstitute.org/gsea/)[22]. The Ts1Rhr gene set was tested for its enrichment in the c1 (positional), c2.cgp (chemical and genetic perturbation), c3.tft (transcription factor targets) and c6 (oncogenic signatures) gene sets deposited in the Molecular Signature Database MSigDB v3.1 (Broad Institute; http://www.broadinstitute.org/gsea/msigdb). The analysis was performed by applying the two-tailed Fisher test method as implemented in the Investigate_GeneSets module at MSigDB. To define the Ts1Rhr B cell gene set, the top 150 most differentially expressed protein-coding genes with an adjusted *P* value below 0.25 were selected. Hierarchical clustering of this signature in DS ALL compared to non-DS ALL revealed a subset of genes most contributing to the distinguishing phenotype, and this branch defined the 'core' Ts1Rhr gene set. Full gene sets for BENPORATH_SUZ12_TARGETS, MIKKELSEN_MEF_HCP_WITH_H3K27ME3 and MIKKELSEN_MEF_NPC_WITH_H3K27ME3 were obtained from MSigDB v3.1. The 100 most differentially expressed genes between the DS ALLs and the non-DS ALLs were determined using the MarkerSelectionModule in Gene Pattern. For E2A target gene expression, we compared *Rag1*$^{-/-}$ pro-B cells to *E2A*$^{-/-}$ pre-pro-B cells to generate probesets with >1.5-fold change and $P < 0.05$ between conditions, exactly as had been done by previous authors[27]. The Ts1Rhr and core gene sets were compared to all probesets for their relative expression in *E2A* wild-type (*Rag1*$^{-/-}$ pro-B) compared to *E2A*$^{-/-}$ cells.

Network enrichment mapping. The gene sets with significant enrichment in genes upregulated in Ts1Rhr cells by GSEA were selected on the basis of the maximum cutoff value 0.05 for *P* value and FDR and visualized with Enrichment Map software[23]. This software organizes the significant gene sets into a network, where nodes correspond to gene sets and the edges reflect significant overlap between the nodes according to a Fisher's test. The size of the nodes is proportional to the number of genes in the gene set. The hubs correspond to collections of genes sets with significant pairwise overlap that have a unifying functional description according to Gene Ontology (GO) biological processes. The node color is associated to the functional description of the hub. The clusters provided by the Enrichment Map are described in **Supplementary Table 1d**.

Visualization of gene expression and mass spectrometry data. RNA-seq–derived expression data from Ts1Rhr and wild-type B cells, B-ALL gene expression data and histone mass spectrometry data were visualized as heat

maps using GENE-E (Broad Institute; http://www.broadinstitute.org/cancer/software/GENE-E/).

Column purification of mouse B-ALLs. For western blotting of mouse B-ALLs, we enriched cryopreserved B-ALL splenocytes using antibody to CD19 conjugated to magnetic microbeads (#130-052-201) and an MS MACS column (#130-042-201), both from Miltenyi Biotec.

Histone mass spectrometry. Mass spectrometry for global histone H3 post-translational modifications was performed as described previously[52] using wild-type or Ts1Rhr passage 1 B cells and BCR-ABL B-ALLs. H3K27 modifications are presented in conjunction with H3K36, as both are present in the same measured peptides because of their close proximity. Significance was calculated as difference from the log2 ratio of zero by *t*-test.

Drug treatment. GSK-J4 (#M60063-2) and GSK-126 (#M60071-2) were purchased from Xcessbio. For methylcellulose experiments, at each passage, DMSO, GSK-J4 or GSK-126 was added to cultures at a final concentration of 1 μM. DS ALLs (deidentified specimens obtained with informed consent under DFCI Institutional Review Board protocol 05-001) were treated *in vitro* in quadruplicate with GSK-J4 at twofold dilutions from 40 nM to 10 μM in RPMI with 20% calf serum supplemented with 10 ng/mL IL-3, IL-7, stem cell factor (SCF), FLT3 ligand and 50 μM β-mercaptoethanol. After 3 d, viability was measured using CellTiter-Glo reagent and normalized to DMSO control (Promega).

ChIP analyses. B cell colonies (>5,000 colonies per genotype) from three wild-type and three Ts1Rhr animals were pooled after 7 d in methylcellulose culture. ChIP was performed as described previously[53]. Libraries for sequencing were prepared following the Illumina TruSeq DNA Sample Preparation v2 kit protocol. After end repair and A tailing, immunoprecipitated DNA (10–50 ng) or DNA from whole-cell extracts (50 ng) was ligated to a 1:50 dilution of Illumina Adaptor Oligo Mix assigning 1 of 24 unique indexes in the kit to each sample. After ligation, libraries were amplified by 18 cycles of PCR using the HiFi NGS Library Amplification kit from KAPA Biosystems. Amplified libraries were then size selected using a 2% gel cassette in the Pippin Prep system from Sage Science set to capture fragments between 200 and 400 bp. Libraries were quantified by qPCR using the KAPA Biosystems Illumina Library Quantification kit according to the kit protocols. Libraries with distinct TruSeq indexes were multiplexed by mixing at equimolar ratios and running together in a lane on the Illumina HiSeq 2000 for 40 bases in single-read mode. Alignment to mouse genome assembly NCBI37/mm9 and normalization were performed as described previously[54]. Regions of modified histones enriched in wild-type and Ts1Rhr cells were identified using a MACS peak calling algorithm at a P value of 1×10^{-9} (ref. 55). Location analysis of ChIP-target enriched regions was performed using the CEAS software suite developed by the Liu lab at DFCI[56]. Promoter states were classified by the presence of H3K4me3, H3K27me3 or both (bivalent) ChIP-seq enriched regions in the ±1 kb region relative to the transcriptional start site (TSS). ChIP-qPCR was performed on two independent sets of pooled B cell colonies from three wild-type and three Ts1Rhr mice (primers available upon request). For analysis of upregulated genes in Ts1Rhr B cells, we excluded the 31 triplicated genes in Ts1Rhr mice. Data are presented as boxplots designating the median (black line), 1 s.d. (box) and 2 s.d. (whiskers). E2A ChIP-Seq data from *Rag1*$^{-/-}$ pro-B cells were obtained from GEO (GSE21978)[27] and mapped to the genome as described above. We defined regions of enriched E2A genomic occupancy using the MACS algorithm as described above. Genes were considered to be associated with E2A if their gene body overlapped an E2A enriched region or if their TSS was within 50 kb of an E2A enriched region, as was performed previously[57].

Statistical analyses. Pairwise comparisons are represented as means ± s.e.m. by two-tailed *t*-test, except where otherwise specified. Categorical variables were compared using a Fisher's exact test. Kaplan-Meier survival curves were compared using the log-rank test.

32. Urbánek, P., Wang, Z.Q., Fetka, I., Wagner, E.F. & Busslinger, M. Complete block of early B cell differentiation and altered patterning of the posterior midbrain in mice lacking Pax5/BSAP. *Cell* **79**, 901–912 (1994).
33. Dildrop, R. *et al.* IgH enhancer-mediated deregulation of N-myc gene expression in transgenic mice: generation of lymphoid neoplasias that lack c-myc expression. *EMBO J.* **8**, 1121–1128 (1989).
34. Abuhatzira, L., Shamir, A., Schones, D.E., Schaffer, A.A. & Bustin, M. The chromatin-binding protein HMGN1 regulates the expression of methyl CpG-binding protein 2 (MECP2) and affects the behavior of mice. *J. Biol. Chem.* **286**, 42051–42062 (2011).
35. Birger, Y. *et al.* Chromosomal protein HMGN1 enhances the rate of DNA repair in chromatin. *EMBO J.* **22**, 1665–1675 (2003).
36. Bustin, M., Crippa, M.P. & Pash, J.M. Immunochemical analysis of the exposure of high mobility group protein 14 and 17 surfaces in chromatin. *J. Biol. Chem.* **265**, 20077–20080 (1990).
37. Trageser, D. *et al.* Pre-B cell receptor–mediated cell cycle arrest in Philadelphia chromosome–positive acute lymphoblastic leukemia requires IKAROS function. *J. Exp. Med.* **206**, 1739–1753 (2009).
38. Tomizuka, K. *et al.* Functional expression and germline transmission of a human chromosome fragment in chimaeric mice. *Nat. Genet.* **16**, 133–143 (1997).
39. Fung, H. & Weinstock, D.M. Repair at single targeted DNA double-strand breaks in pluripotent and differentiated human cells. *PLoS ONE* **6**, e20514 (2011).
40. Weinstock, D.M., Nakanishi, K., Helgadottir, H.R. & Jasin, M. Assaying double-strand break repair pathway choice in mammalian cells using a targeted endonuclease or the RAG recombinase. *Methods Enzymol.* **409**, 524–540 (2006).
41. Ashton, J.M. *et al.* Gene sets identified with oncogene cooperativity analysis regulate *in vivo* growth and survival of leukemia stem cells. *Cell Stem Cell* **11**, 359–372 (2012).
42. Langmead, B. & Salzberg, S.L. Fast gapped-read alignment with Bowtie 2. *Nat. Methods* **9**, 357–359 (2012).
43. Trapnell, C. *et al.* Differential gene and transcript expression analysis of RNA-seq experiments with TopHat and Cufflinks. *Nat. Protoc.* **7**, 562–578 (2012).
44. Trapnell, C. *et al.* Transcript assembly and quantification by RNA-Seq reveals unannotated transcripts and isoform switching during cell differentiation. *Nat. Biotechnol.* **28**, 511–515 (2010).
45. Robinson, M.D., McCarthy, D.J. & Smyth, G.K. edgeR: a Bioconductor package for differential expression analysis of digital gene expression data. *Bioinformatics* **26**, 139–140 (2010).
46. Robinson, M.D. & Smyth, G.K. Moderated statistical tests for assessing differences in tag abundance. *Bioinformatics* **23**, 2881–2887 (2007).
47. Robinson, M.D. & Smyth, G.K. Small-sample estimation of negative binomial dispersion, with applications to SAGE data. *Biostatistics* **9**, 321–332 (2008).
48. Irizarry, R.A. *et al.* Summaries of Affymetrix GeneChip probe level data. *Nucleic Acids Res.* **31**, e15 (2003).
49. Dai, M. *et al.* Evolving gene/transcript definitions significantly alter the interpretation of GeneChip data. *Nucleic Acids Res.* **33**, e175 (2005).
50. Reich, M. *et al.* GenePattern 2.0. *Nat. Genet.* **38**, 500–501 (2006).
51. Kinsella, R.J. *et al.* Ensembl BioMarts: a hub for data retrieval across taxonomic space. *Database (Oxford)* **2011**, bar030 (2011).
52. Peach, S.E., Rudomin, E.L., Udeshi, N.D., Carr, S.A. & Jaffe, J.D. Quantitative assessment of chromatin immunoprecipitation grade antibodies directed against histone modifications reveals patterns of co-occurring marks on histone protein molecules. Molecular & cellular proteomics. *Mol. Cell. Proteomics* **11**, 128–137 (2012).
53. Verzi, M.P. *et al.* Differentiation-specific histone modifications reveal dynamic chromatin interactions and partners for the intestinal transcription factor CDX2. *Dev. Cell* **19**, 713–726 (2010).
54. Lin, C.Y. *et al.* Transcriptional amplification in tumor cells with elevated c-Myc. *Cell* **151**, 56–67 (2012).
55. Zhang, Y. *et al.* Model-based analysis of ChIP-Seq (MACS). *Genome Biol.* **9**, R137 (2008).
56. Shin, H., Liu, T., Manrai, A.K. & Liu, X.S. CEAS: *cis*-regulatory element annotation system. *Bioinformatics* **25**, 2605–2606 (2009).
57. Lovén, J. *et al.* Selective inhibition of tumor oncogenes by disruption of super-enhancers. *Cell* **153**, 320–334 (2013).

doi:10.1038/ng.2949